Title
THE NUCLEAR SPINS AND MOMENTS OF SEVERAL RADIOACTIVE GALLIUM ISOTOPES

Author
Ehlers, Vernon James.

Publication Date
1960-03-18

UCRL 9123

UNIVERSITY OF CALIFORNIA

Ernest O. Lawrence Radiation Laboratory

BERKELEY, CALIFORNIA

DISCLAIMER

UCRL-9123
UC-34 Physics and Mathematic
TID-4500 (15th Ed.)

UNIVERSITY OF CALIFORNIA

Lawrence Radiation Laboratory
Berkeley, California

Contract No. W-7405-eng-48

THE NUCLEAR SPINS AND MOMENTS OF SEVERAL RADIOACTIVE GALLIUM ISOTOPES

Vernon James Ehlers
(Thesis)

March 18, 1960

Printed in USA. Price $2.50. Available from the
Office of Technical Services
U. S. Department of Commerce
Washington 25, D.C.

THE NUCLEAR SPINS AND MOMENTS OF SEVERAL RADIOACTIVE GALLIUM ISOTOPES

Contents

THE NUCLEAR SPINS AND MOMENTS OF SEVERAL RADIOACTIVE GALLIUM ISOTOPES

Vernon James Ehlers
(Thesis)

Lawrence Radiation Laboratory
University of California
Berkeley, California

March 18, 1960

ABSTRACT

The atomic-beam magnetic-resonance technique with radioactive detection has been used to investigate several radioactive gallium isotopes. The nuclear spin of 21-min Ga^{70} has been determined to be 1, and the hyperfine structure separations of 68-min Ga^{68} and 78-hr Ga^{67} have been measured. The Ga^{67} has been measured in both the $^2P_{3/2}$ and the $^2P_{1/2}$ electronic states, allowing a determination of the differential hyperfine structure anomaly $^{67}\delta^{69}$, defined by

$$^{67}\delta^{69} = {}^{67}\Delta^{69}_{\frac{1}{2}} - {}^{67}\Delta^{69}_{\left(\frac{3}{2}\right)} = \left(\frac{\Delta\nu}{a}\right)^{67} \Big/ \left(\frac{\Delta\nu}{a}\right)^{69} - 1.$$

The Ga^{68} has been measured in the $^2P_{3/2}$ state and has shown a very small magnetic moment, causing an inversion of the energy levels. For an assumed positive magnetic moment the decreasing energy level sequence is F = 5/2, 1/2, 3/2. The measurements made on these isotopes yield the following results:

Ga^{67}		Ga^{68}	
$^2P_{3/2}$	$a = 175.092\ (9)$ Mc/sec	$^2P_{3/2}$	$\lvert a\rvert = 3.75\ (20)$ Mc/sec
$^2P_{3/2}$	$b = 71.940\ (25)$ Mc/sec	$^2P_{3/2}$	$\lvert b\rvert = 11.7\ (1.0)$ Mc/sec
$^2P_{1/2}$	$\Delta\nu = 2457.733\ (30)$ Mc/sec	$^2P_{3/2}$	$b/a > 0$
	$\mu_I = 1.8454\ (.8)$ nm		$\lvert\mu_I\rvert = 0.0263\ (14)$ nm
	$Q = 0.219\ (11)$ barns		$\lvert Q\rvert = 0.0356\ (31)$ barns

The nuclear moments are obtained by the use of the Fermi-Segre`

formula and the previously measured moments and interaction constants of Ga^{69}. The magnetic moments quoted do not contain any diamagnetic correction. If we compare the interaction constants of Ga^{69} with our values for Ga^{67}, we obtain $^{67}\delta^{69} = (6 \pm 5) \times 10^{-3}$ %.

The neutron-deficient isotopes were produced by bombarding copper with α particles. The gallium was separated chemically from the copper by an ether-extraction technique. The Ga^{70} was produced by neutron bombardment of gallium and was transported from the reactor to the atomic-beam machine by helicopter, due to the short half life involved. Isotopic detection was accomplished by exposing collector "buttons" to the beam and then counting their radioactivity in either low-background scintillation or Geiger counters, depending on the characteristic radiation emitted.

The theory of the experiment, experimental apparatus and techniques, methods of data analysis, and results are presented. A brief history of studies of gallium is also given.

I. INTRODUCTION

Gallium was discovered spectroscopically by Lecoq de Boisbaudran (BOI 76) in 1875 in a specimen of zinc blend. In the same year he obtained the free metal by electrolysis of a solution of the hydroxide in potassium hydroxide, which is essentially the method used today. He described it as a metallic element of steel-gray color melting at 30°C and boiling at about 1700°C, and recommended it for use in high-temperature thermometers. More recent measurements (HAR 28, KEL 35) have shown the boiling point to be 2071°C, with a melting point of 30°C. At 1349°C, the vapor pressure is 1 mm, which is about the normal operating pressure inside the oven used in atomic-beam research.

Gallium is one of the scarcest elements, although it is widely distributed through nature in minute quantities, occurring in many zinc blends and almost always in bauxite. de Boisbaudran processed 4300 kg of rich Bensberg ore (BOI 78) and determined that gallium was present in the amount of 16 mg/kg of ore. At the present time it is valued at $1360 per pound, roughly three times the value of gold. Remarkably hard and resistant even at a temperature little below its melting point, it is but slightly malleable and flexible. Its chief physical and chemical properties had been predicted six years before its discovery by D. I. Mendeleef, who called it eka-aluminum. However, de Boisbaudran chose to name it gallium in honor of his native country, France.

Early spectroscopic studies were rather difficult because of the scarcity of material and the fact that gallium is liquid at low temperatures. However, the difficulties were overcome, and by 1922 a number of lines had been measured. (FOW 22, PAS 22, UHL 22) In 1925 electron spin was postulated and Sawyer and Lang combined this with previous results and their observations (SAW 29) to obtain a ground state of $4s^2 4p^2 P_{1/2}$ with a fine-structure separation of 826 cm^{-1} from the $^2P_{3/2}$ member of the doublet. Recently the measurements have been extended into the ultraviolet and infrared regions (GAR 50, MEG 52), and all the term values have been

recalculated and summarized by Moore (MOO 52). Approximately 70 lines have now been classified.

A productive approach toward understanding the structure of the nucleus has been provided by measurement of various intrinsic nuclear properties, such as spin and multipole moments. These experimental results can then be compared with theoretical results calculated from an assumed nuclear model and thus can lead to a comprehensive theory of nuclear structure. This method has aided greatly the development of the shell theory of the nucleus (MAY 55), the collective model of Bohr and Mottleson (BOH 53), and various other theories (HOH 50, BLI 57).

Several experimental methods have been extremely useful in furthering the knowledge of ground-state nuclear properties. The principle techniques used are microwave spectroscopy, optical spectroscopy, paramagnetic resonance, electron-nuclear double resonance, atomic and molecular beams, and β^- and γ -ray spectroscopy.

The earliest nuclear information was obtained by using optical spectroscopic methods. In 1931 Campbell and Bacher (CAM 31) observed three components of the $4p\,^2P_{1/2}$—$5s\,^2S_{1/2}$ line at 4032 A, indicating a nuclear spin of 1/2. The relative intensities also agreed with this result, although their resolution was very poor. In 1932, Jackson (JAC 32), using a higher-resolution interferometer, decided the nuclear spin was 3/2 for both Ga^{69} and Ga^{71}, although he could not exclude the possibility that I was 0 for one isotope, in which case he could not say anything about the spin of the other isotope. (This was obviously before the discovery of the neutron!) He later improved his accuracy (JAC 32a) and observed that the magnetic moments were roughly the same for both isotopes, indicating equal spins, i.e. I = 3/2.

Campbell (CAM 32) used a 21-ft grating to measure the hyperfine structure of GaII and also obtained I = 3/2. The following year he noted that the lines of the two isotopes are separated because of differing magnetic moments and obtained the ratio of the moments as 1.27. (CAM 33) Historically, this was important since it was the first instance in which isotopes of the same nuclear spin were found to possess different magnetic moments. Goudsmit (GOU 33) calculated the magnetic

moments from the results of Campbell and obtained μ^{69} = 2.01 nm and μ^{71} = 2.55 nm, in very good agreement with present-day results. In 1936, Schuler and Korsching (SCH 36) made observations on the $4s5s\,^3S_1 - 4s5p\,^3P_{0,1,2}$ triplet of GaII to obtain the quadrupole moments. Their values are in rather poor agreement with present-day values.

The experimental method that treats the atom in the most isolated state is that of atomic and molecular beams. Also, when used in conjunction with the technique of radioactive detection, this method allows a measurement using as few as 10^{10} atoms of the isotope in question. At present this is far less material than is required by any of the other methods. Thus we see the atomic-beam method is ideally suited for the determination of atomic and nuclear properties of an isolated radioactive atom. These properties may best be obtained from a study of the interaction of the nucleus and its associated electrons with an external magnetic field.

The atomic-beam magnetic-resonance technique was originally developed by Rabi (RAB 38). In 1942 Zacharias (ZAC 42) introduced the flop-in modification which greatly enhanced the signal-to-noise ratio, permitting measurements on isotopes with low relative abundance. Development of the radioactive detection technique (SMI 51) resulted in another reduction in the amount of material requied to perform an experiment. This latter method is especially useful for measurements on isotopes having half lives greater than several minutes and less than a month.

Renzetti (REN 40) was the first to perform atomic-beam measurements on stable gallium, using the zero-moment method to obtain rough values of a and b for both stable isotopes. In 1947, Kusch and Foley (KUS 47) applied the much more accurate magnetic-resonance method to the problem and obtained good results. They noted a discrepancy in the values obtained for g_J for the $^2P_{1/2}$ and $^2P_{3/2}$ states, and by combining their results with the value of g_J for sodium, they were able to measure the anomalous magnetic moment of the electron for the first time. (FOL 48, KUS 48) Shortly after this, Becker and Kusch (BEC 48) obtained the values of a and b with an uncertainty of 5 kc/sec and

measured the magnetic moment of both isotopes directly, using a $\Delta m_I = \pm 1$, $\Delta m_J = 0$ transition at 5000 gauss. Using the values of μ_I and a they calculated $\left\langle \frac{1}{r^3} \right\rangle_{Av}$ and thus obtained the first good values of the quadrupole moments from their values of b.

In the same year, Pound (POU 48) used nuclear-resonance techniques to obtain the magnetic moments of Ga^{69} and Ga^{71}. Kusch pointed out (KUS 50) that there was a discrepancy of 0.7 % (about three times the experimental limits of error) between the values obtained by Pound and those obtained by using atomic-beam methods. This discrepancy was explained by Foley (FOL 50) as due to perturbation of the hyperfine structure of the $^2P_{1/2}$ state by the $^2P_{3/2}$ state. Clendenin (CLE 54) has calculated this effect using relativistic electronic wave functions and obtains good agreement between theory and experiment. The main effects are a change in apparent nuclear g factor and a common lowering of all $^2P_{1/2}$ sublevels.

The latest experiments on stable gallium will be mentioned in the main body of this thesis and have resulted in very good values of a, b, $\Delta \nu$, and g_I for Ga^{69} and Ga^{71}. (LUR 56, DAL 54, RIC 55, WAL 55) This has allowed the determination of the hyperfine-structure anomaly for these two isotopes.

The atomic-beam experiment presented in this thesis is part of a continuing program of the Atomic Beam Laboratory of the University of California for the systematic study of the nuclear properties of radioactive isotopes. During the previous four years, a total of 80 nuclear spins have been measured, of which nine are confirmations of work done elsewhere. The half lives involved range from 10 min to 24,000 yr. The hyperfine-structure separations of many of these isotopes have also been measured, which allowed determination of the nuclear multipole moments.

The atomic-beam flop-in apparatus used in the work described here is discussed in detail in the Ph. D. thesis of Robert J. Sunderland (SUN 56). In essence, the system is as follows: Neutral atoms are thermally ejected from a source oven and enter a high-vacuum chamber, where the mean free path is much longer than the length of the chamber.

The beam of atoms is directed sucessively through three magnetic fields, denoted the A, C, and B fields. The A and B fields are very inhomogeneous and thus are able to deflect a neutral atom possessing a magnetic moment. The C field, situated between the A and B fields, is extremely homogeneous and thus has no effect on the direction of travel of the neutral atoms. A radiofrequency magnetic field is superimposed on the C field and is capable of inducing transitions between the energy levels of the atom as it passes through the C field. The frequency necessary to cause a transition is dependent upon the strength of the C field and upon the atomic and nuclear constants of the atom. If the atom undergoes a transition that results in a change in sign of its magnetic moment, the A and B fields act in such a manner as to focus the atoms onto the axis of the apparatus. If such a transition does not occur, the A and B fields will "throw out" the atom. By placing a suitable detector at the focal point of the machine, one can determine when transitions have been induced. From a measurement of the strength of the C field and the frequency at which a transition occurs, various atomic and nuclear constants can be determined.

The experiment presented here resulted in the determination of the nuclear spin of Ga^{70}, and the hyperfine-structure separations, magnetic dipole moments, and electric quadrupole moments of Ga^{67} and Ga^{68}. Preliminary values of these constants had been obtained previously for Ga^{67} (WOR 57) and for Ga^{68} (HUB 58). The accuracy with which the experiment was performed also allowed the determination of the differential hyperfine-structure anomaly for Ga^{67}.

II. THEORY

A. The Hyperfine-Structure Interaction

1. Interaction of a Nucleus with Its Atomic Electrons

In the previous section we noted that one of the advantages of the atomic-beam method is that the atom is studied in a highly isolated state. Thus it is unnecessary to consider interactions between neighboring atoms and in the absence of an external field we need consider only the interaction between the nucleus and its atomic electrons. Perhaps the most fruitful approach is to consider the nucleus as situated in the electric and magnetic fields caused by the moving electrons. We can then expand the electron field in terms of its multipole components and consider the interaction of each component with the corresponding multipole moment of the nucleus. The advantage of this method is that there are certain theoretical restrictions on the order of nuclear multipole moments which serve to reduce the number of terms required to describe the system. They may be summarized as follows: (RAM 56, pp. 58, 70)

(a) For a nuclear spin I, it is impossible to observe a nuclear multipole moment of order 2^k for $k > 2I$.

(b) If there is no degeneracy of nuclear states with different parity and if the nuclear Hamiltonian is unaltered by an inversion of coordinates, then:

(1) if all nuclear electrical effects arise from electrical charges, no odd (k odd) electric multipole can exist;

(2) if all nuclear magnetic effects arise from the circulation of electrical charges, no even (k even) magnetic multipole can exist.

Analagous theorems are applicable to an atom with atomic angular momentum J. Thus a nucleus possessing a nuclear quadrupole moment ($I > \frac{1}{2}$) can have no quadrupole interaction energy with an atom whose J is $\frac{1}{2}$.

The advantages of this method are now evident. The only interactions possible between the nucleus and its electrons are electric monopole, magnetic dipole, electric quadrupole, etc., and the number of terms is limited by the smaller of I and J. The electric-monopole interaction is

well-known and leads to the first-order structure of the atom. It will not be discussed further here. The higher-order terms account for the hyperfine structure of the atom. Schwartz has given an excellent discussion of this in his papers (SCH 55, SCH 57). In practice, the magnetic-octupole interaction is not observable within the accuracy of the machine used in this experiment and will be ignored. Thus we need consider only the magnetic-dipole and electric-quadrupole interactions.

For the case of the dipole interaction, the Hamiltonian has the form

$$\mathcal{H}_D = - \vec{\mu}_I \cdot \vec{B}_J \qquad \text{(II.1)}$$

where $\vec{\mu}_I$ is the nuclear magnetic-dipole moment and $\vec{B}_J$ is the magnetic field at the nucleus due to the circulating electrons. There is a general theorem (RAM 56) to the effect that

$$\vec{\mu}_I = \frac{\mu_I}{I} \vec{I} \qquad \text{(II.2)}$$

for a nucleus of definite spin I. Also $\vec{B}_J$ can be taken as proportional to $\vec{J}$ for matrix elements diagonal in J. (The implications of this will be discussed later.) We can combine these facts and write

$$\mathcal{H}_D = ha\, \vec{I} \cdot \vec{J} \ , \qquad \text{(II.3)}$$

where h is Planck's constant and a is a proportionality constant having the dimensions of frequency. Constant a is usually called the dipole interaction constant and is defined by

$$ha = - \frac{\mu_I}{I} \frac{\vec{B}_J \cdot \vec{J}}{\vec{J} \cdot \vec{J}} \ . \qquad \text{(II.4)}$$

Casimir (CAS 36) has evaluated this expression for a and has obtained

$$a = \frac{g_I \mu_o^2}{h} \left[\frac{2L(L+1)}{J(J+1)}\right] \left\langle \frac{1}{r^3} \right\rangle_{Av} \mathcal{F} \qquad \text{(II.5)}$$

where the average must be taken with respect to the outer electron having orbital angular momentum L. Here $\mathcal{F}$ is a relativistic correction factor given by Casimir (≈ 1), μ_o is the Bohr magneton ($\frac{e\hbar}{2mc}$), and

g_I is the nuclear g factor defined by

$$g_I = \frac{\mu_I}{\mu_o I} \tag{II. 6}$$

and referred to in units of Bohr magnetons.

We note that the majority of the quantities in Eq. (II. 5) depend only on the electronic structure of the atom. Consequently, they will not vary between two neighboring isotopes if we assume a point nucleus. If we then compare the dipole-interaction constants for two isotopes, 1 and 2, we obtain

$$\frac{a_1}{a_2} = \frac{g_{I_1}}{g_{I_2}} . \tag{II. 7}$$

This is the familiar Fermi-Segrè formula. Deviations from this formula are called hyperfine structure anomalies and are a measure of the failure of the approximation used, namely the assumption of a point nucleus (see Sec. II B)

The treatment of the quadrupole interaction is more difficult, since it has a tensor form. Ramsey (RAM 56) presents a good discussion of the problem and arrives at the Hamiltonian

$$\mathcal{H}_Q = \frac{hb}{2I(2I-1)J(2J-1)} \left[3(\vec{I}\cdot\vec{J})^2 + \frac{3}{2}(\vec{I}\cdot\vec{J}) - I(I+1)J(J+1)\right] \tag{II. 8}$$

where b is the quadrupole interaction constant defined by

$$hb = e^2 q_J Q. \tag{II. 9}$$

Here Q is called the nuclear electric-quadrupole moment and is defined by

$$Q = \frac{1}{e} \int_{\tau_n} \rho_{n_{II}} (3z_n^2 - r_n^2)\, d\tau_n, \tag{II. 10}$$

where the subscript n indicates nuclear coordinates and $\rho_{n_{II}}$ is the nuclear charge density when the nucleus is in the orientation state with $m_I = I$. The quantity q_J is defined by

$$q_J = -\frac{1}{e}\left\langle \sum_e \frac{(3\cos^2\theta_e - 1)}{r_e^3} \right\rangle_{Av} \qquad \text{(II. 11)}$$

This has also been evaluated by Casimir with the result

$$b = \frac{e^2 Q}{h}\left(\frac{2L}{2L+3}\right)\left\langle \frac{1}{r^3}\right\rangle_{Av} \mathcal{R}, \qquad \text{(II. 12)}$$

where $\mathcal{R}$ is a relativistic correction factor. We also see that we can obtain the analogue of the Fermi-Segre formula for this case:

$$\frac{b_1}{b_2} = \frac{Q_1}{Q_2}. \qquad \text{(II. 13)}$$

Since it is difficult to evaluate $\left\langle \frac{1}{r^3}\right\rangle_{Av}$, it would be desirable to eliminate this quantity. We see that we can do so by combining Eqs. (II. 5) and (II. 12). For $L = 1$ and $J = 3/2$ we then obtain

$$Q = \frac{8}{3}\,\frac{b}{a}\,\frac{g_I\,\mu_o^2}{e^2}\,\frac{\mathcal{H}}{\mathcal{R}}. \qquad \text{(II. 14)}$$

Since g_I can be measured directly with a nuclear-resonance experiment, and a and b can be obtained accurately with an atomic-beam experiment, we can obtain a reasonably correct value of Q by using this formula.

Up to this point we have assumed the atom to be in a pure state of angular momentum J. The extent to which this holds true can be determined if a can be evaluated for two different states of the atom, since, from Eq (II. 5),

$$\frac{a_{J_1}}{a_{J_2}} = 5\,\frac{\mathcal{H}_{J_1}}{\mathcal{H}_{J_2}} \qquad \text{(II. 15)}$$

for $L = 1$ (p electron).

In the case of gallium, this becomes

$$\left(\frac{a_{1/2}}{a_{3/2}}\right)_{\text{Pure state}} = 5.41, \qquad \text{(II. 16)}$$

while the experimental value is

$$\left(\frac{a_{\frac{1}{2}}}{a_{\frac{3}{2}}}\right)_{\text{Expt.}} = 7.02. \qquad \text{(II. 17)}$$

This poor agreement indicates the necessity of including the effects of configuration mixing. Koster (KOS 52) has considered this problem for gallium and has found it necessary to mix only the 4s4p5s excited state with the $(4s)^2 4p$ ground state. He obtains, in place of Eq. (II. 5),

$$a_{\frac{1}{2}} = -\frac{2 g_I \mu_o^2}{h}\left[-0.280\, a_o^{-3} - 2.67\, \mathcal{F}_{\frac{1}{2}}\left\langle \frac{1}{r^3}\right\rangle_{Av}\right] \qquad \text{(II. 18)}$$

and

$$a_{\frac{3}{2}} = -\frac{2 g_I \mu_o^2}{3h}\left[0.837\, a_o^{-3} - 1.61\, \mathcal{F}_{\frac{3}{2}}\left\langle \frac{1}{r^3}\right\rangle_{Av}\right], \qquad \text{(II, 19)}$$

and for Eq. (II. 12),

$$b = \frac{2 e Q R}{5h}\left\langle \frac{1}{r^3}\right\rangle_{Av} . \qquad \text{(II. 20)}$$

Equation (II. 20) is the same as Eq. (II. 12) with L = 1, i.e. the formula is not changed in this case. This is reasonable, since we are exciting an s electron to a higher s state and thus would not expect it to have any effect on the quadrupole interaction.

Using the experimental values for $a_{\frac{1}{2}}$, $a_{\frac{3}{2}}$, and g_I for Ga^{69} (DAL 54, LUR 56, RIC 55), we can evaluate these expressions. We obtain $\left\langle \frac{1}{r^3}\right\rangle_{Av} = 3.46\, a_o^{-3}$ (a_o, the Bohr radius, is approximately 5.29×10^{-9} cm). To check the validity of this result, we note that now

$$\left(\frac{a_{\frac{1}{2}}}{a_{\frac{3}{2}}}\right)_{\text{Conf. int.}} = 6.67. \qquad \text{(II. 21)}$$

This is now within 5% of the experimental value of Eq. (II. 17) and represents a considerable improvement over Eq. (II. 16).

We must now consider the effect if J is not a good quantum number, that is if we have a near-by level of different J. This is certainly the case for gallium, where the $^2P_{1/2}$ and $^2P_{3/2}$ states have a fine-structure separation of

$$\delta = 826.24 \text{ cm}^{-1} = 2.48 \times 10^7 \text{ Mc/sec} \qquad \text{(II. 22)}$$

Clendenin has discussed this problem, using relativistic wave functions and second-order perturbation theory (CLE 54). He concludes that a in the $^2P_{1/2}$ state must be replaced by

$$a' = a - \frac{2\,(a'')^2}{\delta}\,, \qquad \text{(II. 23)}$$

where

$$\frac{a''}{a} = -\frac{1}{16}\,(1 - 1.396\,Z^2\alpha^2 - 0.121\,Z^4\alpha^4 + \ldots) \qquad \text{(II. 24)}$$

Evaluating this for Ga^{67}, we find that

$$\frac{2\,(a'')^2}{\delta} = 0.4 \text{ kc/sec} \qquad \text{(II. 25)}$$

which is smaller than the accuracy attained in the experiment and thus can be ignored. In this calculation the effect of the quadrupole term has been neglected. However, because of the rather small quadrupole-interaction constants of the gallium isotopes and the relatively large fine-structure separation, this effect is not expected to be significant.

Clendenin also discovered that g_I obtained from Eq. (II. 5) would be altered by about 0.6% due to this effect. However, this is of no consequence to us, because g_I can be measured directly for stable isotopes by using nuclear-resonance techniques. Then g_I for the radioactive isotopes can be obtained by the use of Eq. (II. 7).

2. Interaction with an External Magnetic Field

If we now place the nucleus and its associated electrons in a magnetic field, $\vec{H}$, the Hamiltonian for the interaction with the field will be

$$\mathcal{H}_M = -\vec{\mu}_J \cdot \vec{H} - \vec{\mu}_I \cdot \vec{H}, \qquad \text{(II. 26)}$$

where $\vec{\mu}_J$ is the magnetic moment of the electron system.

Since we have

$$\vec{\mu}_J = \frac{\mu_J}{J} \vec{J} , \tag{II.27}$$

and Eq. (II.2) holds for $\vec{\mu}_I$, we can rewrite Eq. (II.26) as

$$\mathcal{H}_M = - \frac{\mu_J}{J} \vec{J} \cdot \vec{H} - \frac{\mu_I}{I} \vec{I} \cdot \vec{H} . \tag{II.28}$$

In terms of the g factors, we can rewrite Eq. (II.28) as

$$\mathcal{H}_M = - g_J \mu_o \vec{J} \cdot \vec{H} - g_I \mu_o \vec{I} \cdot \vec{H} , \tag{II.29}$$

where g_J is the atomic (Lande) g factor defined by

$$g_J = \frac{\mu_J}{\mu_o J} , \tag{II.30}$$

and g_I is as defined in Eq. (II.6).

We can discuss the behavior of this system in a magnetic field roughly by calculating the magnetic field at the nucleus due to the electrons. For a single s electron, this field is approximately $\frac{2\mu_o}{a_o^3}$, or about 10^5 gauss. The nuclear moment is about $(1/2000)\mu_o$ or 5×10^{-24} ergs/gauss. The interaction energy is thus about 5×10^{-19} ergs, or 100 Mc/sec if frequency is used as the unit of energy. This represents a rather strong coupling of the nuclear spin to the electronic angular momentum. On the other hand, the atomic precession frequency in a magnetic field, if uncoupled, is $\frac{g_J \mu_o H}{h}$, or about 2.8 Mc/sec-gauss. Thus it would take an external field of several hundred gauss to completely decouple the nuclear and electronic systems.

In view of this we can describe the behavior of the system in weak fields as a coupling of $\vec{I}$ and $\vec{J}$ to form a resultant total angular momentum $\vec{F} = \vec{I} + \vec{J}$. The other good quantum number will then be m, the projection of $\vec{F}$ along the magnetic-field direction. Figure 1a shows how $\vec{I}$ and $\vec{J}$ couple to form a resultant $\vec{F}$ which precesses in a weak magnetic field $\vec{H}_o$.

In a strong magnetic field $\vec{I}$ and $\vec{J}$ are decoupled and independently precess about a magnetic field $\vec{H}_o$ as shown in Fig. 1b. In this

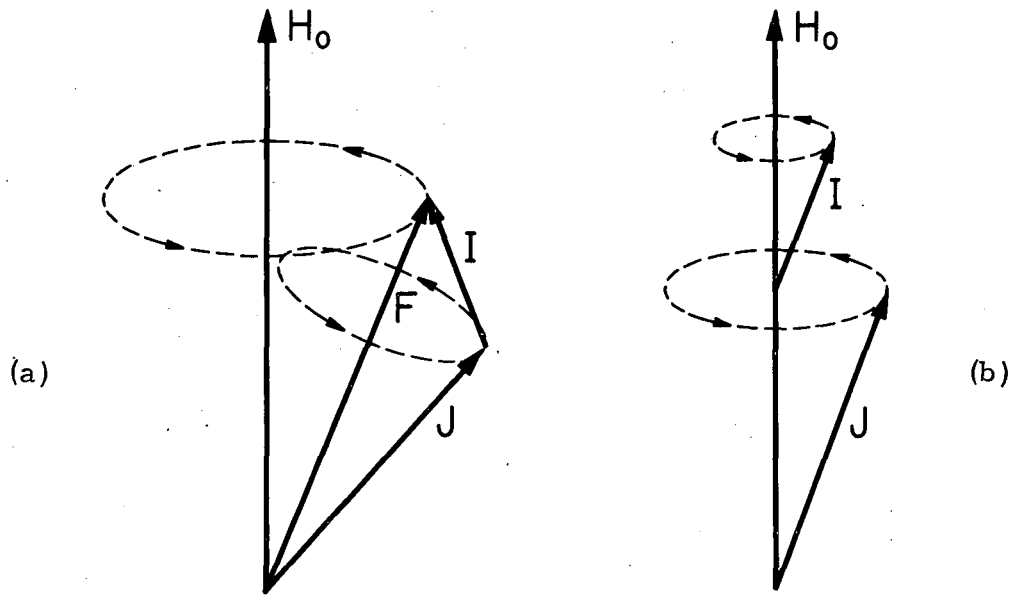

Fig. 1. Precession of $\vec{I}$, $\vec{J}$, and $\vec{F}$ in (a) a weak and (b) a strong magnetic field.

representation, m_I and m_J, the magnetic quantum numbers of $\vec{I}$ and $\vec{J}$, are good quantum numbers.

3. Solution of the Secular Equation

a. Case I: No magnetic field

When there is no magnetic field, the Hamiltonian is

$$\mathcal{H}_o = \mathcal{H}_D + \mathcal{H}_Q \tag{II.31}$$

or

$$\mathcal{H}_o = ha\,\vec{I}\cdot\vec{J} + \frac{hb}{2I(2I-1)\,J(2J-1)}\left[3(\vec{I}\cdot\vec{J})^2 + \frac{3}{2}(\vec{I}\cdot\vec{J}) - I(I+1)\,J(J+1)\right] \tag{II.32}$$

At zero field, F and m are good quantum numbers and the solution of the equation is fairly simple, since the matrix is diagonal in the (F, m) representation. We need the matrix elements of $\vec{I}\cdot\vec{J}$ in this representation. They are easily obtained by noting

$$(\vec{F})^2 = (\vec{I}+\vec{J})^2 = (\vec{I})^2 + (\vec{J})^2 + 2\,\vec{I}\cdot\vec{J}, \tag{II.33}$$

for which we can write

$$\vec{I}\cdot\vec{J} = \frac{1}{2}\left[F(F+1) - I(I+1) - J(J+1)\right] = \frac{1}{2}\,C\,. \tag{II.34}$$

Thus the expression for the energy becomes

$$W_F = (F, m\,|\,\mathcal{H}_o\,|\,F, m) = \frac{1}{2}\,ha\,C + \frac{hb}{2I(2I-1)\,J(2J-1)} \times\left[\frac{3}{4}\,C\,(C+1) - I(I+1)\,J(J+1)\right]. \tag{II.35}$$

We note that this expression is degenerate in m. We shall see later that this degeneracy is removed by a magnetic field.

When $J = 1/2$, we have no quadrupole term and there are only two possible F values, $F = I + 1/2$ and $F = I - 1/2$. The hyperfine-structure energy separation between these levels is customarily designated $\Delta\nu$ (in units of Mc/sec) and is given by

$$\Delta\nu = \frac{W_{I+1/2} - W_{I-1/2}}{h} = a\,(I+1/2)\,. \tag{II.36}$$

For $J > 1/2$, we must include the quadrupole term, and the computation becomes more involved, although by no means difficult. To eliminate the tedium involved in the calculation, Baker (BAK 60) has utilized

the IBM-653 computer to obtain tables of coefficients relating $\Delta\nu_{F_1, F_2}$ to a and b. Using these tables, we obtain for J=3/2, I=1:

$$\Delta\nu_{\frac{5}{2},\frac{3}{2}} = \frac{5}{2}\,a + \frac{5}{4}\,b$$
$$\Delta\nu_{\frac{3}{2},\frac{1}{2}} = \frac{3}{2}\,a - \frac{9}{4}\,b\,, \qquad \text{(II.37)}$$

and for J = 3/2, I = 3/2;

$$\Delta\nu_{3,2} = 3\,a + b$$
$$\Delta\nu_{2,1} = 2\,a - b$$
$$\Delta\nu_{1,0} = -\,a - b\,. \qquad \text{(II.38)}$$

The order of the various levels depends on the ratio $b/a=\xi$. It is of interest to determine the dependence. If we write our energy as

$$W' = \frac{W}{ha} = \frac{1}{2}\,C + \frac{\xi}{2I(2I-1)\,J(2J-1)} \times\left[\frac{3}{4}\,C\,(C+1) - I(I+1)\,J(J+1)\right] \qquad \text{(II.39)}$$

we can plot W' against ξ. Marino (MAR 59) has done this and obtained Fig. 2 for J = 3/2, I = 1, and Fig. 3 for J = 3/2, I = 3/2.

b. Case II: Magnetic field

When the effect of the magnetic field is included, the Hamiltonian becomes

$$\mathcal{H} = \mathcal{H}_o + \mathcal{H}_M \qquad \text{(II.40)}$$

or

$$\mathcal{H} = ha\,\vec{I}\cdot\vec{J} + \frac{hb}{2I(2I-1)\,J(2J-1)} \times\left[3\,(\vec{I}\cdot\vec{J})^2 + \frac{3}{2}(\vec{I}\cdot\vec{J}) - I(I+1)J(J+1)\right] - g_J\mu_o\vec{J}\cdot\vec{H} - g_I\mu_o\vec{I}\cdot\vec{H}. \qquad \text{(II.41)}$$

We have already obtained the matrix elements of $\mathcal{H}_o$ in Eq. (II.35). Ramsey (RAM 56) gives the diagonal matrix elements of $\mathcal{H}_M$ as

$$(F, m)\left|\mathcal{H}_M\right|F, m) = -\,g_J\mu_o\,H\,\frac{F(F+1) + J(J+1) - I(I+1)}{2F(F+1)}\,m - g_I\mu_o\,H\,\frac{F(F+1) + I(I+1) - J(J+1)}{2F(F+1)}\,m\,. \qquad \text{(II.42)}$$

There will be off-diagonal elements of $\mathcal{H}_M$ in the (F, m) representation due to the terms in I_z and J_z (from $\vec{I}\cdot\vec{H}$ and $\vec{J}\cdot\vec{H}$). Now, since $F_z = I_z + J_z$ is diagonal in F and m, we will have

$$(F, m \;|\; I_z|\, F', m') = -\,(F, m \;|\; J_z \;|\; F', m'). \qquad \text{(II.43)}$$

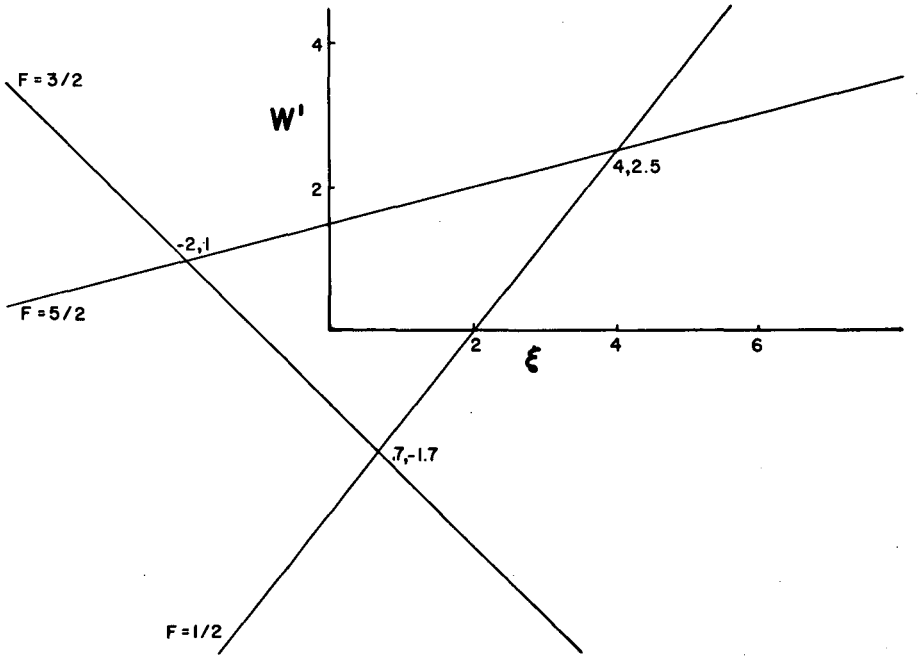

MU-17219

Fig. 2. W' versus ξ for $J = \frac{3}{2}$, $I = 1$.

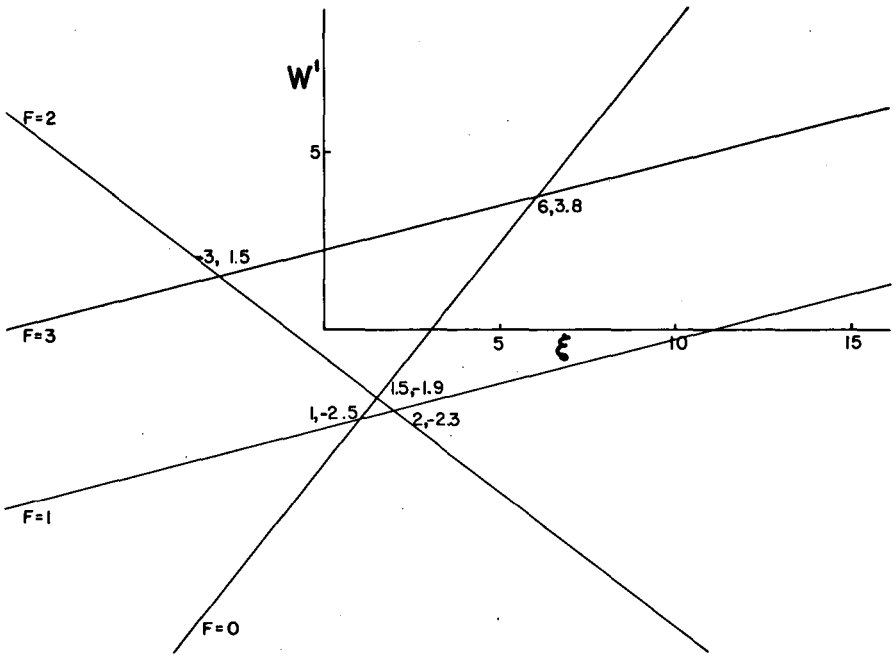

MU-17203

Fig. 3. W' versus ξ for $J = \frac{3}{2}$, $I = \frac{3}{2}$.

Also, since J_z can connect only states for which F changes by ±1, and since the matrix of J_z is diagonal in m (EDM 57), the only nonzero off-diagonal matrix elements of $\mathcal{H}$ will be of the form

$$(F, m \left| \mathcal{H} \right| F \pm 1, m) = (-g_J + g_I)\, \mu_o\, H\, (F, m \left| J_z \right| F \pm 1, m) \tag{II.44}$$

where (RAM 56)

$$(F, m \left| J_z \right| F - 1, m) = (F - 1, m \left| J_z \right| F, m)$$

$$= -\left\{ \frac{(F-I+J)(F+I-J)(I+J+1+F)(I+J+1-F)(F^2-m^2)}{4F^2(2F-1)(2F+1)} \right\}^{1/2} \tag{II.45}$$

The sign of the last matrix element is a phase factor and therefore is arbitrary.

Because the matrix is diagonal in m, it can be arranged as a group of submatrices along the diagonal, each corresponding to a different m. The maximum order of these submatrices is given by the number of different possible F values. This method of arrangement greatly facilitates the solution of the determinant.

For the case J = 1/2, we have two different F levels. Consequently the secular equation is quadratic, and the solution can be obtained in closed form. This solution is known as the Breit-Rabi equation: (BRE 31)

$$W(F, m) = -\frac{h\,\Delta\nu}{2(2I+1)} - g_I\, \mu_o\, Hm \pm \frac{h\,\Delta\nu}{2} \left[1 + \frac{4mx}{2I+1} + x^2 \right]^{1/2}, \tag{II.46}$$

where

$$x = (-g_J + g_I) \frac{\mu_o\, H}{h\,\Delta\nu}, \tag{II.47}$$

and $\Delta\nu$ is the hyperfine-structure separation. The sign of the square root is positive for the state $F = I + 1/2$ and negative for $F = I - 1/2$.*

If we plot the energy in units of $h\Delta\nu$ as a function of x, we obtain what is called a Breit-Rabi diagram. Figure 4 shows such a diagram for the case J = 1/2, I = 3/2.

For J > 1/2, the secular determinant has a dimensionality greater than 2 (unless I = 1/2), and a solution in closed

*Ewbank (EWB 60) has recently pointed out that this rule does not hold for the $F = I + 1/2$, $m = -I - 1/2$ level, but instead we must use the positive sign for $x \leq 1$ and the negative sign for $x \geq 1$.

(Footnote continued on following page)

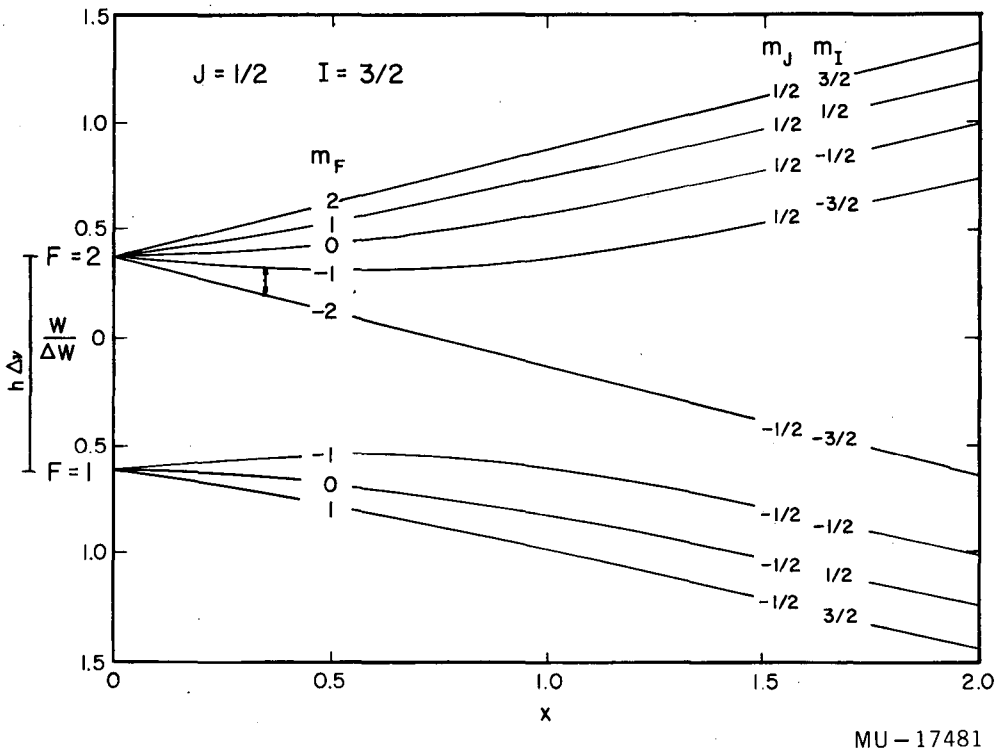

Fig. 4. Breit-Rabi diagram for $J = \frac{1}{2}$, $I = \frac{3}{2}$.

form is not attainable. In this case, two methods of solving the problem are available; we can obtain an approximate solution by using perturbation theory, or we can obtain an exact solution by using numerical methods on a high-speed digital computer.

Although in principle any accuracy desired can be obtained by using higher-order perturbation theory, in practice the problem becomes rather complicated beyond third order. The author has written a program for the IBM 653 that solves the problem to third order (Appendix B 1). In terms of the only nonzero matrix elements of our Hamiltonian [Eq. (II. 41)], the appropriate equations for the energy of the level (F, m) are: (CON 57)

$$
\begin{aligned}
W^{F,m} &= W_o^{F,m} + W_1^{F,m} + W_2^{F,m} + W_2^{F,m} + \ldots . \\
W_o^{F,m} &= (F,m\,|\,\mathcal{H}_o\,|\,F,m) \\
W_1^{F,m} &= (F,m\,|\,\mathcal{H}_M\,|\,F,m) \\
W_2^{F,m} &= \frac{(F,m\,|\,\mathcal{H}_M\,|\,F+1,m)^2}{W_o^{F,m} - W_o^{F+1,m}} \\
&\quad + \frac{(F,m\,|\,\mathcal{H}_M\,|\,F-1,m)^2}{W_o^{F,m} - W_o^{F-1,m}}
\end{aligned}
\qquad \text{(II.48)}
$$

---

*(Footnote continued from p. 20) The difficulty arises because for this level the quantity in brackets becomes

$$\left[1 + \frac{4mx}{2I+1} + x^2\right]^{\frac{1}{2}} = \left[1 - 2x + x^2\right]^{\frac{1}{2}} = 1 - x. \qquad \text{(II.47a)}$$

we see that as the value of x passes through 1, the quantity $1 - x$ changes sign. Because we always take the positive square root of the quantity in Eq. (II. 46), we see we much choose the negative sign for this level for $x \geq 1$.

$$W_3^{F,m} = \frac{(F,m|\mathcal{H}_M|F+1,m)^2[(F+1,m|\mathcal{H}_M|F+1,m)-(F,m|\mathcal{H}_M|F,m)]}{\left(W_o^{F,m} - W_o^{F+1,m}\right)^2}$$

$$+ \frac{(F,m|\mathcal{H}_M|F-1,m)^2[(F-1,m|\mathcal{H}_M|F-1,m)-(F,m|\mathcal{H}_M|F,m)]}{\left(W_o^{F,m} - W_o^{F-1,m}\right)^2}.$$

We can easily obtain the first-order expression for the frequency of a $\Delta F = 0$, $\Delta m = \pm 1$ transition. Since $\mathcal{H}_o$ is degenerate in m, we can write

$$\nu = \frac{W_1^{F,m} - W_1^{F,m_2}}{h}$$

$$= -\left[g_J \frac{F(F+1)+J(J+1)-I(I+1)}{2F(F+1)} + g_I \frac{F(F+1)+I(I+1)-J(J+1)}{2F(F+1)}\right] \times \frac{\mu_o H}{h}(m_1 - m_2). \quad \text{(II.49)}$$

We introduce a quantity g_F defined by

$$g_F = \left[g_J \frac{F(F+1)+J(J+1)-I(I+1)}{2F(F+1)} + g_I \frac{F(F+1)+I(I+1)-J(J+1)}{2F(F+1)}\right]$$

$$\approx g_J \frac{F(F+1)+J(J+1)-I(I+1)}{2F(F+1)}, \quad \text{(II.50)}$$

where we can neglect the last term to first order because $g_I \approx (1/2000)\, g_J$. Since we have $m_1 - m_2 = \pm 1$, Eq. (II. 49) now becomes

$$\nu = g_F \frac{\mu_o H}{h} \quad \text{(II. 51)}$$

Higher-order expressions for the frequency are listed in Appendix B 1.

A method of solving the secular determinant exactly has been developed by Nierenberg (NIE 58) and has been programmed for the IBM-653 computer (Appendix B 3). The method utilizes two properties of the matrix; there is one submatrix corresponding to each m value, and there are no matrix elements more than one off the diagonal. The solution is simpler if we rewrite our Hamiltonian in the following manner (using Mc/sec as our unit of energy):

$$\mathcal{H}' = a\,\vec{I}\cdot\vec{J} + \frac{b}{2I(2I-1)J(2J-1)}\left[3(\vec{I}\cdot\vec{J})^2 + \frac{3}{2}(\vec{I}\cdot\vec{J}) - I(I+1)J(J+1)\right] + \frac{(-g_J + g_I)\,\mu_o H}{h} J_z - \frac{g_I\,\mu_o H}{h} F_z. \tag{II. 52}$$

We temporarily neglect the last term and define:

$$a_n = (F, m \,|\, \vec{I}\cdot\vec{J} \,|\, F, m)$$

$$b_n = \frac{3\,a_n^2 + \frac{3}{2}\,a_n - I(I+1)\,J(J+1)}{2\,I(2\,I-1)\,J(2\,J-1)} \tag{II. 53}$$

$$c_n = (F, m \,|\, J_z \,|\, F, m)$$

$$d_n = (F, m \,|\, J_z \,|\, F+1, m)^2.$$

The diagonal elements of a given m submatrix will then be given by

$$A_n = a\,a_n + b\,b_n + (-g_J + g_I)\,\frac{\mu_o H}{h}\,c_n, \tag{II. 54}$$

and the square of the elements one off the diagonal will be

$$E_n = \left[(-g_J + g_I)\,\frac{\mu_o H}{h}\right]^2 d_n. \tag{II. 55}$$

Now let H_p be the submatrix for the particular m value we are interested in, and let X be an eigenvalue of that submatrix. Then we must solve the determinantal equation

$$D_p = |H_p - X\,I| = 0, \tag{II. 56}$$

where I is the identity matrix. If we now let D_1 be the 1x1 determinant in the lower right-hand corner of the submatrix, D_2 be the 2x2 determinant in that same corner, etc., then we see that the following recursion relation holds true:

$$D_n = (A_n - X)\,D_{n-1} - E_{n-1}\,D_{n-2}, \tag{II. 57}$$

when we define $D_{-1} = 0$ and $D_0 = 1$. We can differentiate this with respect to X to obtain

$$\frac{\partial D_n}{\partial X} = (A_n - X)\,\frac{\partial D_{n-1}}{\partial X} - D_{n-1} - E_{n-1}\,\frac{\partial D_{n-2}}{\partial X}. \tag{II. 58}$$

Other derivatives can be obtained in a similar manner, for example,

$$\frac{\partial D_n}{\partial H} = (A_n - X)\frac{\partial D_{n-1}}{\partial H} + (g_J + g_I)\frac{\mu_o}{h} c_n D_{n-1}$$
$$- E_{n-1}\frac{\partial D_{n-2}}{\partial H} - \frac{2 E_{n-1} D_{n-2}}{H}, \qquad \text{(II. 59)}$$

Using these recursion formulae, we can use Newton's method to solve the equation $D_p = 0$ for the eigenvalue of interest. The problem of root identification and other details are explained in Appendix B 3.

Since we neglected the last term in Eq. (II. 52), the eigenvalues calculated in this manner will not be the true energies but will be related to them by

$$W(F, m) = X - \frac{g_I \mu_o H}{h} m. \qquad \text{(II. 60)}$$

B. The Hyperfine-Structure Anomaly

We noted that the derivation of Eq. (II. 7),

$$\frac{a_1}{a_2} = \frac{g_{I_1}}{g_{I_2}} \qquad \text{(II. 7)}$$

involved the assumption of a point nucleus. Actually the requirements for this equation to hold true are not that stringent. If the nuclear radius and the distribution of nuclear magnetism and charge are the same for the two nuclei involved, the electronic part of Eq. (II. 5) should be the same for both, and thus Eq. (II. 7) would still be valid.

In 1949, Bitter (BIT 49) noted a discrepancy when applying Eq. (II. 7) to Rb^{85} and Rb^{87}. He ascribed it to a difference in distribution of nuclear magnetism for the two isotopes. Bohr and Weisskopf (BOH 50) developed a theory to explain the quantitative effect this would have on the hyperfine structure. This made it possible to use the experimentally observed hyperfine-structure anomaly $^1\Delta^2$, defined by

$$\frac{a_1}{a_2} = \frac{g_{I_1}}{g_{I_2}} \left(1 + {}^1\Delta^2 \right) \qquad \text{(II. 61)}$$

as an indication of the distribution of nuclear magnetism. The subject has been ably reviewed and extended by Eisinger and Jaccarino (EIS 58). In essence, the method used is to calculate the fractional hyperine-interaction reduction, ϵ, for a given isotope from the fractional contributions of spin and orbital moment to the nuclear magnetic moment. The anomaly will then be given by

$$^1\Delta^2 = \epsilon_1 - \epsilon_2 . \qquad \text{(II. 62)}$$

The value of $^1\Delta^2$ will depend on some coefficient b which represents the density at the nucleus of the electrons responsible for the hyperfine structure.

Other effects can also enter into $^1\Delta^2$, but in general the only one of importance for heavier nuclei is the Breit-Rosenthal effect (ROS 32, CRA 49), caused by a difference in the distribution of charge in the two nuclei. Theoretical estimates indicate that its effect on

$^1\Delta^2$ is in general less than one part in 10^4. However, in some cases it may exceed the Bohr-Weisskopf effect.

For an atom in the $S_{1/2}$ state, the anomaly is generally of the order of 0.3%. For an atom in a $P_{1/2}$ or $P_{3/2}$ state, the anomaly is much smaller, since the p-electron wave function vanishes at the origin. The majority of the anomaly for a P state arises from the s-electron components of the relativistic wave function ($b_{P_{1/2}}/b_{S_{1/2}} \approx Z^2\alpha^2$) and from admixture of excited s-electron states with the ground state.

We see from Eq. (II.61) that in order to determine $^1\Delta^2$ it is necessary to measure both a and g_I very accurately for two different isotopes. The a's can easily be obtained by use of the atomic-beam method. The g_I's can be measured by use of nuclear-resonance techniques if the isotope is present in sufficient relative abundance. Unfortunately, for the case of radioactive isotopes where there is an extremely low abundance, this method can not be used. The atomic-beam method can be used to measure g_I if the atom is in an $S_{1/2}$ state, but the accuracy leaves something to be desired.

However, we note that if we write Eq. (II. 61) for two different states, J = 1/2 and J = 3/2, we have

$$\left(\frac{a_1}{a_2}\right)_{1/2} = \left(\frac{g_{I_1}}{g_{I_2}}\right)_{1/2} (1 + {}^1\Delta^2{}_{1/2}) \qquad \text{(II. 63)}$$

and

$$\left(\frac{a_1}{a_2}\right)_{3/2} = \left(\frac{g_{I_1}}{g_{I_2}}\right)_{3/2} (1 + {}^1\Delta^2{}_{3/2}). \qquad \text{(II. 64)}$$

Since the ratio of the moments is entirely independent of the state of the atom, we have

$$\left(\frac{g_{I_1}}{g_{I_2}}\right)_{1/2} = \left(\frac{g_{I_1}}{g_{I_2}}\right)_{3/2}, \qquad \text{(II. 65)}$$

and therefore we can take the ratio of Eq. (II. 63) to Eq. (II. 64) to obtain

$$\frac{\left(\frac{a_1}{a_2}\right)_{1/2}}{\left(\frac{a_1}{a_2}\right)_{3/2}} = \frac{(1 + {}^1\Delta^2_{1/2})}{(1 + {}^1\Delta^2_{3/2})} \approx 1 + {}^1\Delta^2_{1/2} - {}^1\Delta^2_{3/2}. \qquad \text{(II. 66)}$$

We now define the differential hyperfine-structure anomaly as

$${}^1\delta^2 = {}^1\Delta^2_{1/2} - {}^1\Delta^2_{3/2} \qquad \text{(II. 67)}$$

and obtain

$${}^1\delta^2 = \frac{\left(\frac{a_1}{a_2}\right)_{1/2}}{\left(\frac{a_1}{a_2}\right)_{3/2}} - 1. \qquad \text{(II. 68)}$$

Thus we see that if we can measure the value of a in two different states of the atom, we can obtain the difference between the anomalies in the two states.

The ratio of the anomalies depends only on the difference in electronic density at the nucleus for the two states involved. Thus we should expect the ratio to vary only slightly from one pair of isotopes to another pair of the same element. Therefore if the ratio can be measured directly for a pair of stable isotopes, the value obtained can be used in conjunction with Eq. (II. 67) to obtain the individual anomalies for a radioactive isotope. The advantage of the method is that it eliminates the necessity of measuring g_I directly.

We shall now attempt to calculate the ratio of the anomalies for gallium. Normally, we should expect that ${}^1\Delta^2_{1/2}$ is much greater than ${}^1\Delta^2_{3/2}$ because of the much smaller density of $p_{3/2}$ electrons at the nucleus. However, if we consider configuration mixing, it is possible to have a noticeable admixture of excited s states contributing to both anomalies. For that case, we must replace the electron-density coefficient, b, by an effective value given by (SCH 55a)

$$b_{eff} = (1 - \beta_j)\, b_{p_j} + \beta_j\, b_s. \qquad \text{(II. 69)}$$

Where β_j, the fractional contribution of s-electrons to the hyperfine

structure in the state ^2P_J, may be calculated from $a_{1/2}$ and $a_{3/2}$ by the use of (SCH 55)

$$\beta_{1/2} = \frac{\left(1-5\theta \frac{a_{3/2}}{a_{1/2}}\right)}{1+5\theta} \qquad \text{(II. 70)}$$

and

$$\beta_{3/2} = -\frac{a_{1/2}}{a_{3/2}} \beta_{1/2},$$

where θ is a relativistic correction factor ≈ 1.10. For gallium, we have $a_{1/2}/a_{3/2} = 7.02$ and we obtain $\beta_{1/2} = 0.033$, $\beta_{3/2} = -0.23$. Also, $b_s/b_{p_{1/2}}$ for Bohr-Weisskopf theory is 23 and so we get

$$^2P_{1/2} \qquad b_{eff} = 1.7\, b_{p_{1/2}},$$

and (II. 71)

$$^2P_{3/2} \qquad b_{eff} = -5.3\, b_{p_{1/2}},$$

where we assume $b_{p_{3/2}}$ is zero.

The experimental values for the anomalies of Ga^{69} and Ga^{71} are, in percent, (DAL 54, RIC 55, SCH 55a, LUR 56)

$$^{69}\Delta^{71}_{1/2} = (6.2 \pm 2.3) \times 10^{-4}\,\%$$

$$^{69}\Delta^{71}_{3/2} = (-25.2 \pm 3.2) \times 10^{-4}\,\% \qquad \text{(II. 72)}$$

and

$$^{69}\delta^{71} = (31.4 \pm 2.4) \times 10^{-4}\,\%$$

The experimental value of the ratio of the two anomalies is

$$\left(\frac{^{69}\Delta^{71}_{3/2}}{^{69}\Delta^{71}_{1/2}}\right)_{\text{Expt.}} = -4.1 \pm 1.5, \qquad \text{(II. 73)}$$

while the value calculated from Eq. (II. 71) is

$$\left(\frac{{}^{69}\Delta^{71}_{3/2}}{{}^{69}\Delta^{71}_{1/2}}\right)_{\{\text{Theo.}\}} = -3.1. \qquad \text{(II. 74)}$$

Perhaps the best comparison of theory and experiment is made by taking

$$\left(\frac{{}^{69}\Delta^{71}_{3/2}}{{}^{69}\delta^{71}}\right)_{\text{Expt.}} = -0.80 \pm .16 \qquad \text{(II. 75)}$$

and comparing it to the theoretical value,

$$\left(\frac{{}^{69}\Delta^{71}_{3/2}}{{}^{69}\delta^{71}}\right)_{\text{Theo.}} = -0.76\ . \qquad \text{(II. 76)}$$

The excellent agreement indicates the validity of the theoretical assumptions used.

C. Nuclear Structure

1. Individual-Particle Model

It is of interest to attempt to correlate observed nuclear spins and moments with a theory of nuclear structure. The theory which at the present time gives the most consistent interpretation of observed data is the shell theory of Mayer (MAY 55).

The discovery of the neutron in 1932 opened the way for the development of models of nuclear structure. Early attempts were made to develop individual-particle models patterned after the electronic configurations in atoms. All these models assumed LS coupling, since jj coupling was not expected because of the very small absolute values of the nucleon magnetic moments.

Because of the failure of the individual-particle models to explain nuclear discontinuities, or "magic numbers" for heavier nuclei, interest turned toward the liquid-drop model of Bohr and the uniform model of Wigner. However, in 1948 Mayer (MAY 48) listed an impressive accumulation of experimental evidence (spins, moments, isomers, binding energy, and pairing energy) for closed nucleon shells at the magic numbers 2, 8, 20, 28, 50, 82, and 126. Since the liquid-drop and uniform models are inherently incapable of predicting any discontinuities, attention immediately returned to the individual-particle model.

It was not until Mayer (MAY 49) and, independently, Haxel, Jensen, and Suess (HAX 49) introduced strong spin-orbit forces that the individual-particle model was able to explain the observed magic numbers. The only justification for introducing these forces with the resultant jj coupling lay in its noteworthy success in matching experimental facts.

The basic assumption of the individual-particle model is that each nucleon can be considered as moving independently in an average central potential due to all the other nucleons. By assuming a nuclear potential intermediate between the harmonic oscillator and square-well potentials, with a strong spin-orbit interaction, we obtain the nuclear energy-level order shown in Fig. 5.

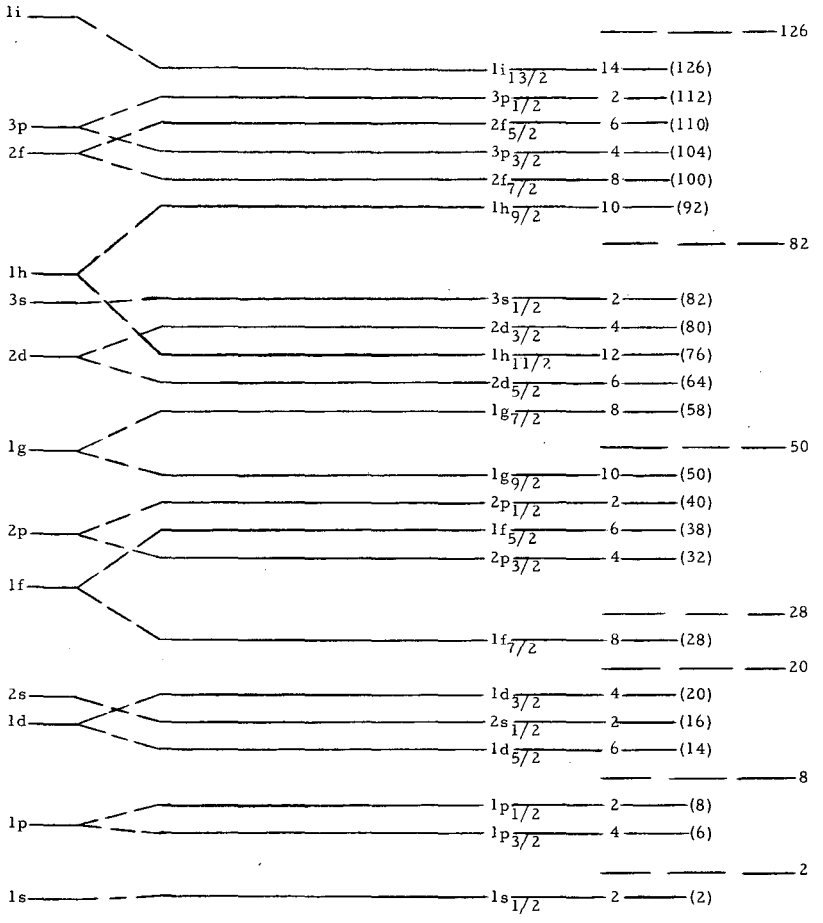

MU-17154

Fig. 5. Shell-model energy-level sequence. The levels without spin-orbit forces are shown on the left.

A note concerning nomenclature should be injected at this point. In atomic models, the principle quantum number n determines the first-order term for the total energy of the state, and is included in the notation. Thus an electron state with n = 3, orbital angular momentum $\ell = 2$, and total angular momentum j = 3/2 would be designated $3d_{3/2}$. In a nuclear potential well, the energy does not depend primarily on n, but on ℓ and the radial quantum number r (= n - ℓ). Thus a nucleon with n = 3, $\ell = 2$, j = ℓ - s = 3/2, would have r = 1 and would be denoted $1d_{3/2}$, i.e. r takes the position occupied by n in the electronic notation.

2. Nuclear Spins

In order to correlate the observed nuclear spins with the shell model, it has been necessary to adopt the following empirical coupling rules (MAY 55, NOR 51):

(a) The ground states of all nuclei with an even number of protons and neutrons have zero angular momentum.

(b) In nuclei of odd A, the ground-state properties are determined only by the type of nucleons present in odd number.

(c) In a nucleus of odd A, the nucleons of the type that is present in odd number will usually couple their spins in such a way that the total nuclear angular momentum is that of the last partially filled orbit, j.

(d) (Nordheim's Strong Rule). In an odd-odd nucleus, if one of the odd nucleons is in a level with intrinsic spin and orbital angular momentum parallel, and the other is in a level where they are anti-parallel ($j_n = \ell_n \pm 1/2$, $j_p = \ell_p \mp 1/2$), the total angular momentum of the ground state is the smallest possible one, $I = |j_n - j_p|$.

(e) (Nordheim's Weak Rule). In an odd-odd nucleus, if both odd proton and odd neutron are in levels in which intrinsic spin and orbital angular momentum are parallel ($j_n = \ell_n + 1/2$, $j_p = \ell_p + 1/2$) or if both are in levels in which these quantities are antiparallel ($j_n = \ell_n - 1/2$, $j_p = \ell_p - 1/2$), the spin should be $I > |j_n - j_p|$. (Recently Gallagher and Moszkowski have advanced coupling rules

for odd-odd nuclei based on the collective model (GAL 58); however, these rules are not necessary to explain the spins presented here.)

In applying this theory to gallium (Z = 31), we see from Fig. 5 that for the odd-A isotopes we need consider only the three $2p_{3/2}$ protons outside the closed shells. From the coupling rules, we expect I = 3/2 for all odd-A isotopes. This has been borne out for all the isotopes for which the spin is known.

In the case of the even-A gallium isotopes, for Ga^{68} we have N = 37, and we expect the $1f_{5/2}$ neutron to couple with the $2p_{3/2}$ proton to give I = 1. For Ga^{70}, we expect the thirty-ninth neutron to be in the $2p_{1/2}$ level and to couple with the $2p_{3/2}$ proton to again give spin 1. Both are predicted by the strong rule and have been verified by the experiment presented in this thesis.

3. Nuclear Moments

One of the first attempts to correlate nuclear angular momenta with nuclear magnetic dipole moments was made by Schmidt (SCH 37). He assumed a single-particle model in which the spin and magnetic moments for odd-A nuclei are due only to the one odd nucleon. Using this assumption, he calculated the moment to be expected for odd-proton and odd-neutron nuclei. The results are listed in Table I.

Table I

Schmidt formulae for nuclear moments

Type of nuclei	Parallel $I = \ell + 1/2$	Antiparallel $I = \ell - 1/2$
odd proton	$\mu = I - 1/2 + \mu_p$	$\mu = I + \frac{I}{I+1}(1/2 - \mu_p)$
odd neutron	$\mu = \mu_n$	$\mu = -\frac{I}{I+1}\mu_n$

If we substitute the emperical values for the proton and neutron magnetic moments -- μ_p = 2.79 nuclear magnetons (nm) and μ_n = - 1.91 nm, we obtain what are called the Schmidt limits. If we substitute the Dirac values --μ_p = 1 nm, μ_n = O, we obtain the Dirac limits. Although few moments lie on these limits, it is interesting to note that almost all nuclear moments lie between the two limits. This would indicate that there is some "quenching" of the anomalous magnetic moments of the proton and neutron when they are bound to the nuclear core. Qualitatively, this is to be expected from meson theory.

Several modifications of the theory have been developed. Consideration of intermediate coupling and configurational mixing has given promising results. (NOY 58) The collective model of Bohr and Mottleson (BOH 53) has been extremely useful in regions far removed from closed-shell configurations and has also shown some promise for calculating quadrupole moments. For an excellent review of the subject of nuclear moments, the reader is referred to Blin-Stoyle (BLI 57).

III. EXPERIMENT

A. Experimental Apparatus

1. Atomic-Beam Machine

The atomic-beam machine used in this research is described in detail in the thesis of Sunderland (SUN 56). Several modifications were made to it and are discussed by Shugart (SHU 57). The essential principles of operation of an atomic-beam machine are discussed in the introduction to this thesis. Figure 6 is a schematic diagram of the machine used and shows the trajectories followed by two different atoms in the machine. Atom 2 undergoes a transition in the C field which changes the sign of its effective atomic magnetic moment, and so it is refocused onto the detector D. Atom 1 starts out along the same path as atom 2 but does not undergo such a transition and thus is "thrown-out". The stop wire, S, is an obstacle which prevents the high-energy tail of the Maxwellian velocity distribution from traveling undeflected through the machine and reaching the detector.

Figure 7 is a photograph of the atomic-beam machine used in this research. Since many of the samples used in this machine were quite radioactive (about 50 roentgens per hr at 4 in.), various precautions were taken to protect the experimenters. The lucite box shown mounted on the machine served to surround the side oven loader while ovens were being inserted into or removed from the machine. This prevented stray particles of radioactive material from being dropped on the floor. A vacuum cleaner with a special filter was attached to the box and kept it at a negative pressure to prevent radioactive dust from entering the room.

To protect personnel from receiving too much radiation while operating the machine, a portable lead shield was place around the machine after the oven was inserted. This proved to be rather unwieldy and provided insufficient protection so it was replaced by the lead shield shown in Fig. 8. This shield consists of 4-in.- thick lead bricks supported by a steel frame. Lead doors encased in steel can be opened to allow insertion and removal of ovens. The chalk numbers

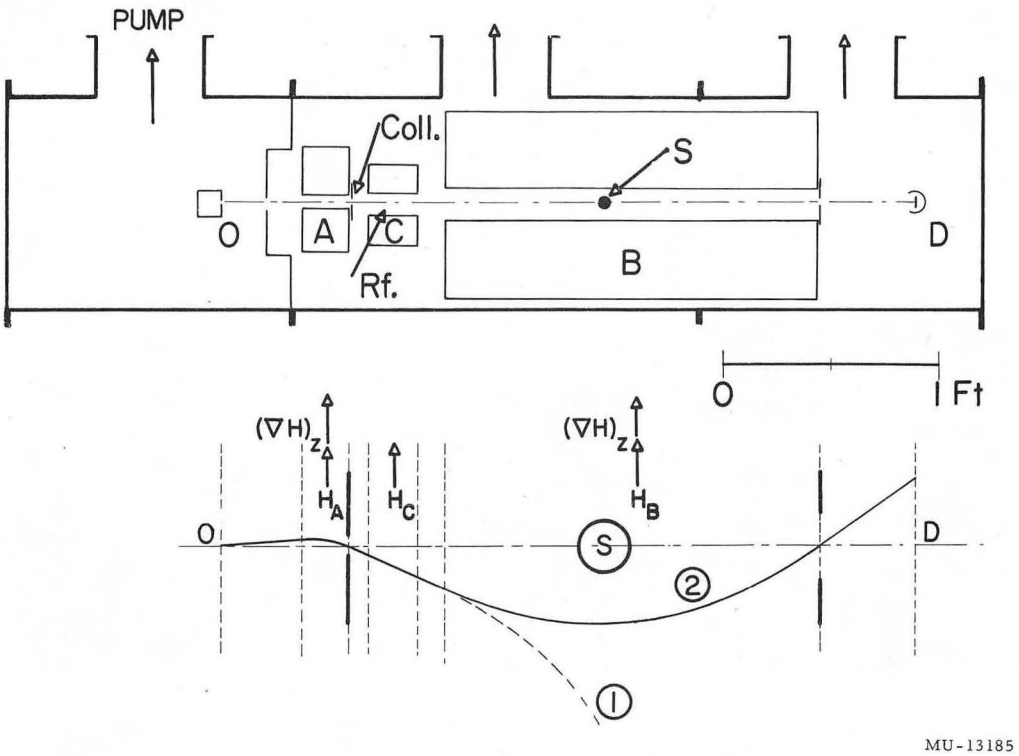

Fig. 6. Schematic arrangement and trajectory in an atomic-beam flop-in machine.

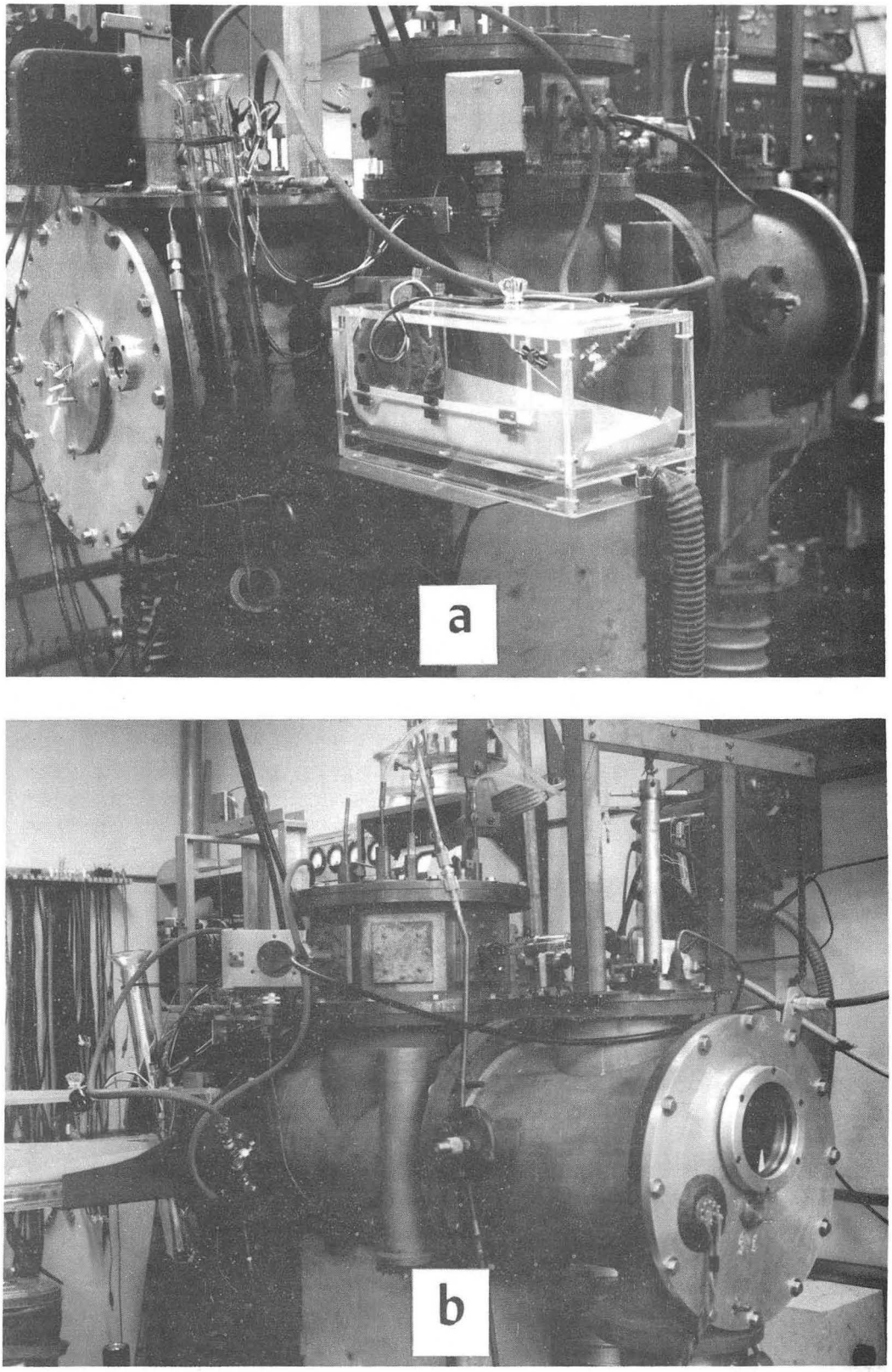

ZN-2370

Fig. 7. The atomic-beam machine as viewed from (a) the oven end and (b) the detector end of the apparatus.

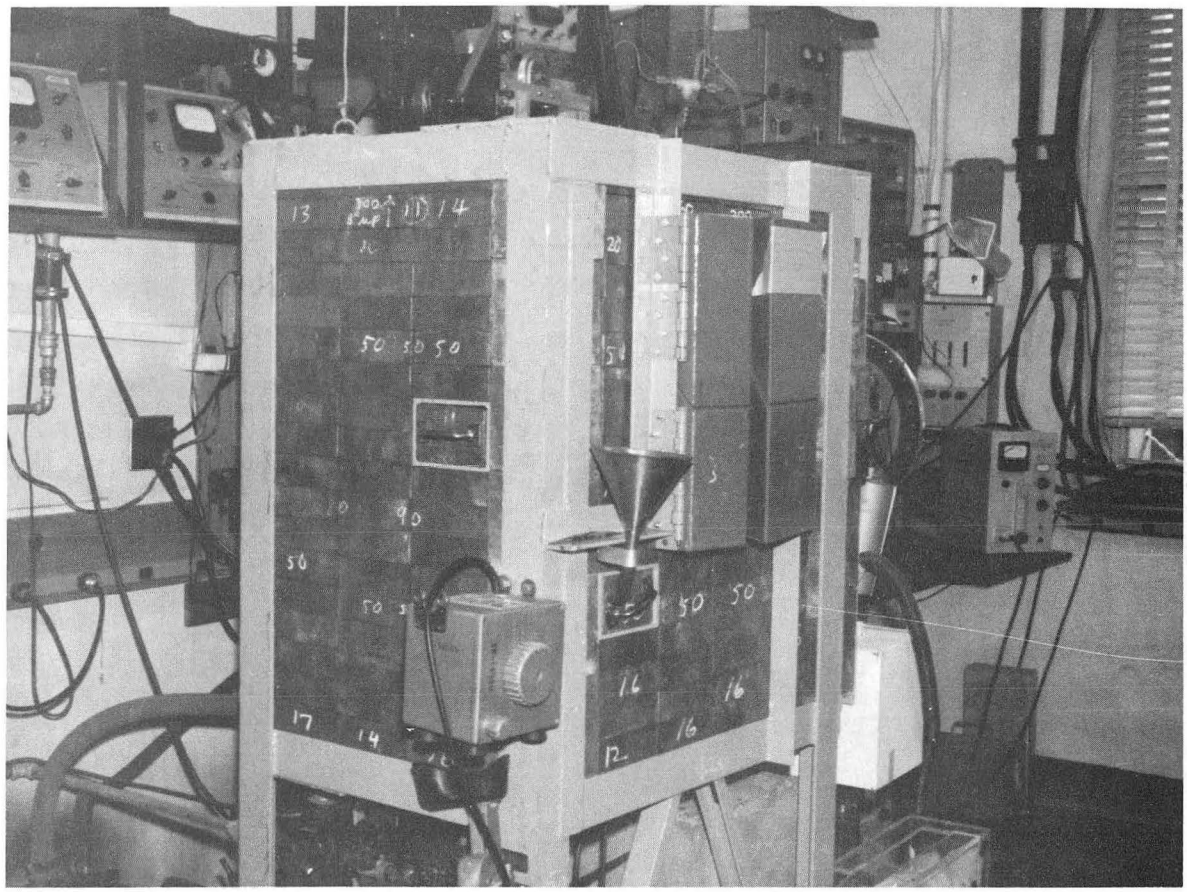

ZN-2362

Fig. 8. The atomic-beam machine with the lead shielding installed.

visible on the lead bricks indicate the radiation in milliroentgens per hr at those points when an extremely radioactive La^{140} sample was placed in the machine. The radiation is normally about a factor of ten lower than that shown.

Two ovens were used while the machine was in operation; the radioactive oven contained the sample of interest, while the calibration oven contained RbCl and some calcium filings. The calcium reduces the RbCl at moderate temperatures and the beam of Rb atoms coming from the oven was used to calibrate the C field. Originally, the calibration oven was mounted on a stand in the oven chamber of the machine. However, this meant that refilling the oven involved opening the machine and working in the rather radioactive oven chamber. Thus it was deemed advisable to build an oven loader for the calibration oven, utilizing a large port available on top of the oven chamber. It was decided to place another larger oven loader in this port, in addition to the calibration oven loader (see Fig. 9). The larger loader was designed to accomodate snouted ovens of the type shown in Fig. 10 and to provide independent heating of the body and the snout of the oven. This permits operation of the snout at extremely high temperatures which allows dissociation of polymers given off by some substances such as antimony. Several attempts have been made to obtain a beam of antimony, but to date the results have not been promising.

Carbon ovens of the type shown in Fig. 11 were used to obtain a beam of radioactive gallium atoms. The oven was placed in the machine through the side oven loader and was heated to the proper temperature by electron bombardment. Figure 12 shows the filament and high-voltage power supplies used for this purpose.

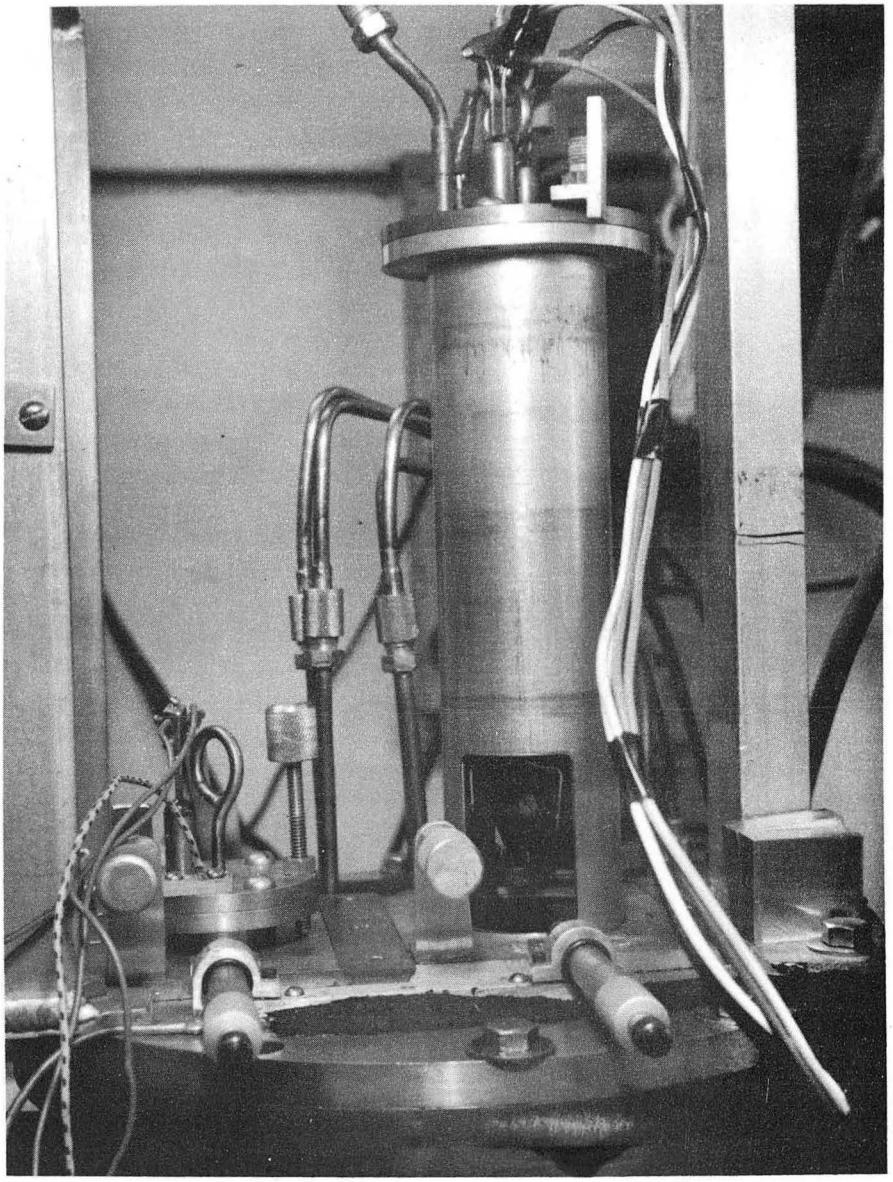

ZN-2361

Fig. 9. The calibration oven loader in operating position on the left with the snouted-oven loader on the right removed.

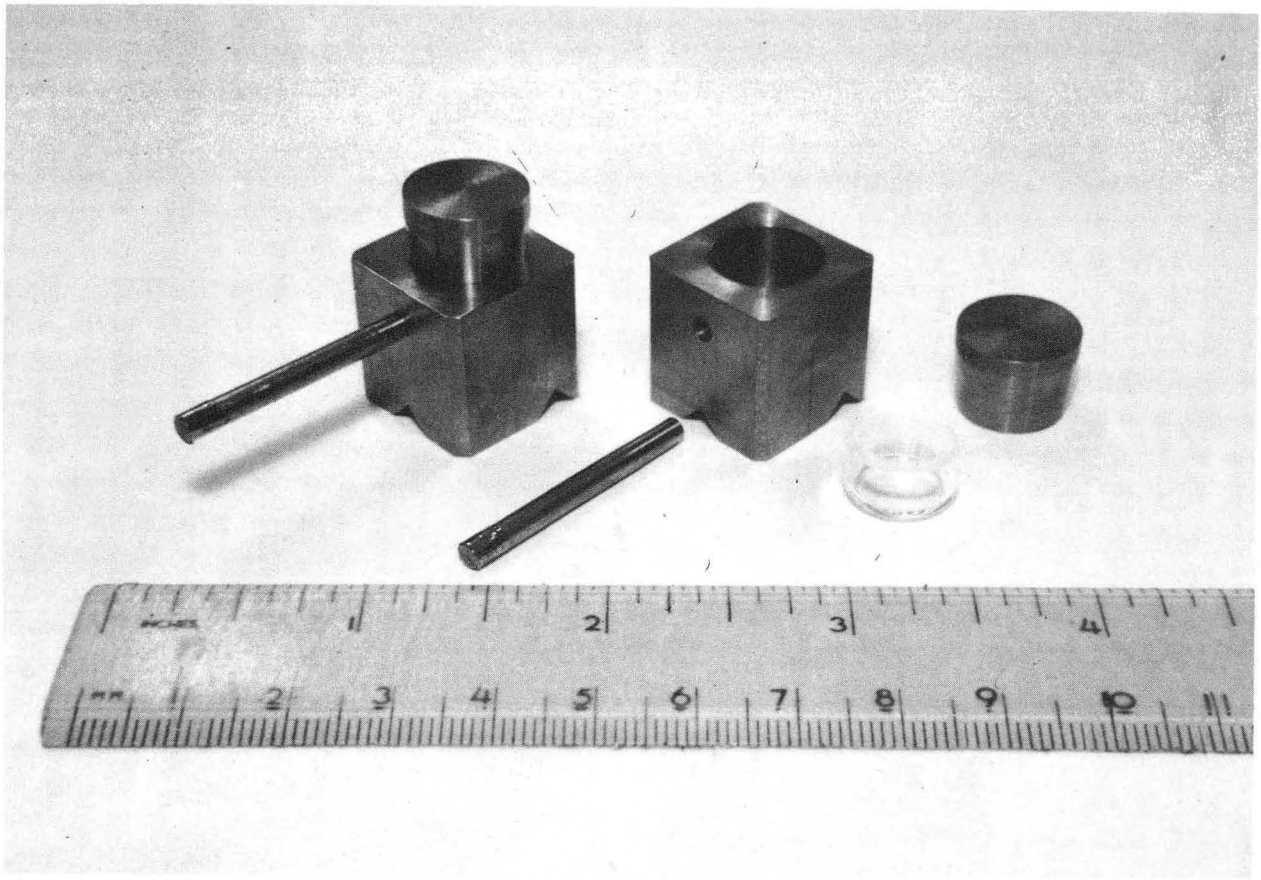

Fig. 10. Snouted ovens of the type used for antimony.

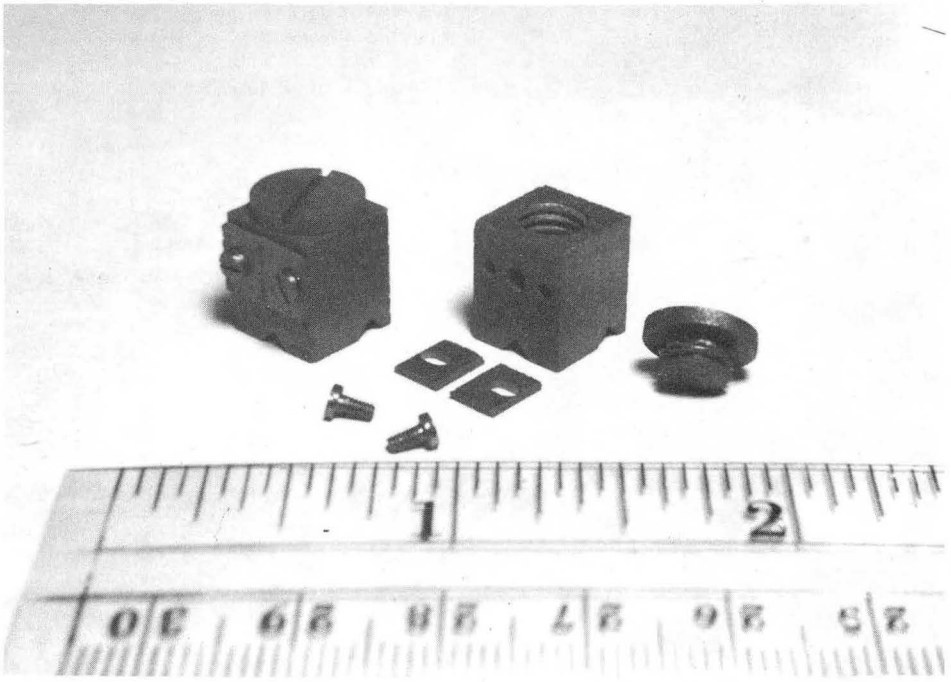

ZN-2369

Fig. 11. Carbon ovens of the type used for Ga. Tantalum screws were used to hold the slits in place.

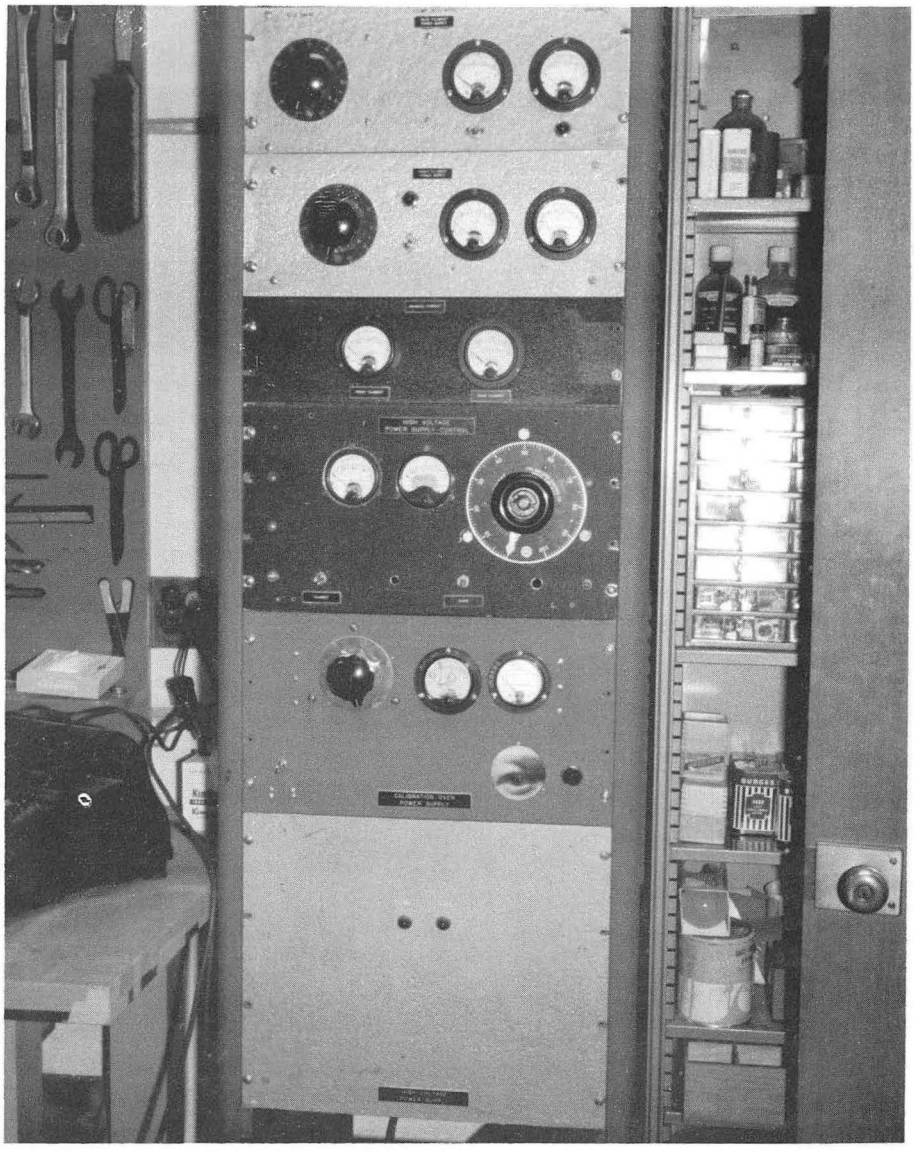

ZN-2357

Fig. 12. Power supplies used for electron-bombardment heating of the oven.

2. Radiofrequency Equipment

The measurements on Ga^{68} and Ga^{70} were all made in the frequency range from 0.5 to 35 Mc/sec. A Tektronix Type-190 signal generator was used to cover this range. The frequency was measured with a Hewlett-Packard 524 frequency counter with a 525A plug-in unit. The internal crystal of this counter was checked weekly by comparison with a National Atomichron time standard.

An Airborne Instruments Model 124c power oscillator was used to supply the rf field for the work on Ga^{67}, where frequencies between 250 and 2500 Mc/sec were desired. Because of the high-power output of this oscillator, it was necessary to monitor the power continuously with a Hewlett-Packard Model 430CR microwave power meter. The frequency was determined by beating against harmonics of a Hewlett-Packard 540A transfer oscillator. The frequency of the 540A was then measured with the 524B and a 525B plug-in unit. Figure 13 shows much of the radiofrequency equipment used in this experiment.

Since the width of a resonance line is inversely proportional to the length of the rf field through which the atom passes, it is desirable to make this length as great as possible. Unfortunately, if the length is too great the inhomogeneities of the C field will wash out any advantage gained. Thus a compromise must be reached. Since the rf hairpin in the machine was a simple loop (SHU 57), it was felt that some improvement could be made. The hairpin shown in Fig. 14 was installed and, indeed, cut down the line width by a factor of three or four. However, this design did cause some difficulty in the measurement of $\Delta m = 0$ transitions, since they are excited by an rf field parallel to the C field. As the atom traverses the hairpin it sees two components of the rf field 180 deg out of phase with each other. This tends to give line shapes of the type discussed by Ramsey, (RAM 56, p. 132) and, indeed, several were observed. While these lines permit greater accuracy in some types of work, they proved to be somewhat of a hindrance when the radioactive detection method was used.

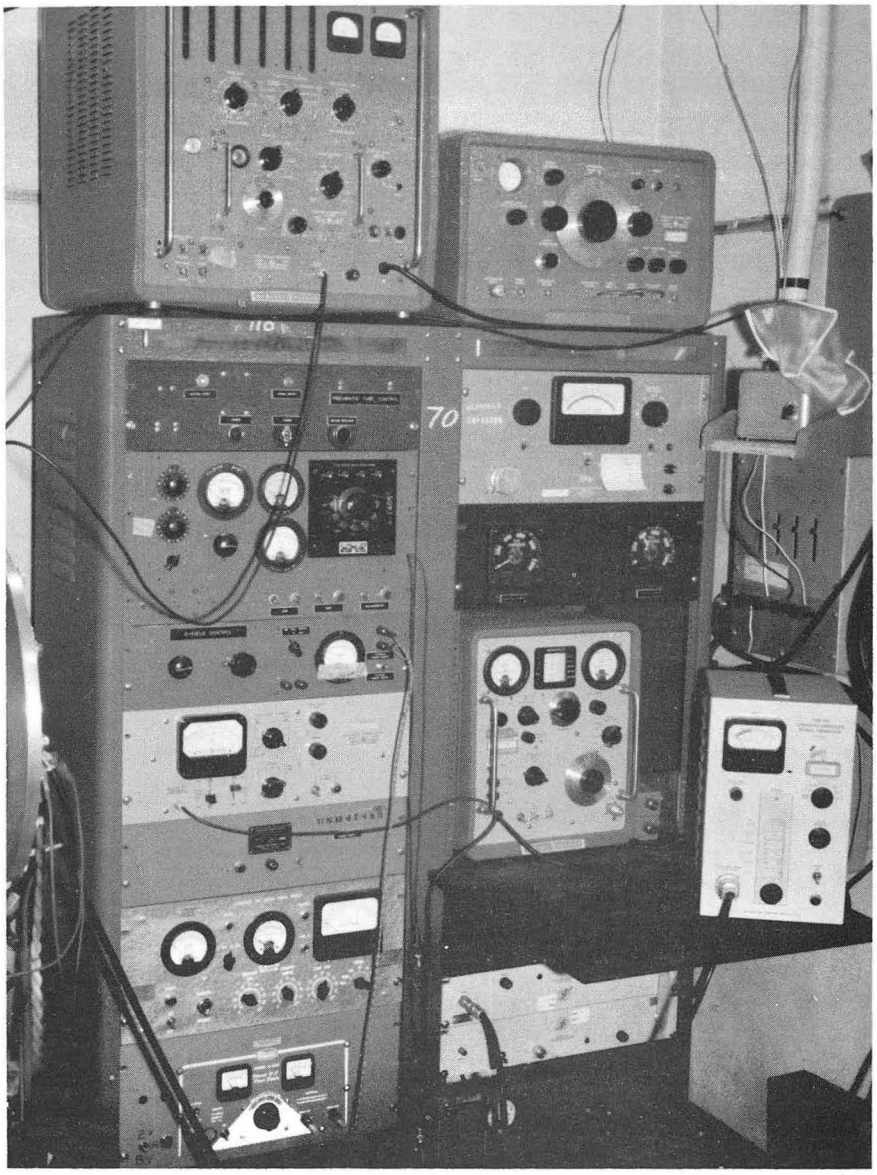

ZN-2365

Fig. 13. The radiofrequency equipment.

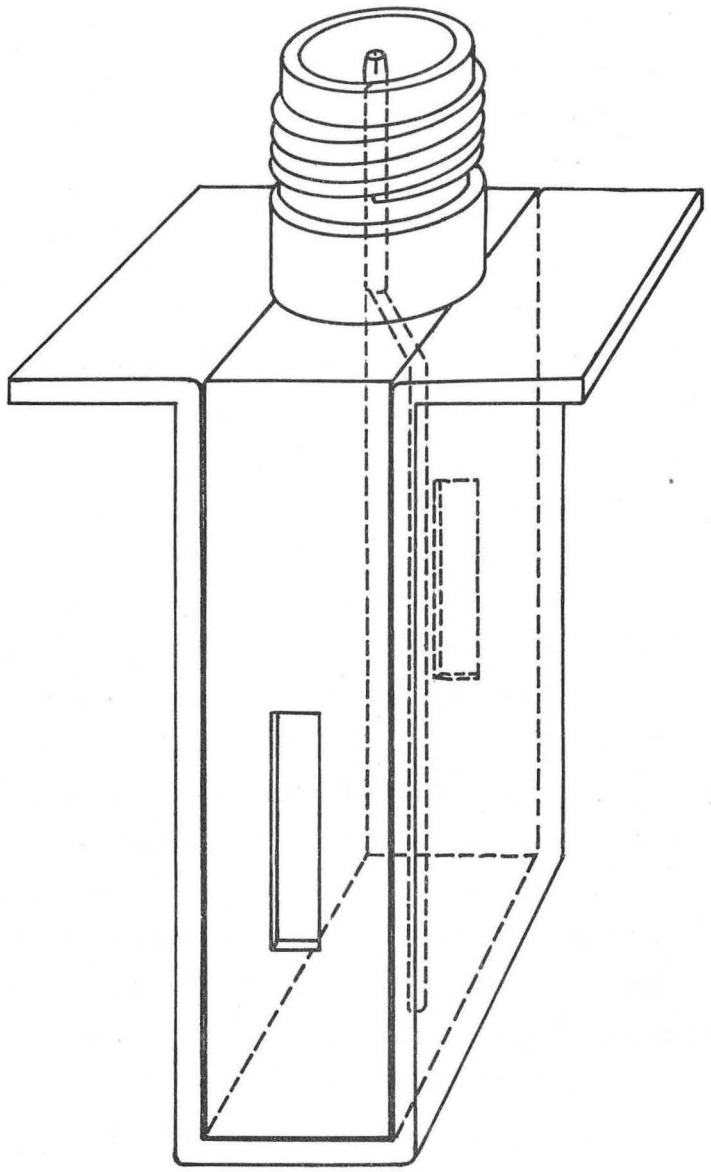

MU-19576

Fig. 14. Sketch of the radiofrequency hairpin.

3. Counting Equipment

The radioactive detection technique involves the collecting and counting of radioactive samples. In general, the counting rates of the samples are very low (often 5 counts per minute) and so it is desirable to have counting equipment possessing a very low background counting rate. Since most neutron-deficient isotopes decay by K capture, the problem can be solved for this case by using a very thin NaI(Tl) crystal in conjunction with a photomultiplier tube (SUN 56). A single-channel pulse-height analyzer can then be used to discriminate against all but the desired K x-ray counts. Because of the small size of the crystal, few higher-energy gamma rays are absorbed. In practice, background counting rates of the order of 1 count per minute (cpm) are achieved. Figure 15 shows a collector button and the assembly in which the crystal and photomultiplier are mounted.

Since the crystal counters described above have an extremely low efficiency for observing beta rays, it was felt desirable to design a β counter for use in this work. The continuous-flow Geiger counter shown in Fig. 16 seems to give the best results. (PET 60) The collector button is inserted directly into the active volume of the counter. The small tungsten wire is kept at about 3200 v with respect to ground, and the pulses arising from ionization in the chamber are amplified by a pre-amplifier and counted by a scaler. Various gases were tested, but methane seems to give the best results, yielding a background of about 2 cpm. This is quite tolerable, since the efficiency of the counters is quite high and the sample counting rates are generally at least 10 cpm. Since the counting chambers are open, some dust collects in them tending to raise the background. Thus they must be cleaned out periodically.

The counting equipment used in this experiment is shown in Fig. 17. Four counters of each type were used in order to increase the counting time for each sample and thus reduce the statistical uncertainity. The counting equipment is situated in a room some distance away from the atomic-beam machines to prevent the very radioactive samples in the machines from affecting the counter backgrounds.

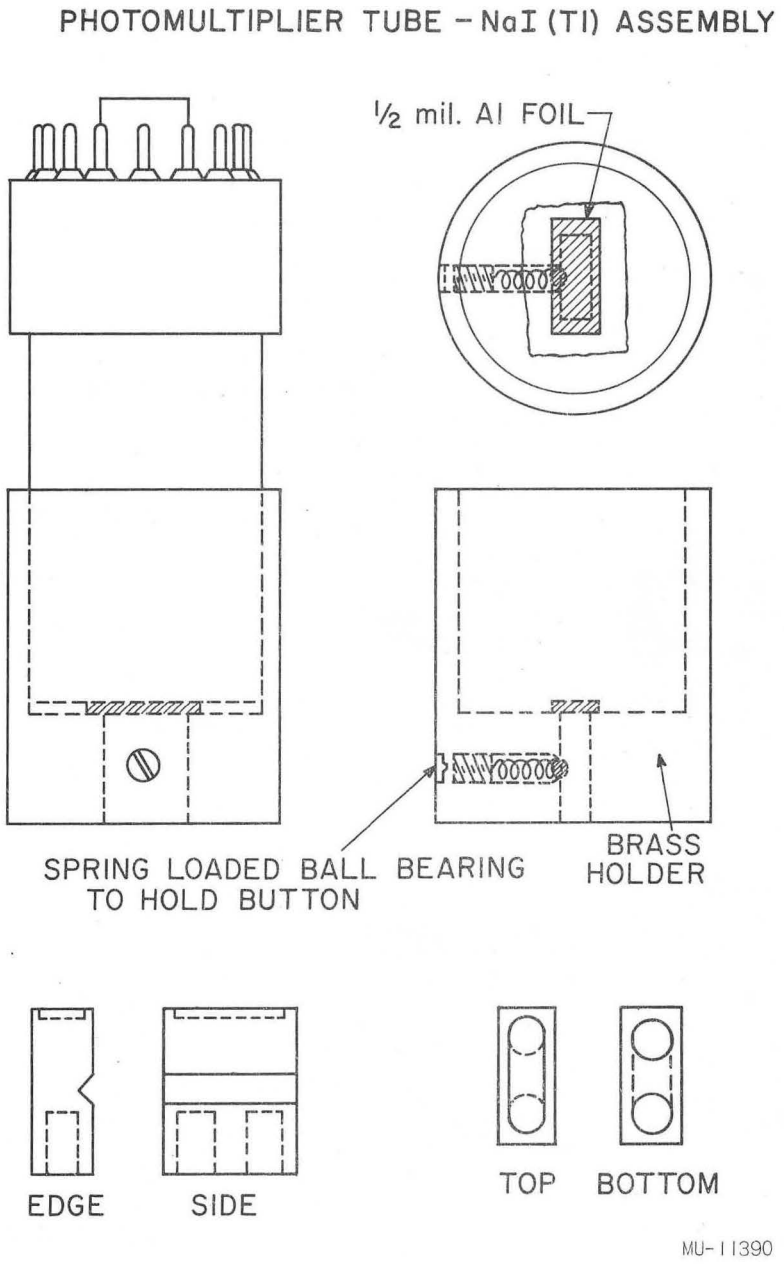

Fig. 15. (Top) NaI (Tl) crystal and photomultiplier assembly, (Bottom) Sample collector or button.

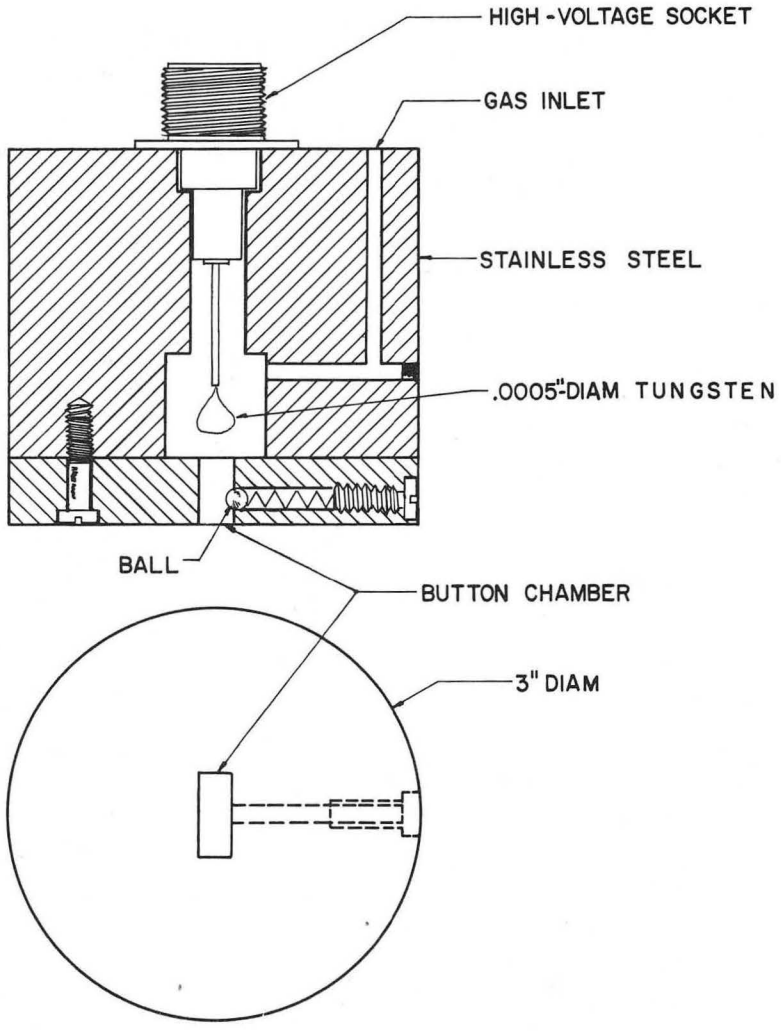

Fig. 16. Cross-sectional view of the counting head for continuous-flow Geiger counter.

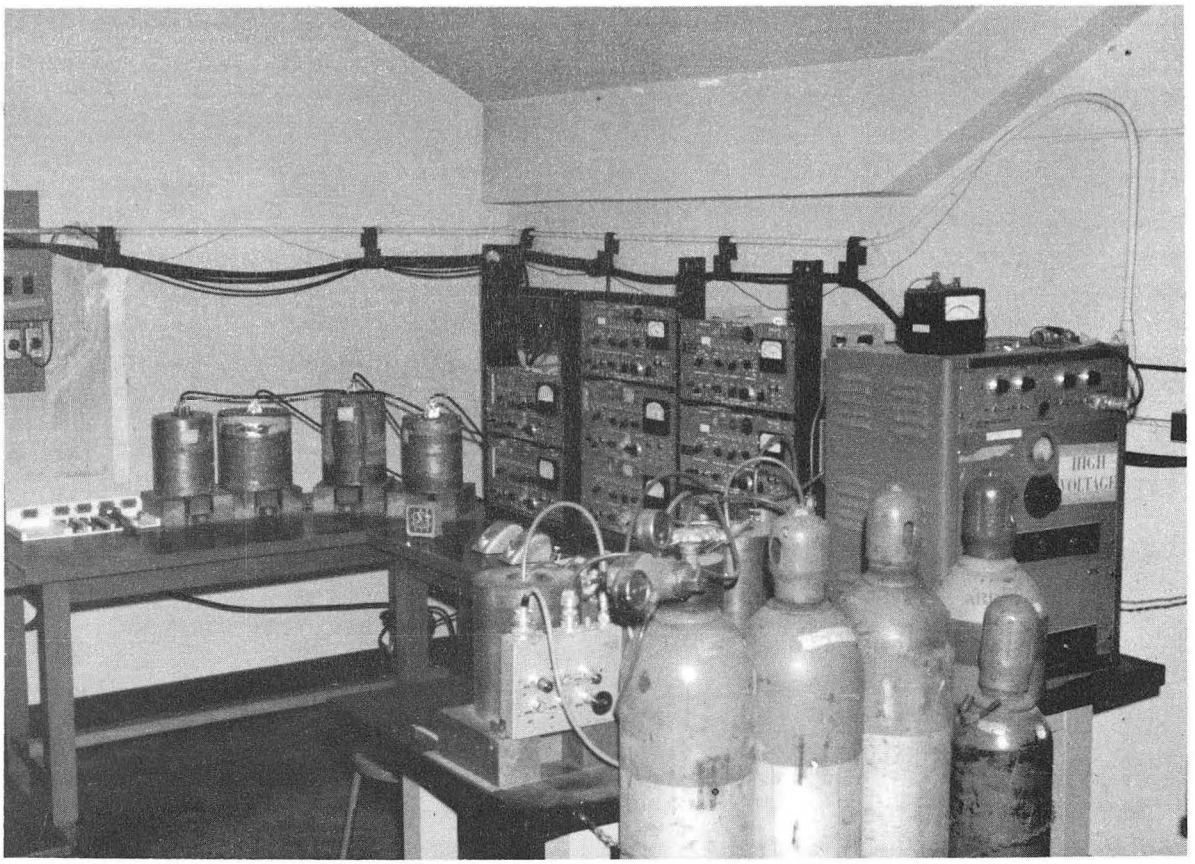

ZN-2363

Fig. 17. Counting equipment, showing β counters in foreground and K x-ray counters in background.

4. Pulse-Height Analzer

In the production of isotopes, it is often of interest to obtain an idea of the relative amounts of the various isotopes produced and to identify all the isotopes present. One method of doing this is to analyze the decay curve of the sample into its component decay curves. However, this implies that the half lives of all the isotopes present are known. Often this is not the case.

A far better method of isotope identification is to look at the gamma-ray spectrum of the sample. This can be done with a single-channel analyzer, but at best the procedure is very laborious. The acquisition of a Radiation Counter Laboratories Model-20611 256-channel pulse-height analyzer has made the task trivial and has proved invaluable in identification of isotopes. Figure 18 shows the analyzer with the associated Moseley Autograf plotter.

The procedure employed is to look at the spectrum of the sample at a convenient high voltage. The energy scale is then calibrated by using radioactives sources of known gamma-ray energy. From this, the gamma-ray energies of the sample may be obtained, and a correlation can be made with the isotopes which are expected to be present. A typical gamma-ray spectrum for Ga^{67} is shown in Fig. 19.

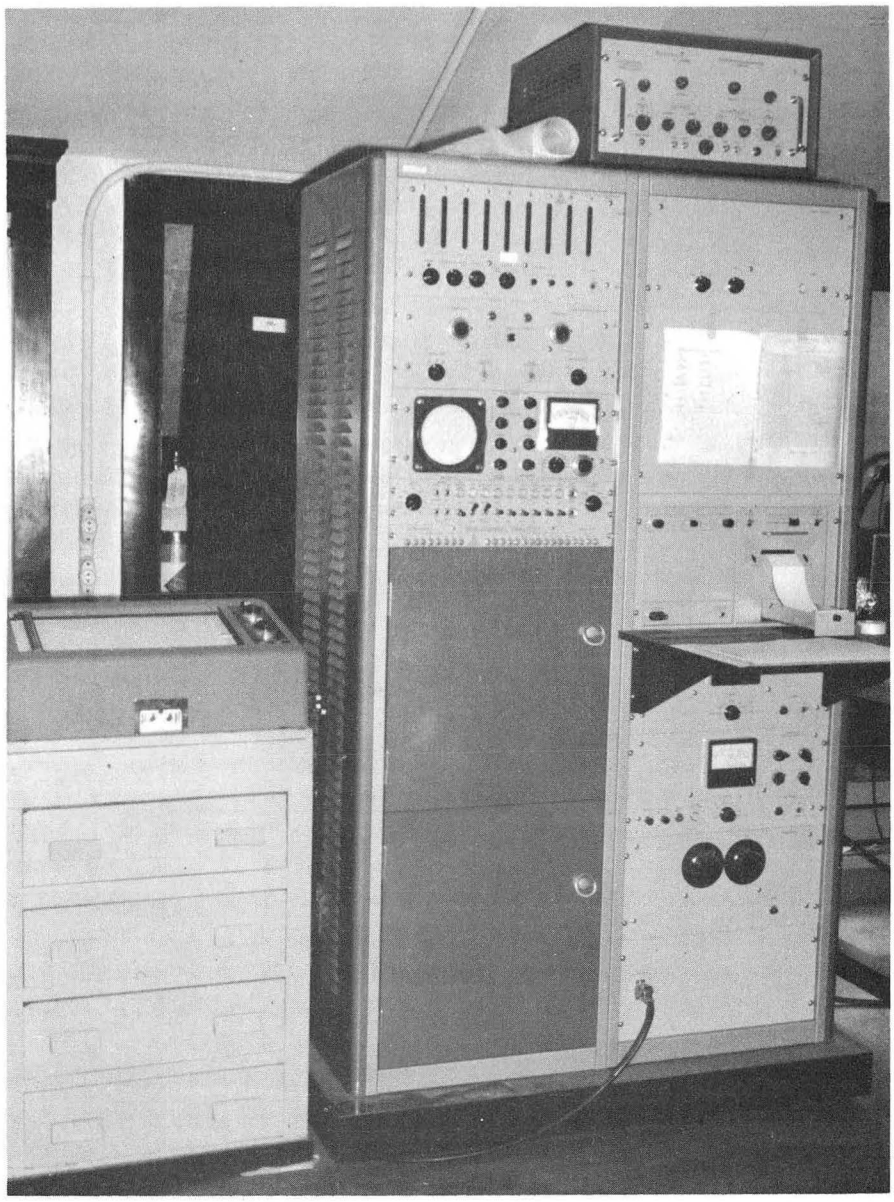

ZN-2358

Fig. 18. RCL 256-channel pulse-height analyzer and Mosely x-y plotter.

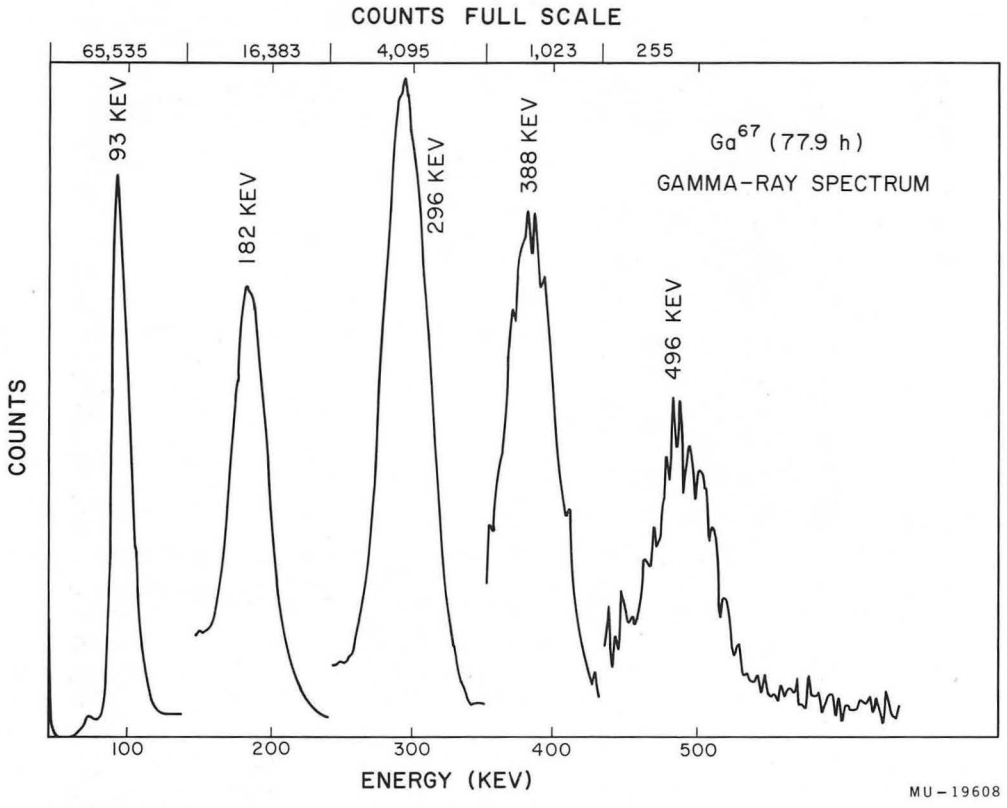

Fig. 19. Ga^{67} gamma-ray spectrum obtained with the 256-channel analyzer using a NaI(Tl) crystal. 2-in-long by 1-3/4-in-diam.

B. Experimental Techniques

1. Isotope Production and Preparation

The isotopes used in this experiment were produced by two different means. The 78-hr Ga^{67} and the 68-min Ga^{68} were produced by α-particle bombardment of copper, and the 21-min Ga^{70} was produced by neutron bombardment of gallium. This meant that the Ga^{67} and Ga^{68} had to be separated chemically from the copper, while the Ga^{70} could be used just as it came from the reactor.

The Ga^{67} was produced from Cu^{65} by an (α, 2n) reaction, while the Ga^{68} was produced from the same isotope by an (α, n) reaction. Unfortunately, a great deal of 9-hr Ga^{66} was also produced by the reactions Cu^{65} (α, 3n) Ga^{66} and Cu^{63} (α, n) Ga^{66}. The Ga^{66} presented no problem in the work on Ga^{67}, since the target was allowed to cool for about 36 hours and most of the Ga^{66} had decayed away by that time. However, in the Ga^{68} experiments, the Ga^{66} background presented quite a problem. The amount of Ga^{66} produced by the (α, 3n) reaction could be reduced by decreasing the energy of the bombarding particles, since the cross section for this reaction drops to zero at about 25 Mev. However, the amount of Ga^{66} produced by the (α, n) reaction can not be reduced, since the same reaction is used to produce Ga^{68}. This is especially a problem because the Cu^{63} is present in 69% relative aboundance while Cu^{65} is only 31% abundant. The problem could be solved by using copper enriched in the Cu^{65} isotope, but the cost would be prohibitive. The procedure adopted was to bombard the copper for about 45 min. and perform the chemical separation as rapidly as possible.

The α-particle bombardments were done using the internal probe of the Berkeley 60-in. cyclotron. The probe was extended until the target was at the 19-1/2-in. radius, giving a maximum energy of 33 Mev for the α particles. A lower energy would have been desirable but could not be attained because inserting the probe further had the effect of detuning the cyclotron. The target itself was a copper foil, 1-3/4- by 1-1/2-by 0.010 in. which was mounted on the probe

and was water-cooled on the back face. Since copper is a very good conductor, it was possible to run with fairly high beam currents. The average current was generally about 100 μa, but several targets were run at more than 120 μa without showing visible damage. The Ga^{67} targets were bombarded for about 4 hr for a total of 400 μamp-hrs, while the Ga^{68} targets usually received about 70 μamp-hr.

The usual method of separating gallium from copper is the ether-extraction method reported by Swift (SWI 24). He reports a 97% efficiency for the diethyl-ether extraction of $GaCl_3$ from a 6N HCl solution. The procedure used is as follows (WOR 57a). The copper target was dissolved in about 20 ml of 12N HNO_3 which contained about 20 mg of gallium carrier. This was evaporated to near dryness by using a hot plate and a hot nitrogen jet. The solution was then re-dissolved in 60 ml of 6N HCl which had previously been saturated with ether. This was then poured into a separatory funnel which contained 60 ml of ether saturated with 6N HCl. The solution was stirred vigorously; a shaded-pole arc-less stirring motor was used to reduce the danger of the ether fumes exploding. The HCl containing the copper chloride was then separated off while the gallium chloride remained in the ether. The ether solution was washed with 30 ml and then 20 ml of 6N HCl to remove any copper chloride that might have gone into the ether. The $GaCl_3$ was extracted from the ether with 15 ml of distilled H_2O, which was then drained off into a beaker containing some bromcresol-green indicator solution. Since some HCl got into the solution, the solution was fairly acidic at this point, causing the indicator to be yellow. A pipette was used to add 10N NaOH dropwise until the solution turned blue, indicating a pH of about 5. A Beckman Model-G pH meter was then used to measure the pH accurately. Ten percent acetic acid and 10N NaOH were added dropwise to adjust the pH to exactly 5.5. At this point, the gallium precipitates as $Ga(OH)_3$. After the solution was centrifuged and the supernatant poured off, the $Ga(OH)_3$ was redissolved in one or two drops of 10N NaOH. The Ga was then electroplated onto a short length of 0.006-in. diam platinum wire by using a current of 0.5 amps at about 8 v. For Ga^{68} the electroplating was discontinued after about 15 min due to the short

half life, but for Ga^{67} it was allowed to continue for about 45 min. Since the temperature of the solution was above the melting point of Ga, a nice globule of Ga formed on the wire and was easily scraped off into the oven. The entire separation procedure took about 45 min exclusive of the electroplating. Generally, separation efficiencies of the order of 60% were achieved for Ga^{68} and up to 85% for Ga^{67} for which the chemistry could be performed more carefully because of the longer half life.

Since the targets, particularly those used for the Ga^{68} experiments, were very radioactive (about 50 r/hr at 3 ft) the entire chemical separation was performed inside the cave shown in Fig. 20. The lead walls of the cave are 2-in.-thick while the lead-glass window is 7-in.-thick. The radiation at the surface of the cave was generally about 10 mr/hr for Ga^{68} and negligible for Ga^{67} targets. All operations were performed remotely by using the manipulators. The pipettes were controlled with a syringe mounted outside the cave. A Mag-mix stirrer was used to stir the solution while reagents were being added dropwise and an Electro Model-D-612T power supply was used for electroplating. Figure 21 shows the interior of the cave as it is viewed through the lead-glass window, while Fig. 22 shows a view through the open side door of the cave.

In the case of Ga^{70}, no chemical separation was necessary, since it was produced by neutron bombardment of stable gallium. The main problem in this case was transportation, because the gallium was bombarded in the General Electric Test Reactor at Vallecitos Atomic Laboratory near Pleasanton, California, some 40 miles from the campus in Berkeley. Since the Ga^{70} has a half life of only 21 min, if it were transported by land most of the material would have decayed by the time it arrived. The possibility of transporting the atomic-beam machine to Vallecitos Laboratory for the experiment was briefly considered, but both the cost and labor involved were prohibitive. The thought of using a helicopter arose and the Office of Naval Research was contacted. They made arrangements and permission was granted to the Commanding Officer of the Oakland Naval Air Station to provide helicopter service for us. Lieutenant-Commander

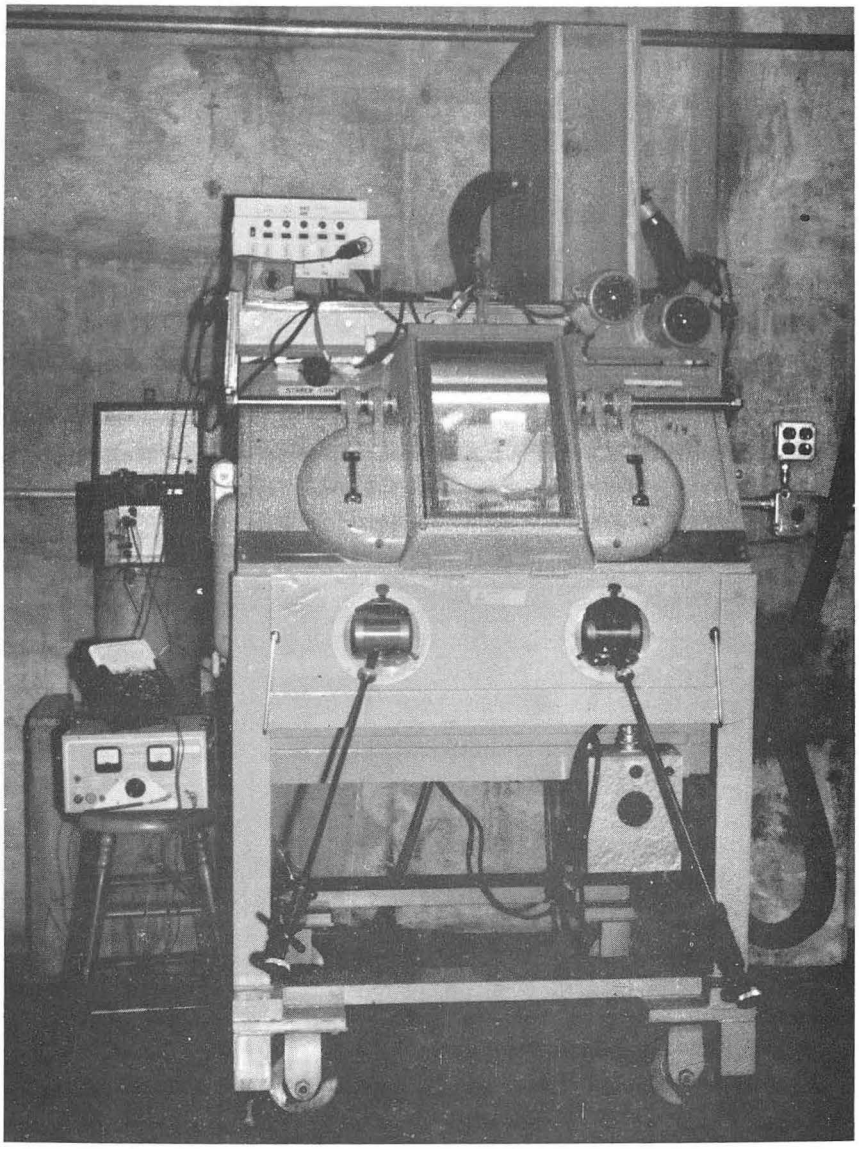

ZN-2366

Fig. 20. The cave in which the chemical separations were performed, showing the pH meter and electroplating power supply on the left.

ZN-2359

Fig. 21. The interior of the cave as seen through the lead-glass window. Note the separatory funnel and centrifuge on the right and the electroplating electrodes held in the manipulator tong on the left.

Fig. 22. The interior of the cave as seen through the open side door. Note the pipettes and pH-meter electrodes in the background, and the ether and 6N HCl-$CuCl_2$ layers in the separatory funnel.

ZN-2355

Fig. 23. The helicopter used to fly the Ga^{70} samples from Vallecitos Laboratory to Berkeley.

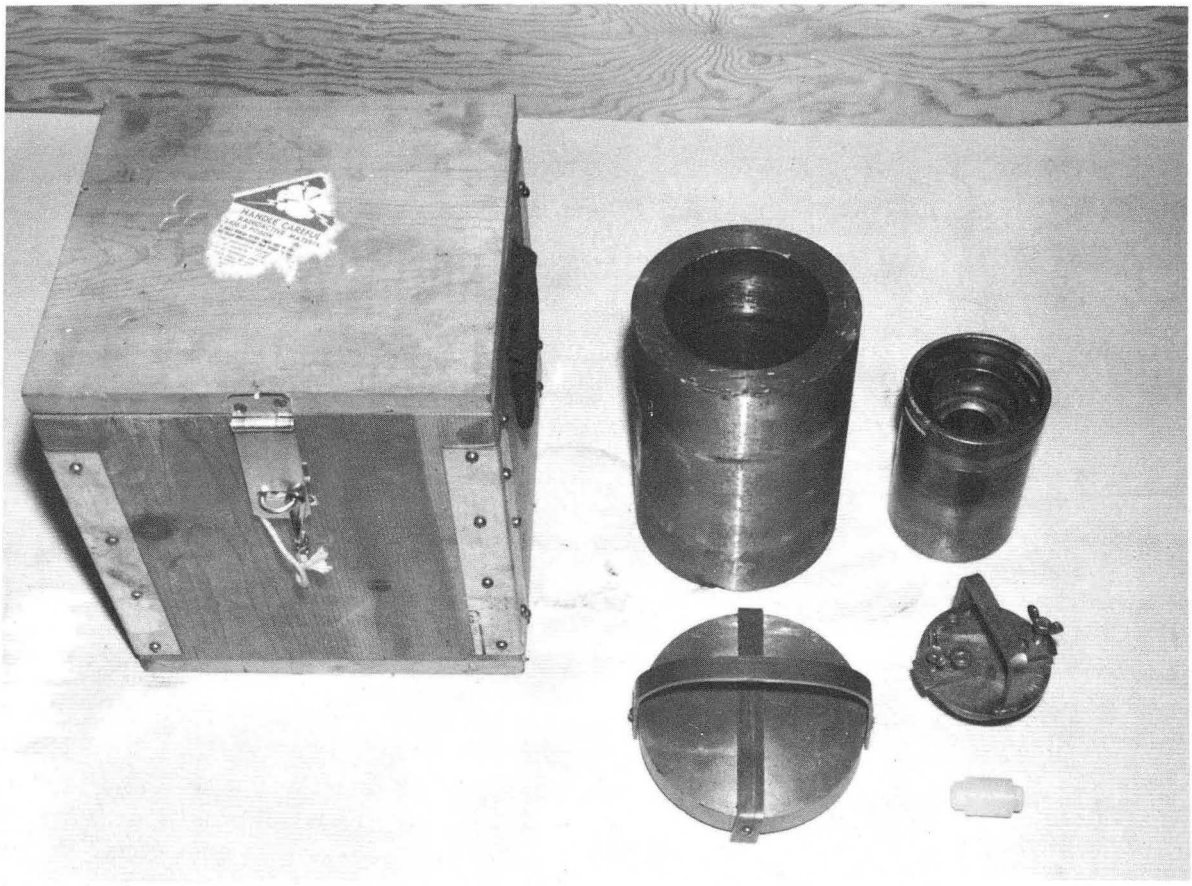

ZN-2368

Fig. 24. The nesting containers used for transporting the Ga^{70} samples. (Left) containing box; (center) 80-lb lead container; right, 35-lb uranium container and polyethylene capsule.

R. E. Roby was assigned to fly the samples from Vallecitos Laboratory to Berkeley, using the helicopter shown in Fig. 23.

All the planning for the experiment centered aroung making every operation as rapid as possible. In order to save the time it would take to transfer the bombarded material to an oven after arrival in Berkeley, the entire oven was bombarded with the material already in it. This was possible because of the extremely low neutron-capture cross section of carbon. Although the tantalum screws became slightly activated this did not interfere with the experiment. Usually about 30 mg of Ga were used. Four mg of CsF were also placed in the oven to aid in lining it up when placed in the atomic-beam machine. The oven was placed inside a 2-by 1-1/16-in. diam. polyethylene capsule which was then filled with helium and sealed. The entire capsule was then bombarded in the hydraulic shuttle tube at the reactor. This facility was chosen because the sample could be removed from the core in about 20 sec, much less than the other facilities required. The flux used was about 10^{14} neutrons/cm^2.

The nesting containers used to hold the sample during transportation are shown in Fig. 24, along with one of the small polyethylene capsules. These containers again were designed for utility and speed. The outer box and 80-lb lead container were placed in readiness in the helicopter as soon as it landed at Vallecitos Laboratory. The 35-lb uranium container was at the exit of the shuttle tube. As soon as the capsule was removed from the reactor it was placed in the uranium container which was then carried to the helicopter. Although the radiation through the walls of this container was fairly high, it was handled for such a short time that very little danger was involved for the person carrying it. When it reached the helicopter, the uranium container was placed inside the 80-lb lead container, the box was latched, and the helicopter immediately took off. The radiation at the surface of the containing box was about 5 mr/hr. Since the nearest crew member sat about 3 ft from the box, there was absolutely no danger involved for any of the crewmen.

Kleeburger Field, an intramural playfield, was chosen as the landing spot on the campus in Berkeley since it was the largest field in proximity to the atomic-beam machine in LeConte Hall. The helicopter was able to approach from only one direction since there are obstructions on three sides of the field. This seemed to present no great difficulty to the pilot and a beautiful landing was made each time. When the helicopter landed the containing box was immediately transferred to a truck (see Fig. 25) which was escorted to LeConte Hall by a police motorcycle. During the trip to LeConte, the various containers were opened. When the truck arrived at LeConte, the polyethylene capsule was dropped through a tube which led directly into the portable glove box shown in Fig. 26. The glove box was situated adjacent to the atomic-beam machine and contained equipment for opening the capsule. A 30-amp current run through a nichrome wire made it hot enough to cut easily through the polyethylene. Two completely separate nichrome-wire systems were set up in case of failure of one of the systems. After the capsule was opened, the oven was removed, placed on the oven loader, and inserted into the atomic-beam machine. The timetable for a typical run is shown below:

Time	Operation
12:55	The capsule is placed in the reactor.
13:55	The capsule is removed from reactor.
13:59	Helicopter takes off.
14:13	Helicopter lands in Berkeley.
14:15	Truck arrives at LeConte, capsule is opened.
14:18	Oven is placed on loader and pushed into pump-out chamber.
14:21	Oven is inserted into machine.
14:24	Oven is lined up by using CsF.
14:27	Oven is at operating temperature; exposure of buttons begins.
About 15:00	Exposure of buttons ends.
About 18:00	Counting of exposed buttons ends.

ZN-2354

Fig. 25. Transferring the Ga^{70} sample from the helicopter to a truck.

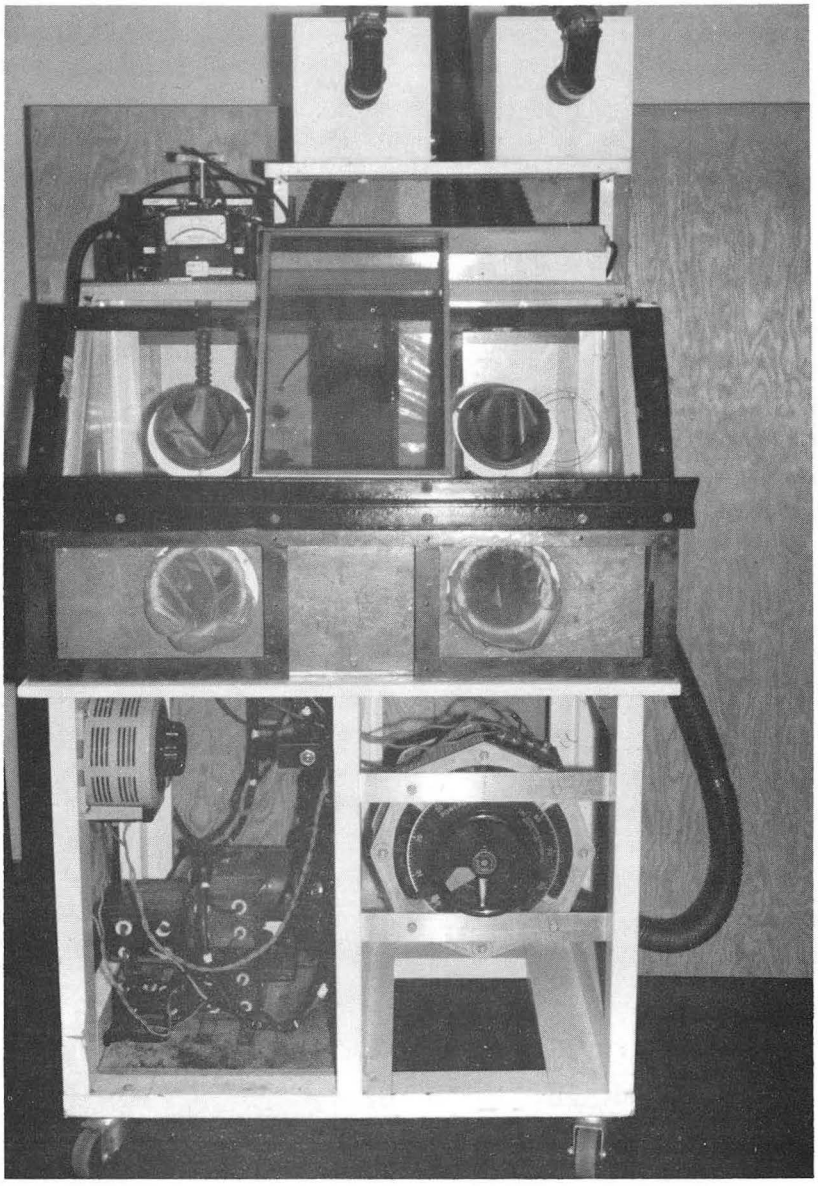

ZN-2364

Fig. 26. The portable glove box used for opening the polyethylene capsule.

2. Beam Production and Detection

A beam of gallium is easily produced if one has metallic gallium in a carbon oven at an oven temperature of about 1300°C. This temperature is easily obtained by electron bombardment of the oven. For Ga^{67} and Ga^{68}, where the specific activity was controlled by the amount of gallium carrier used in the chemical separation, a good beam was usually obtained at a high voltage of about 400 v and a bombardment current of 350 ma. This represents a power of 140 w. For Ga^{70}, where the specific activity was much lower, power inputs as high as 210 w were required to get a good beam.

A calibration beam of rubidium atoms was obtained by heating a mixture of RbCl and calcium filings to about 400° C. At this temperature the Ca reduces the RbCl and a beam of Rb atoms is obtained. The Rb beam is then used to calibrate the C field. The advantage of using an alkali metal as a calibrating material is twofold. First, the atomic and nuclear constants are well known and $J=1/2$ so the Breit-Rabi equation can be used to solve for the field if the resonant frequency in the field is measured. Second, because of the low ionization potential of these materials they can easily be detected on a hot tungsten or rhenium wire. The hot wire ionizes the atoms with almost 100% efficiency and the ions are then attracted to a collector plate. In this experiment, the ion current was measured with a Cary Model-31 vibrating-reed electrometer.

The easy detectability of the alkali metals was also used to good advantage in lining up the radioactive oven. A small amount of alkali halide was placed in the oven before it was inserted into the machine. The alkali compound would come out of the oven in molecular form at very low temperatures (about 10-w input power). Since the molecules have only very small molecular-rotational and nuclear-magnetic moments, they were not deflected by the A and B fields and thus could be detected with the hot wire when the oven was in the correct position. By observing ion current versus oven position, we could position the oven at the point where the maximum amount of beam would go through the machine. This of course was done with the stop wire removed.

The choice of an alkali halide to be used in lining up the Ga^{70} oven was complicated by the fact that the material was put in the oven before the neutron bombardment and thus would become activated. About 4 mg of CsF were used, since the activities produced from this material were least likely to interfere with the experiment.

Detection of the radioactive beam was accomplished by collecting the radioactive atoms on sulfur-coated collector buttons of the type shown in Fig. 15 and 27. The buttons were then counted in scintillation or Geiger counters to determine the radioactivity collected. The sulfur seemed to work very well as a collecting surface for gallium.

Three different types of button exposures were made during a typical run. An exposure made with the magnetic fields off and the stop wire removed was termed a full-beam exposure. A half-beam exposure was identical to this except that the magnetic fields were turned on. These were used to check the beam intensity during a run. A spin button was one exposed with the fields on, the stop wire in place, and the rf field applied.

The throw-out of the machine is defined as

$$1 - \frac{\text{half-beam counting rate}}{\text{full-beam counting rate}} . \qquad \text{(III. 1)}$$

For gallium the throw-out was typically 60%.

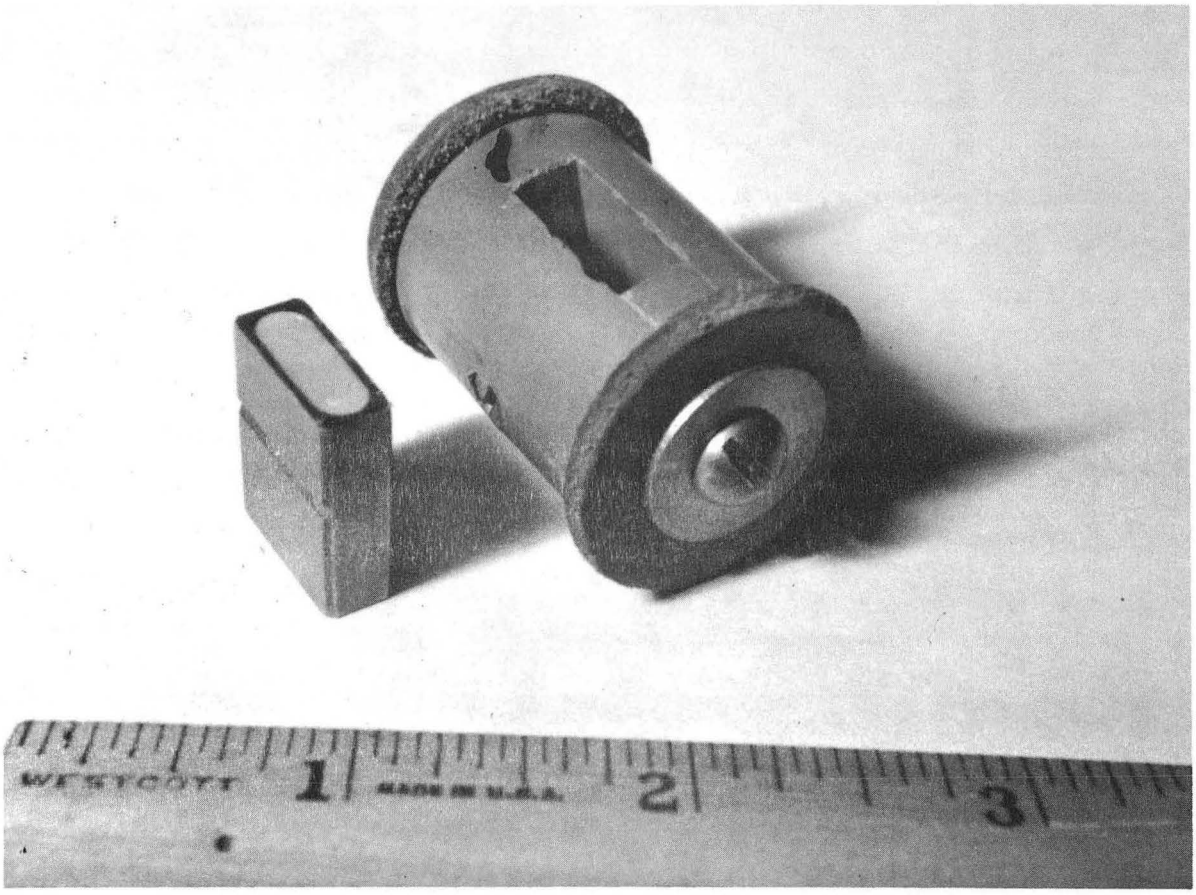

ZN-2367

Fig. 27 A collector button and a carrier used to transport the button through the pneumatic tube.

3. Isotope Identification

Since more than one isotope is usually present in the beam, some method must be used to identify the isotope of interest. Although the pulse-height analyzer is well suited for this type of work, in general the counting rates of the spin samples are too low to permit effective use of the analyzer. In this case, the best procedure is to obtain the decay curve of the sample and analyze it into its various components, since we know which isotopes will be present. This analysis is aided by a program written for the IBM-653 computer by H. B. Silsbee. (EWB 59)

In the case of Ga^{67}, we are particularly fortunate because there are some low-energy gamma rays present (Fig. 28). This means we will be able to see these gamma rays with the K x-ray counters and thus will be able to discriminate against counts caused by other isotopes. Figure 29 shows a typical counter response for Ga^{67}. By setting the high voltage on peak "A", we should be able to see Ga^{67} almost exclusively.

4. Experimental Procedure

The ultimate object of an atomic-beam experiment is to measure the relative number of atoms that reach the detector as a function of the frequency of the oscillating field. To this end, it is desirable to keep all other parameters as constant as possible. Ideally, the only variable that changes from exposure of one button to exposure of the next is the frequency. In practice, it is virtually impossible to keep all parameters constant. The beam intensity fluctuates, the magnetic field drifts, etc. The best that can be done is to minimize these effects and to correct them when possible.

The principle problem is that of fluctuating beam intensity. Fortunately, a gallium beam does not generally exhibit any rapid short-term fluctuations, but does show a long-term decrease of beam intensity. This can be compensated for by gradually increasing the temperature of the oven, but this is a rather haphazard procedure.

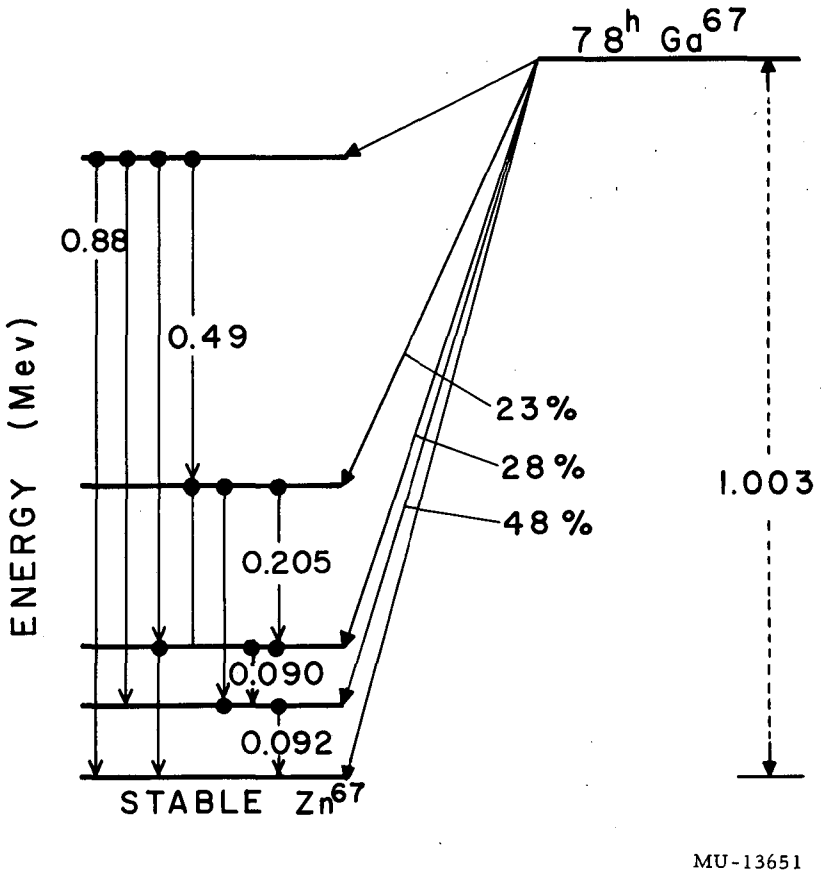

Fig. 28. The decay scheme for Ga^{67}.

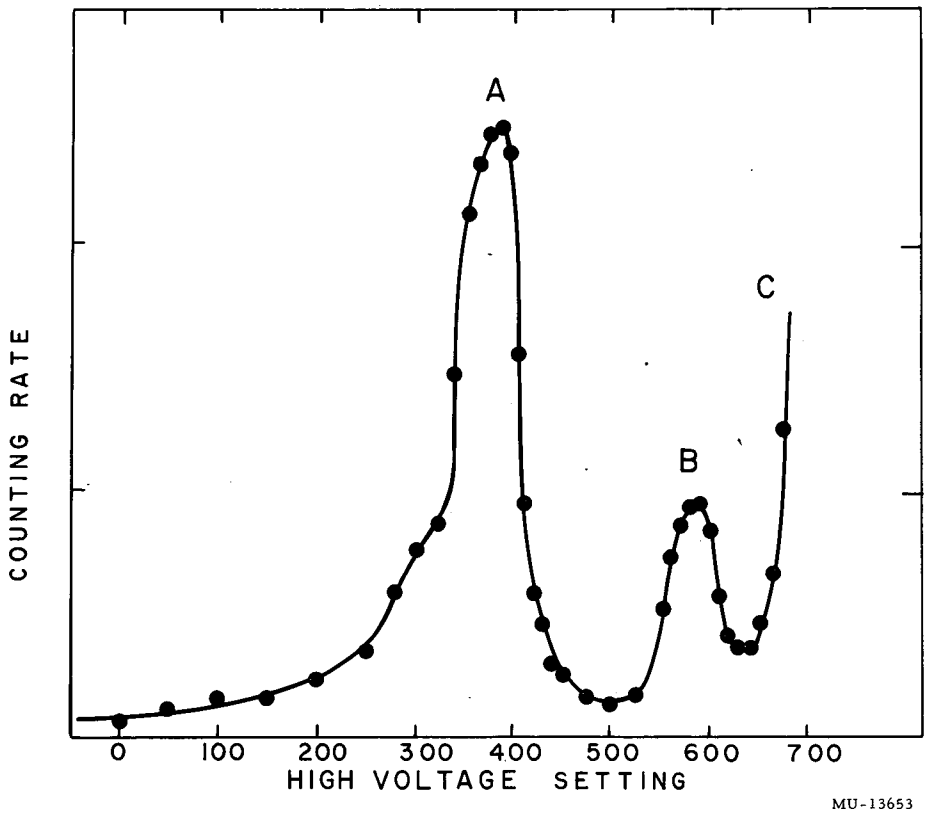

Fig. 29. Typical counter response for Ga^{67}. (A) the 92-kev gamma ray of Ga^{67}; (B) K x-ray peak; (C) region of excessive counter noise.

The method adopted is to check the beam intensity between spin-button exposures by taking a half-beam exposure. This provides a method of normalizing the counting rates of the spin buttons to the rates they would have for a constant beam. If the change in beam intensity becomes too large, the temperature of the oven can be adjusted.

The C-field power supply was quite stable at low magnetic fields, although it did exhibit some drift at higher fields. Since the majority of the experiments presented here were performed at fairly low fields, the drift was not a critical problem. The drift of the A and B fields did tend to change the value of the C field, but the current in these fields is now regulated, and therefore the drift is no longer a problem. In a typical run, the calibration frequency changed by about 15 kc/sec, which is within the accuracy of measuring the resonance peak.

The length of time for which the buttons are exposed is determined primarily by the half life of the material involved. For 78-hr Ga^{67}, the spin buttons were exposed for 10 min, while the half-beams were exposed for one min. In the case of 68-min Ga^{68}, greater speed was necessary, and the spin buttons were exposed for 4 min, with 1-min exposures for half-beams. For 21-min Ga^{70}, speed was essential and the exposures were for 2.5 min and for 30 sec.

The half-beam buttons were counted by the atomic-beam-machine operator in a counter located some 25 ft from the machine. Because of the high counting rate (from 200 to 2000 cpm) of these buttons, the higher counter background due to the proximity of the machine did not present a problem. The spin buttons were counted by a collaborator in the counters located about 500 ft and four floors away from the machine. For short-half-life materials, it was essential to get the sample from the machine to the counters as rapidly as possible. A pneumatic tube was installed to transport the buttons (PET 60), using carriers of the type shown in Fig. 27. The average transit time is about 15 sec. Several carriers have made the trip in 2 sec under higher air pressure but then arrived in N pieces,

where N was generally greater than or equal to three.

The length of time the samples are counted is determined by the half life involved. Generally an attempt is made to obtain the counting rate at intervals less than the half life with which the sample is decaying at the moment of counting. Also, it is desirable to have the sample cycled through all four counters before one half life has elapsed.

The choice of operating frequencies depends on the type of experiment to be performed. During the first stages of work on a new isotope, the nuclear spin is unknown and must be determined. This is best done by noting from Eqs. (II. 50) and II. 51) that the frequency of a $\Delta F = 0$, $\Delta m = \pm 1$ transition at low fields is given by

$$\nu = g_J \frac{F(F+1) + J(J+1) - I(I+1)}{2F(F+1)} \frac{\mu_o H}{h} . \qquad \text{(III. 2)}$$

Since the electronic configuration is usually well known, we know g_J and J. Thus for a particular F level, the resonant frequency at a field H depends only on I. By calculating the frequencies corresponding to different values of I and exposing buttons at these frequencies, one usually obtaines one button with a high counting rate, indicating the value of the spin. This procedure is termed a spin search. In practice, the procedure is somewhat simplified since a likely value of the spin is usually known from shell theory and β- and γ-ray spectroscopy. After the spin search has indicated the spin, a few resonances are taken at different magnetic fields to assure the correct field dependence of the transition and thus confirm the spin.

Once the spin has been determined, attempts are made to obtain resonances at higher magnetic fields in order to observe deviations from Eq. (III. 2), since these deviations are dependent on the hyperfine-structure separations. Because the amount of the deviation is not known, there is somewhat of a search problem involved. The usual procedure is to change the frequency by increments of about one third of the expected line width for each button exposed. Then when a high button is observed, smaller steps of frequency are taken about that point. After each run, the hyperfine-structure separations (or equivalently, the interaction constants a and b) are calculated from the results and are used to predict the frequency at a higher field. The next run then is an attempt to see the resonance at that higher field, etc. When the transitions have been observed at such high fields that the hyperfine-structure separations are known to within a few Mc/sec, an attempt is made to measure them directly by observing the $\Delta F = 1$ transitons. Once these transitions have been observed and identified, the experiment has been done to the highest accuracy attainable with the machine.

IV. RESULTS

A. Data Processing

The results obtained using the experimental procedure described in the preceding section will be the decay rates of the various samples which have been exposed at different frequencies. In the treatment of these data, we must extrapolate the decay rate of the isotope of interest to some common time for all the samples and apply whatever correction may be necessary for variations in beam intensity. If the magnetic-field drift is excessive, a correction must also be applied to the frequencies at which the samples were exposed. The end result of this procedure will be a table of sample counting rate vs frequency. Theoretically, the points obtained should lie along a bell-shaped curve, with the actual resonant frequency determined by the peak of the curve. In practice, one usually observes distortions of the curve; however, in this experiment the distortions observed were not severe. Using the resonant frequency obtained with this procedure, we can calculate the hyperfine-structure separations, or, equivalently, the interaction constants a and b.

The data analysis is aided greatly by several programs which have been written for the IBM-653 and IBM-704 computers (see Appendix B). The Omnibus program (EWB 59) uses a least-squares method to analyze the observed decay curve and obtain the contribution of each isotope present to that decay curve. It then gives the counting rate (and statistical uncertainity) at time zero for each isotope. It will also fit a bell-shaped curve to the resonance obtained and give the frequency of the peak.

Several different methods are used to calculate the hyperfine-structure seperations from the observed resonant frequency. Routine JO-7 uses third-order perturbation theory to solve the problem for arbitrary I and J. The Shugart routine performs the calculation for J = 1/2 by solving the Breit-Rabi equation. The JO-10 and Hyperfine programs solve the problem exactly for arbitrary I and J greater than 1/2 by a least-squares method employing the interaction constants a and b as the parameters to be varied.

Normalization of the sample counting rates to correct for variations in beam intensity can be accomplished in two different ways. The first method, half-beam normalization, depends on the assumptions that beam intensity is porportional to the half-beam counting rate and that no short-term fluctuations in beam intensity occur. This means that beam intensity can be measured by exposing a half-beam button between each pair of spin buttons. The normalized counting rate for a spin sample is then obtained by dividing the observed counting rate by the average of the counting rates of the half-beam buttons taken before and after the spin sample.

The second method, called ratio normalization, can be used if there are two different isotopes present in the beam, as in the case of Ga^{70} and Ga^{72}. If the background isotope does not have a resonance in the frequency range that is being swept, we can assume that the amount of that isotope deposited on the spin sample is proportional to the intensity of the beam. By dividing the counting rate of the isotope of interest by the background isotope counting rate, we obtain the normalized counting rate. The half-beam method is always applicable, the ratio method only when two isotopes are present. When both methods can be applied, they can be used to check each other and generally yield nearly identical results, which indicates the validity of the assumptions made.

The drift of the C field was generally quite small, and thus a correction can be applied quite easily. The procedure used is to assume a linear drift with time and choose the value the field had when the peak button was exposed.

B. Ga^{67}

Preliminary values of the interaction constants a and b for Ga^{67} had been obtained previously by Worcester (WOR 57a). He also determined the signs of these quantities. Using his values we began a search for $\Delta F = 1$ transitions in the $^2P_{3/2}$ state. A resonance was observed at 280.775 Mc/sec, and its field dependence proved it to be an unresolved doublet composed of the $(2, 2) \leftrightarrow (1, 1)$ and $(2, 1) \leftrightarrow (1, 0)$ transitions. From this information, a search was begun for less field-dependent transitions, and several were observed.

At this point it was observed that the (2, 0), (1, 0), and the (3, -1), (2, -1) levels are perturbed in such a manner that the frequencies of the transitions between them decrease at low fields. Since these frequencies must increase at high fields, we see that at some field their derivative with respect to field must be zero. Figure 30 shows the frequency of these transitions as a function of magnetic field. In the field-independent region we should expect to obtain very narrow line widths, yielding greater accuracy.

These transitions were observed in the field-independent region and indeed yielded narrow lines. Some difficulty was experienced in that the resonances observed had the shape expected when the rf field has two components 180 deg out of phase (see disscussion in Sec. III, A. 2). The most extreme example of this observed is shown in Fig. 31. To be certain that the resonant frequency was actually at the minimum of such a curve, the $\Delta F = 1$, $\Delta m = 0$ transition for K^{39} was observed, since it is in the same frequency range. The same curve shape was observed, and the minimum was at the correct frequency, within the limits of error. However, the agreement was not as good as could be desired, and thus slightly larger uncertainties than usual were assigned to these peaks.

The data observed on the $^2P_{3/2}$ state of Ga^{67} is summarized in Table II. The first three digits of the run number indicate the run during which the resonance was obtained, while the fourth digit indicates the order in which the resonances were observed, if more than one was observed during the run. The first field-dependent transition

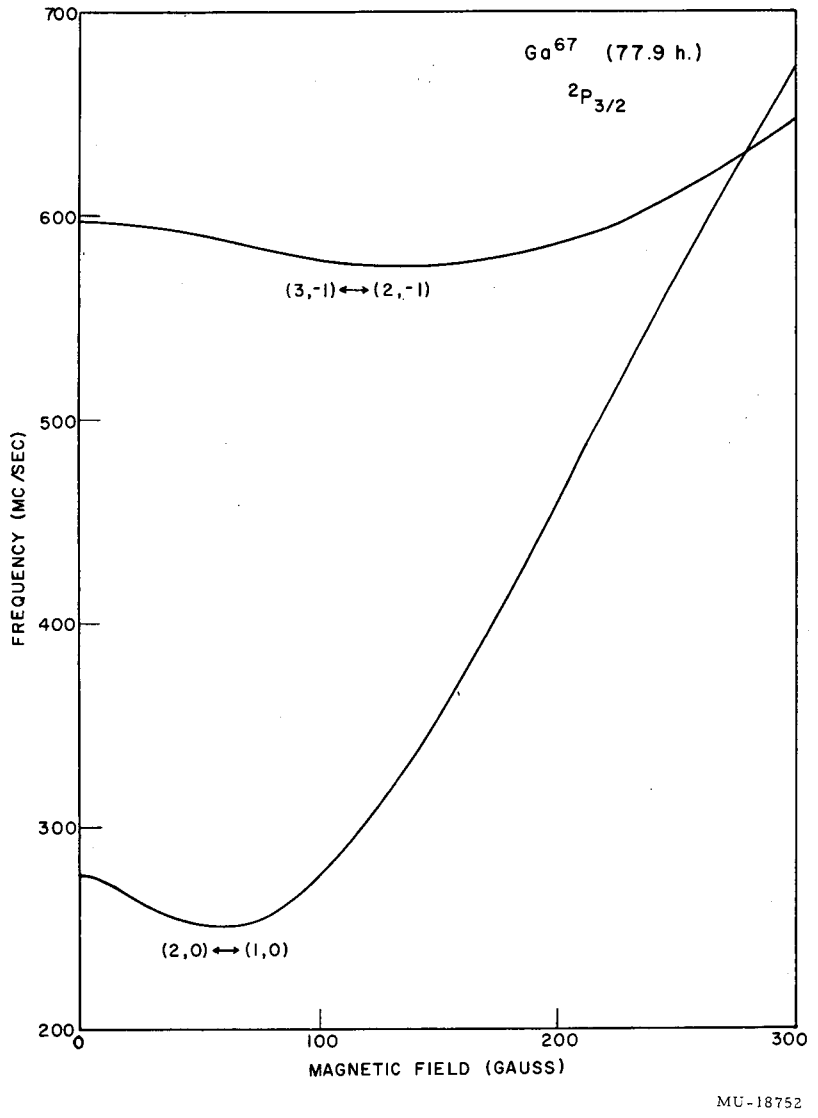

Fig. 30. The frequency of two $\Delta F = 0$ transitions as a function of magnetic field. Note the field-independent regions at the minima.

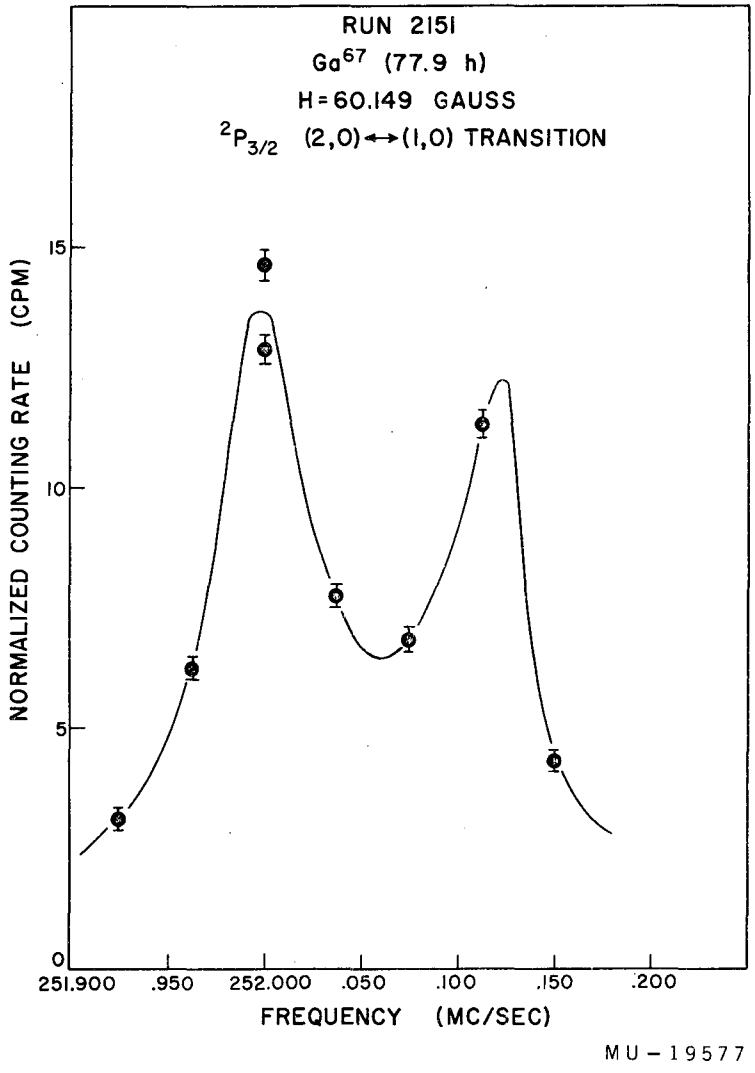

Fig. 31. The resonance shape observed when the rf field has two components 180 deg out of phase. The two points at 252.000 Mc/sec were taken 3 hr apart, indicating the extent to which normalization is valid over long periods of time.

Table II

Summary of Ga^{67} $^2P_{3/2}$ data

Run No.	Calibration frequency[a]	Ga^{67} frequency	F_1	M_1	F_2	M_2	Residual
2101	1.656(25)	277.882(75)	2	0	1	0	-0.053
2102	1.647(30)	278.439(75)	2	1	1	1	+0.038
214	1.629(25)	597.170(40)	3	-1	2	-1	-0.012
2151	29.426(25)	252.058(40)	2	0	1	0	+0.000
2201	1.813(25)	278.464(60)	2	1	1	1	+0.029
2202	1.791(30)	277.838(75)	2	0	1	0	-0.045
248	74.932(25)	575.736(35)	3	-1	2	-1	+0.010

[a]Calibration is in terms of Rb^{85} frequency.

Summary of least-squares fit:

$a = 175.092 \pm .005$ Mc/sec, $b = 71.940 \pm .014$ Mc/sec, $\chi^2 = 1.52$.

observed is not included in the analysis, since it was an unresolved doublet and thus does not contribute to the accuracy of determing a and b because of the large uncertainties involved. The data was processed with the Hyperfine program with the results shown in the table. The residual is the quantity $f-X_1 + X_2$, where f is the observed frequency and the X's are the term values calculated using the final value of a and b. The χ^2 is low for this number of points, indicating a very good fit. If we look at a standard table of χ^2, n, and probability, (FIS 46) we get $P \approx 90\%$ for this case (since n is the number of observations less the degrees of freedom, or n=5 for our case). Thus the actual values of a and b have a 90% probability of lying within the limits of error given by the routine. To be on the conservative side, we increase the limits of error somewhat and obtain for our final result for the $^2P_{3/2}$ state:

$$\begin{aligned} a &= 175.092 \pm .009 \text{ Mc/sec} \\ b &= 71.940 \pm .025 \text{ Mc/sec} \end{aligned} \qquad \text{(IV. 1)}$$

The Breit-Rabi diagram for these values of a and b is shown in Fig. 32. This diagram was calculated with Routine JO-9 and was plotted with the aid of Routine JO-9A.

Using the value of a obtained in the $^2P_{3/2}$ state, we can predict quite accurately the value to be expected for $\Delta\nu$ in the $^2P_{1/2}$ state using Eq. (II. 68) and neglecting any anomalies that may be present. We then have

$$\left(\frac{a_1}{a_2}\right)_{3/2} = \left(\frac{a_1}{a_2}\right)_{1/2} . \qquad \text{(IV. 2)}$$

Using Eq. (II. 36) and the values of $\Delta\nu$ and a for Ga^{69}, we obtain, since I = 3/2 for both isotopes,

$$\Delta\nu_{67_{\text{Predicted}}} = \left(\frac{a_{67}}{a_{69}}\right)\Delta\nu_{69} = 2457.594 \text{ Mc/sec} \qquad \text{(IV. 3)}$$

A search was made at low fields for the $\Delta F=1$, $\Delta m = 0$ transition with the result shown in Fig. 33. Several more observations were made

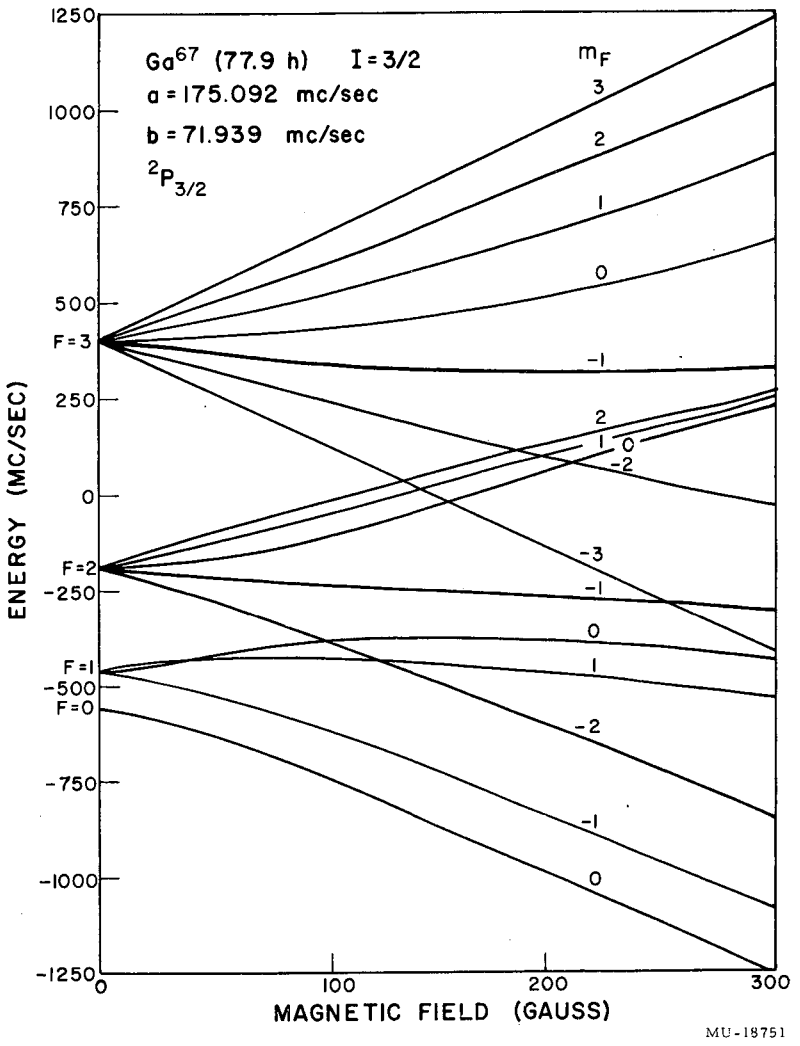

Fig. 32. The Breit-Rabi diagram for the $^2P_{3/2}$ state of Ga^{67}.

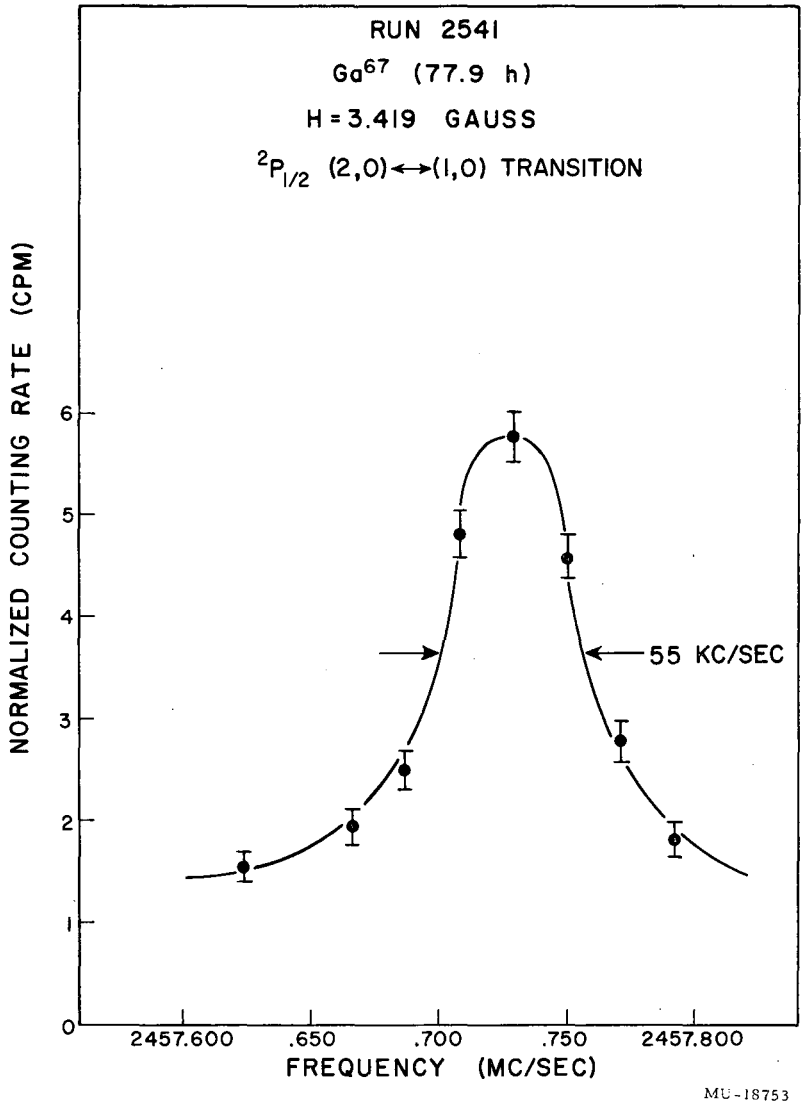

Fig. 33. A resonance observed in the $^2P_{1/2}$ state of Ga^{67}.

and are summarized in Table III. The $\Delta\nu$ values were calculated by the Shugart routine. Again assigning conservative errors, we obtain as the final result for the $^2P_{1/2}$ state of Ga^{67}:

$$\Delta\nu = 2457.733 \pm .030 \text{ Mc/sec.} \qquad \text{(IV. 4)}$$

The accuracy with which these constants have been obtained allows us to determine the differential hyperfine structure anomaly of Ga^{67} and Ga^{69}, which is defined from Eqs. (II. 68) and (II. 36) as

$$^{67}\delta^{69} = \frac{\Delta\nu_{67}}{\Delta\nu_{69}} \Big/ \frac{a_{67}}{a_{69}} - 1. \qquad \text{(IV. 5)}$$

Substituting our values for Ga^{67} and those previously obtained for Ga^{69} (DAL 54, LUR 56), we obtain

$$^{67}\delta^{69} = (6 \pm 5) \times 10^{-3}\%, \qquad \text{(IV. 6)}$$

where all the uncertainty is due to the uncertainty in our value of a.

We can now use the theoretical value of the ratio of the anomalies in the two states [Eq. (II. 74)] to obtain approximate values for the individual anomalies. We get

$$^{67}\Delta^{69}_{3/2} = -(4.5 \pm 6) \times 10^{-3}\%$$

and $\qquad \text{(IV. 7)}$

$$^{67}\Delta^{69}_{1/2} = +(1.5 \pm 6) \times 10^{-3}\%$$

where we have increased the limits of error slightly to include any uncertainty in Eq. (II. 74).

The value of $\Delta\nu$ obtained can be combined with Eq. (II. 7) and the values of $\Delta\nu$ and μ_I for Ga^{69} (WAL 53) to obtain the nuclear magnetic moment of Ga^{67}. Because we have $I = 3/2$ for both isotopes, Eq. (II. 7) becomes

$$\mu_I = \mu_{I_{69}} \frac{\Delta\nu_{67}}{\Delta\nu_{69}}. \qquad \text{(IV. 8)}$$

Table III

Summary of Ga^{67} $^2P_{1/2}$ data

Run No.	Calibration frequency[a]	Ga^{67} frequency	F_1	M_1	F_2	M_2	Calculated $\Delta\nu$
2541	1.600(25)	2457.728(15)	2	0	1	0	2457.726(15)
2542	3.660(25)	2457.740(40)	2	0	1	0	2457.729(40)
2571	2.194(25)	2457.740(25)	2	0	1	0	2457.736(25)
2572	2.946(20)	2457.752(20)	2	0	1	0	2457.745(20)

[a] Calibration is in terms of Rb^{85} frequency.

Weighted average: $\Delta\nu_0$ = 2547.733 Mc/sec

Substituting the measured values, we obtain the uncorrected nuclear moment,

$$\mu_I = 1.8454 \pm .0008 \text{ nm}, \qquad \text{(IV. 9)}$$

where the uncertainty includes the uncertainty of the Ga^{69} moment and possible anomaly effects.

Using Eq. (II. 20) and the value of 3.46 a_o^{-3} for $\left\langle \frac{1}{r^3} \right\rangle_{Av}$, Koster (KOS 52) finds that the quadrupole moment of Ga^{69} is 0.190 barns. From this, using Eq. (II. 13) and our value of b, we get

$$Q = 0.219 \pm .011 \text{ barns} \qquad \text{(IV. 10)}$$

for Ga^{67}. The uncertainty has been assigned in view of the implications of Eq. (II. 21).

C. Ga^{68}

The nuclear spin of Ga^{68} was found to be 1 by Worcester (HUB 58), who also obtained rough preliminary values for a and b. These values indicated the possibility that the energy levels might not follow the so-called normal order, in which any F level always lies below the (F + 1)st level. A more careful analysis of this data was made, and further experiments verified that the level order is inverted.

The experiments involving Ga^{68} were much more difficult than those performed on Ga^{67}. One great disadvantage is the short half life. In general, the first button was not exposed until about 100 min had elapsed since the target was removed from the cyclotron, because of the involved chemical separation. Since this is about one and one-half half-lives of Ga^{68}, the experiment was rather marginal because of the large amount of Ga^{66} produced [see Sec. (III. B 1)]. A run was usually discontinued if no resonance was observed in the first 45 min of running, since continuance would have been futile. Also, due to the statistical effects of the Ga^{66} background, many of the resonances obtained were rather poor.

Another factor contributing to the difficulty of the experiment is that Ga^{68} has an extremely small nuclear magnetic moment and thus shows large deviations from the first-order frequency expression [Eq. (III. 2)] even at very low fields. The shift at 10 gauss is already about 3.1 Mc/sec for the $\Delta m = 1$ transition in the $F = 5/2$ level. This makes the search problem more difficult unless the field is increased very little from one run to the next. In spite of the experimental difficulties, a few good resonances were obtained for the $\Delta m = \pm 1$ transition in the $F = 5/2$ level. These indicated that the value of $b/a = \xi$ is about 3. If we look at Fig. 2 we see this value corresponds to a $5/2 - 1/2 - 3/2$-level order. Figure 34 shows the Breit-Rabi diagram for Ga^{68} using some preliminary values of a and b. We note that one consequence of this level ordering is that a transition in the $F = 1/2$ level is observable with an atomic-beam

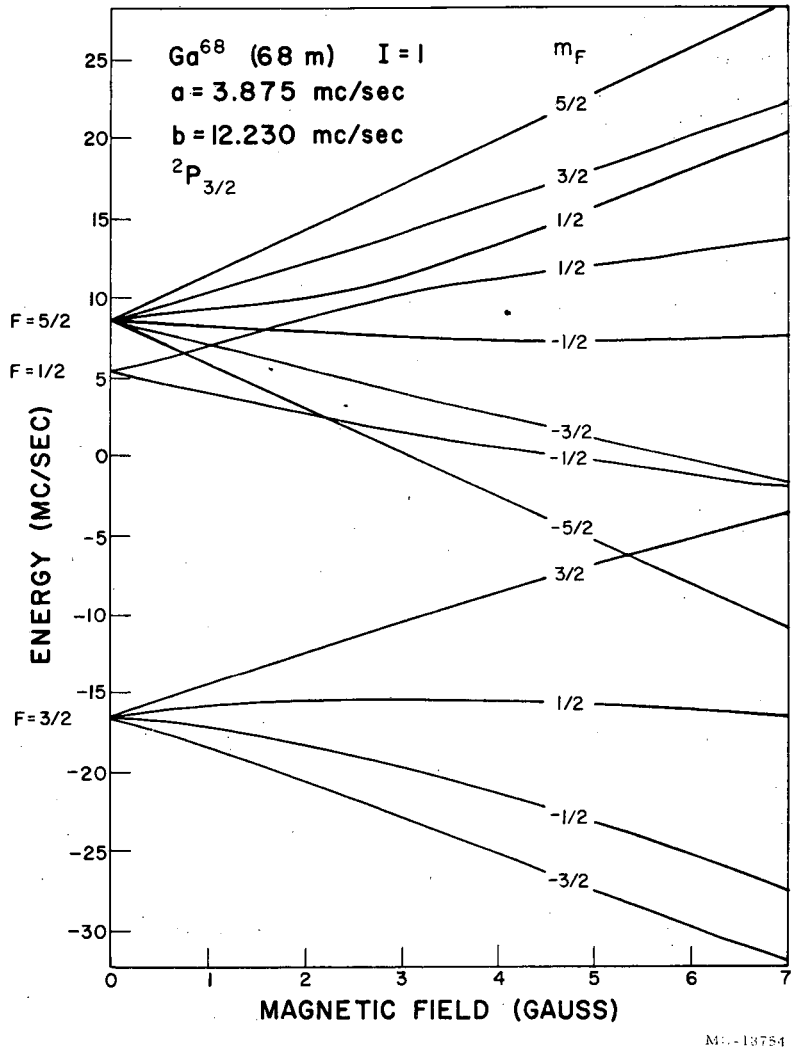

Fig. 34. The Breit-Rabi diagram for the $^2P_{3/2}$ state of Ga^{68}.

machine, while for normal ordering this transition is not observable. A search was made for this transition and a resonance was observed, establishing this level order.

The Ga^{68} data is summarized in Table IV. Worcester's data, as analyzed by the author, are also included. Several poorer resonances have been omitted from the summary. While they were valuable as indications of the field dependence of the lines, they are of little value in determining the constants a and b. We note that if Run 5 is included in the summary, it has a residual three times larger than its uncertainty, whereas if it is omitted, the χ^2 drops by a factor of six. This would indicate that some error has been made. Since the Ga^{68} frequency was obtained from a graph made by Worcester, it seems that the only likely place for error is in the calibration frequency. In view of the poor fit for Run 5, it was deemed advisable to omit it from the final analysis.

Because of the very small magnetic moment of Ga^{68}, we can not reach any conclusion about its sign from our data. Thus we must list the absolute values of a and b. Also, we find that a $\chi^2 = 0.98$ for $n = 7$ corresponds to a probability of about 99%. However, in view of the experimental difficulties encountered, we feel that this good fit is rather fortuitous, and again we shall be conservative and increase the errors by a factor of about 2.5. Thus we have

$$|a| = 3.75 \pm .20 \text{ Mc/sec},$$
$$|b| = 11.7 \pm 1.0 \text{ Mc/sec}, \qquad \text{(IV. 11)}$$

and

$$\frac{b}{a} > 0.$$

Using the method outlined in the previous section, we may obtain the uncorrected nuclear moments from these values. We get

$$|\mu_I| = 0.0263 \pm .0014 \text{ nm}$$

and (IV. 12)

$$|Q| = 0.0356 \pm .0031 \text{ barns},$$

where the limits of error are due only to the uncertainty in a and b.

Table IV

Summary of Ga^{68} $^2P_{3/2}$ data

Run	Calibration isotope	Calibration frequency	Ga^{68} frequency	F_1	M_1	F_2	M_2	Residuals With run 5	Residuals Without run 5
1[a]	K^{39}	0.500(25)	0.800(50)	5/2	-1/2	5/2	-3/2	-0.006	-0.006
2[a]	K^{39}	1.000(25)	1.630(60)	5/2	-1/2	5/2	-3/2	+0.003	+0.002
3[a]	K^{39}	2.000(25)	3.250(100)	5/2	-1/2	5/2	-3/2	-0.083	-0.089
4[a]	K^{39}	1.000(25)	2.145(50)	3/2	3/2	3/2	1/2	+0.000	-0.005
5[a]	K^{39}	3.010(25)	5.030(50)	5/2	-1/2	5/2	-3/2	-0.145	
6[a]	K^{39}	1.500(25)	3.370(50)	3/2	3/2	3/2	1/2	+0.032	+0.019
7[a]	K^{39}	2.000(25)	4.635(65)	3/2	3/2	3/2	1/2	+0.042	+0.022
252	Rb^{85}	2.980(25)	8.285(85)	5/2	-1/2	5/2	-3/2	-0.014	-0.048
282	Rb^{85}	4.708(25)	14.435(100)	5/2	-1/2	5/2	-3/2	+0.087	+0.018
294	Rb^{85}	2.294(25)	12.125(100)	1/2	1/2	1/2	-1/2	-0.012	-0.006

[a]Data obtained by Worcester.

Summary of least-squares fit, including Run 5 is $a = 3.831 \pm .083$ Mc/sec, $b = 12.076 \pm .410$ Mc/sec, and $\chi^2 = 5.83$. Not including Run 5, the summary is $a = 3.752 \pm .084$ Mc/sec, $b = 11.703 \pm .417$ Mc/sec, and $\chi^2 = 0.98$.

D. Ga^{70}

Since the nuclear spin of Ga^{70} was not known, the first run consisted of a spin search. Whereas the hyperfine-structure separations of the other odd-odd gallium isotopes are very small, causing large shifts in frequency at low fields, there was some concern that the same might hold true for Ga^{70}. Thus the search was conducted at the lowest field feasible with the machine used. Also, since the most likely spins were I = 1 and I = 3, buttons were also exposed at points 200 kc/sec above those for I = 1 and I = 3, in case the frequency should be shifted up. The normalized Ga^{70} counting rates obtained from the search are shown in Fig. 35. This indicates the spin of Ga^{70} to be 1, with the frequency shifted very little, if at all. If we plot the normalized Ga^{72} counting rate of the same samples, we obtain Fig. 36. This confirms that Ga^{72} has spin 3, as previously reported by Goodman (GOO 58). Since the points for I = 2, 3, 4, and 3 + 200 kc/sec lie so close together we see that we actually have a resonance curve for Ga^{72} in Fig. 36.

In order to confirm the spin of Ga^{70}, four resonances were taken at various magnetic fields. Table V gives a summary of all the data. All observable $\Delta F = 0$ transitions were observed at least once. The data from Run 328 are plotted in Fig. 37. The two different methods of normalization are used; note how closely they agree.

In the last column of Table V, the observed frequencies are compared with the frequency expected for an infinite hyperfine-structure separation, that is, that given by Eq. (III. 2). We see that the shift is quite small, which indicates that Ga^{70} has rather large nuclear moments.

Several resonances were also observed for Ga^{72}, confirming the spin. Transitions were seen in the F = 9/2, 7/2, and 5/2 levels, confirming that Ga^{72} has the inverted level order previously reported. (KIE 59)

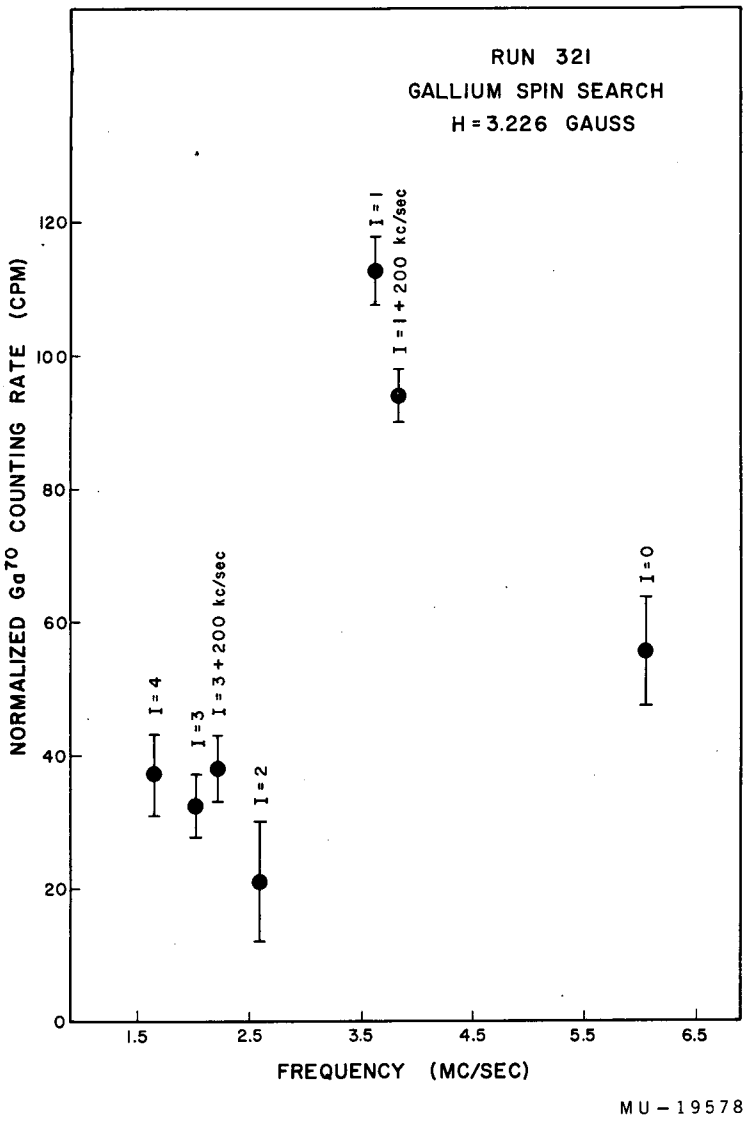

Fig. 35. Spin search for Ga^{70}. Normalized counting rate of Ga^{70} versus frequency.

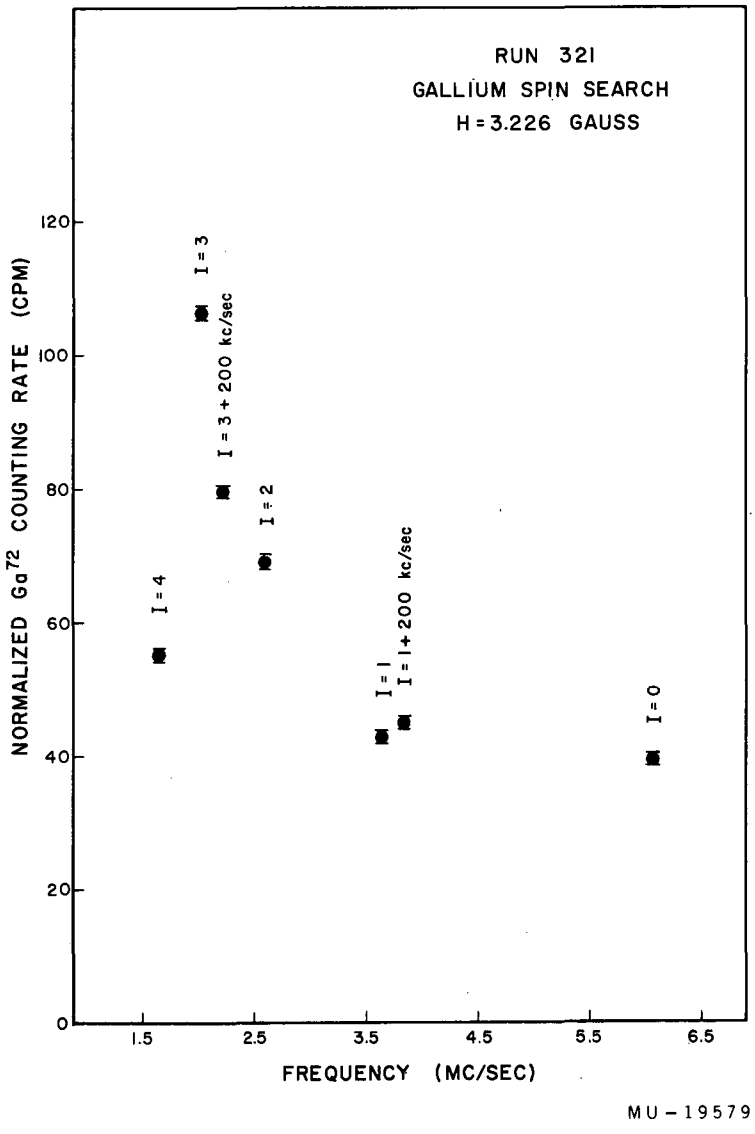

Fig. 36. Spin search for Ga^{70}. Normalized counting rate of Ga^{72} versus frequency.

Table V

Summary of Ga^{70} data

Run No.	Calibration frequency[a]	Ga^{70} frequency	State	F_1	M_1	F_2	M_2	$\nu - \nu_o$
321	1.510(20)	Spin = 1	$^2P_{3/2}$					
328	1.867(30)	4.470(90)	$^2P_{3/2}$	5/2	-1/2	5/2	-3/2	-0.011
338	1.633(25)	1.135(100)	$^2P_{1/2}$	3/2	-1/2	3/2	-3/2	+0.046
365	1.730(25)	5.250(125)	$^2P_{3/2}$	3/2	1/2	3/2	-1/2	+0.176
387	4.616(25)	11.125(90)	$^2P_{3/2}$	5/2	-1/2	5/2	-3/2	+0.045

[a] Calibration in terms of Rb^{85} frequency.

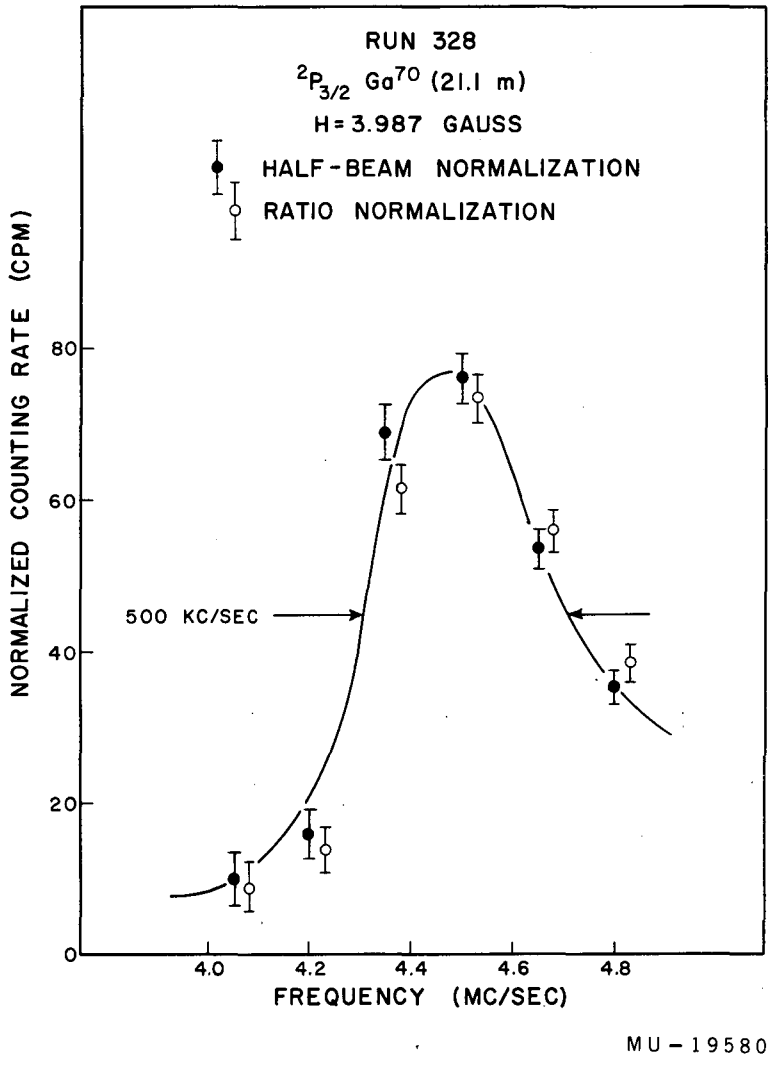

Fig. 37. Counting rate of Ga^{70} versus frequency, using both methods of normalization. The ratio-normalized points have been shifted 50 kc/sec for display purposes.

V. DISCUSSION OF RESULTS

A. Ga^{67}

The results obtained for Ga^{67} are perhaps the most interesting. Because of the relatively long half life and unique field-independence of several transitions, very accurate results were obtained, enabling the determination of the differential hyperfine-structure anomaly.

One thing of interest is to note the relationship of the Ga^{67} magnetic moment to the Schmidt and Dirac limits. We see from Table I that for an odd proton with parallel spin and orbital angular momentum--as we have for the $p_{3/2}$ proton in Ga^{67}--the Schmidt limit is 3.79 nm and the Dirac limit is 2 nm. Since the Ga^{67} moment is 1.845 nm, we see that it lies below the Dirac limit. Although there are several other nuclei with moments outside the Dirac limits, it is a rather rare occurence. No suitable explanation has yet been advanced to explain this phenomenon other than to say that the collective effects of the nuclear core overcome the single-particle effects of the odd particle.

If we plot the nuclear magnetic and quadrupole moments of the odd-A gallium isotopes as a function of A, we obtain Fig. 38. If we assume that the contribution of the odd proton to the quadrupole moment does not change from one isotope to the next, then we may assume that the change in quadrupole moment is due only to a change in deformation of the core. Thus we see that as the deformation decreases, the magnetic moment increases, approaching the Schmidt limit. This is reasonable, since the Schmidt limit is calculated with the assumption that the magnetic moment and spin of the nucleus are due entirely to the single odd particle. Thus as the collective effects of the nuclear core decrease, we expect the single-particle properties to manifest themselves more strongly.

It is difficult to draw any conclusions about the effect causing the hyperfine-structure anomalies because of their very small size. Since the spins are identical and the magnetic moments are nearly the same for the two isotopes, one would not expect a radically different

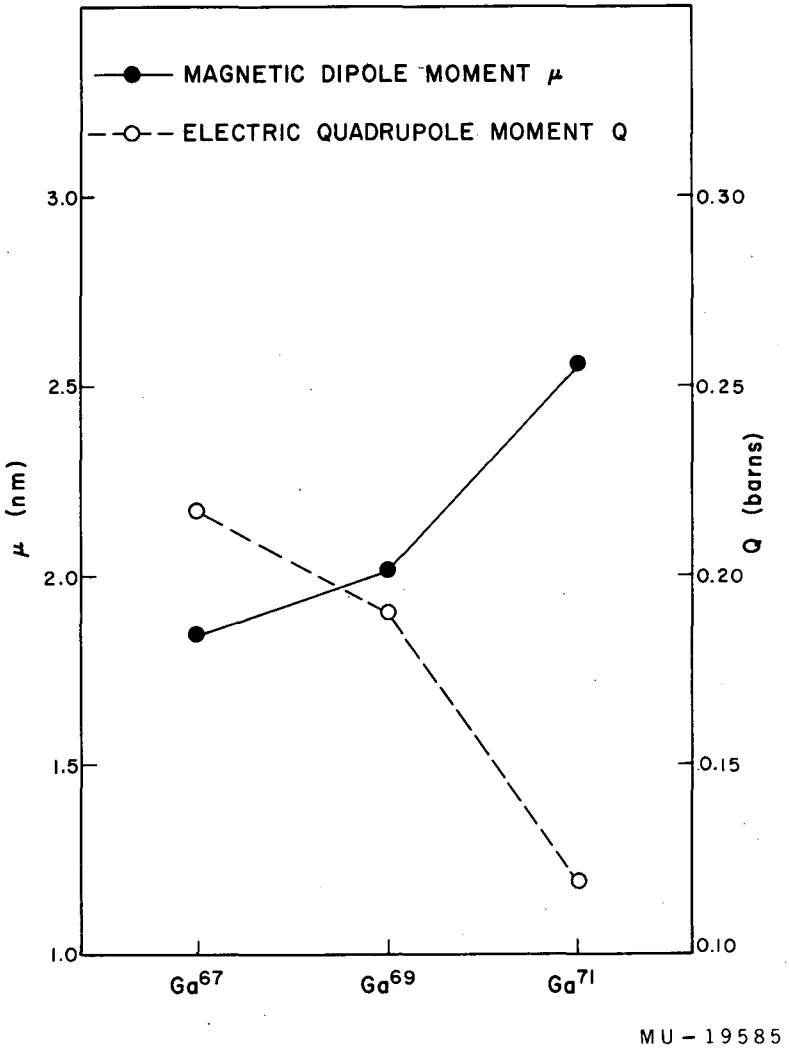

Fig. 38. The nuclear moments of the odd-A gallium isotopes.

distribution of magnetism in the two nuclei. Thus we do not expect a very large Bohr-Weisskopf effect. There is a possibility, therefore, that part of the observed anomaly is due to the Breit-Rosenthal effect.

B. Ga^{68}

The short half life and small magnetic moment of Ga^{68} greatly increased the difficulty of the experiment, leaving something to be desired in the accuracy of the results. Nevertheless, it is quite certain that the level order is inverted, with the $F = 1/2$ level lying between the $F = 5/2$ and $F = 3/2$ levels.

The accuracy with which a and b are known would indicate that a search for the $\Delta F = 1$ transitions is now feasible. A search has been made over a portion of the region lying within the limits of error of a and b, but nothing has been observed. The search problem is tremendous, since only a small region can be covered on each run because of the short half life.

C. Ga^{70}

The result obtained for the nuclear spin of Ga^{70} is exactly that predicted by shell theory [Sec. (II. C. 2)], indicating that we have strong coupling of the $^2P_{1/2}$ neutron to the $^2P_{3/2}$ proton. This result is also in agreement with the prediction of beta-ray spectroscopy (WAY 55).

However, one surprising result has been obtained; there is very little quadratic shift of the resonances that have been observed, indicating a large nuclear magnetic and/or quadrupole moment. This is surprising in view of the fact that all the other odd-odd gallium isotopes exhibit extremely small magnetic moments. It would be interesting to continue the experiment and obtain the moments accurately. However, in view of the difficulties involved in transporting the sample, and since only eight buttons can be exposed per run because of the short half-life, the extended search required to do this is not considered advisable at this time.

VI. ACKNOWLEDGMENTS

It is a pleasure to express my gratitude to all the individuals who have contributed to the success of this research. I would especially like to express my deep appreciation to Professor William A. Nierenberg, who has an uncanny ability of exciting the transition of a faltering graduate student from the ground state to a highly excited state. His boundless energy and enthusiasm have been a constant source of inspiration throughout this research. I would also like to express my profound thanks to Professor Howard A. Shugart for suggesting this research topic, for his continual encouragement, and for his never-failing presence and assistance in all phases of the work. I would like to thank Dr. W. Bruce Ewbank and Mr. F. Russell Petersen for helpful discussions and assistance in the experiment, and Mr. Irving Y. W. Chan and Miss Barbara Dodsworth for help rendered during the later phases of the work.

Special thanks are due LCDR "Mike" Roby and the United States Navy for transporting the Ga^{70} samples from Vallecitos to Berkeley. Without their very willing cooperation, the experiment would have been impossible.

I am also indebted to Mr. John Bowen and Mrs. Ruth-Mary Larimer of the Health Chemistry Division for their excellent assistance during the dangerously radioactive portions of the experiment, to Mr. Douglas McDonald for his valuable engineering advice and assistance, to the crews of the Crocker 60-inch cyclotron and the General Electric Test Reactor for their speedy handling of the short half-life bombardments, and to Messrs. Forrest Baker, Ray Sanchez, and Ralph Stein for their technical contributions to the work.

In addition, I would also like to express my appreciation to my parents for the encouragement received during my collegiate career, and my loving gratefulness to my wife Jo, for cheerfully and patiently enduring the trials and odd hours of being a physicist's wife.

VII. APPENDIX

A. Constants Used in Calculations

Certain constants have been used in the calculations performed in this thesis. It was deemed advisable to list them for the benefit of anyone who might wish to repeat the calculations. The fundamental constants used are (COH 57):

$$a_o = 5.29172(2) \times 10^{-9} \text{ cm}$$
$$\frac{M}{m} = 1836.12(2)$$
$$\alpha = 7.29729(3) \times 10^{-3}$$
$$h = 6.62517(23) \times 10^{-27} \text{erg-sec}$$
$$\mu_o = 0.92731(2) \times 10^{-20} \text{ erg/gauss}$$
$$\frac{\mu_o}{h} = 1.399677(57) \text{ Mc/gauss.}$$

Various atomic and nuclear constants used in the calculations are (BED 52, DAL 54, KOS 52, LUR 56, RAM 56, WAL 55):

K^{39} $I = 3/2$
$\Delta\nu = 461.71971(15)$ Mc/sec
$\mu_I = 0.39094(7)$ nm
$g_J = 2.00228(2)$

Rb^{85} $I = 5/2$
$\Delta\nu = 3035.735(2)$ Mc/sec
$\mu_I = 1.348190(5)$ nm
$g_J = -2.00238(4)$

Ga^{69} $I = 3/2$
$a = 190.794270(55)$ Mc/sec
$b = 62.522490(100)$ Mc/sec
$\Delta\nu = 2677.9875(10)$ Mc/sec
$\mu_I = 2.01081(52)$ nm
$Q = 0.190(10)$ barns

Ga^{71} $I = 3/2$

$a = 242.433955(55)$ Mc/sec

$b = 39.399030(100)$ Mc/sec

$\Delta\nu = 3402.6946(13)$ Mc/sec

$\mu_I = 2.55492(26)$ nm

$Q = 0.120(6)$ barns

Here, as elsewhere in this thesis, all moments listed are uncorrected for diamagnetic or other effects.

B. Computer Routines

The principles and techniques used in the various computer routines discussed in this thesis are described in greater detail here, although only the basic principles involved will be considered. For a more detailed description the interested reader is referred to the various program instruction sheets which have been prepared for internal distribution in the Atomic Beam Laboratory. Several of the routines used are discussed in other theses (EWB 59, MAR 59) and will not be considered here.

The majority of the programs described here are written for the IBM-653 computer. With the installation of the new IBM-704 in Campbell Hall, we may expect that most of the routines in the future will be programmed for this more advanced computer.

1. Routine JO-7

This program, written by the author for the IBM 653, solves the Hamiltonian given in Eq. (II.41) (neglecting the g_I term) using third-order perturbation theory. If it is given the necessary hyperfine-structure separations, it will calculate the frequency of any transition satisfying the selection rules $\Delta F = 0, \pm 1$; $\Delta m = 0, \pm 1$, and will print out tables of frequency versus magnetic field. If given the frequency of a $\Delta F = 0$, $\Delta m = \pm 1$ transition and one of the adjoining hyperfine structure separations it will calculate the other adjoining separation.

The expression for the energy of the (F, m) level is given to third order in Eq. (II.48). We see that the frequency for any $\Delta F = 0$ transition can be expressed in the form

$$\nu = AH + \left(\frac{B_+}{\Delta\nu_{F,\,F+1}} + \frac{B_-}{\Delta\nu_{F,\,F-1}} \right) H^2 + \left(\frac{C_+}{(\Delta\nu_{F,\,F+1})^2} + \frac{C_-}{(\Delta\nu_{F,\,F-1})^2} \right) H^3 , \tag{VII.1}$$

where $\Delta\nu_{F,\,F\pm1} = \dfrac{W_o^{F,m} - W_o^{F\pm1,m}}{h}$ and is independent of m.

We can also solve this equation for $\Delta\nu_{F,\,F\pm1}$, using the familiar quadratic formula

$$\Delta\nu_{F,\,F\pm1} = \frac{-2c}{b \pm \sqrt{b^2 - 4ac}}, \qquad \text{(VII. 2)}$$

where

$$a = \nu - AH - \frac{B_{\mp} H^2}{\Delta\nu_{F,\,F\mp1}} - \frac{C_{\mp} H^3}{(\Delta\nu_{F,\,F\mp1})^2},$$

$$b = -B_{\pm}H^2, \qquad \text{(VII. 3)}$$

and

$$c = -C_{\pm}H^3.$$

To evaluate the constants A, B_+, B_-, C_+, and C_-, let us adopt the shorthand notation

$$J^{F}_{F,m} = (F, m \,|\, J_z \,|\, F, m),$$

and

$$J^{F\pm1}_{F,m} = (F, m \,|\, J_z \,|\, F \pm 1, m), \qquad \text{(VII. 4)}$$

where these matrix elements are given by Eqs. (II. 42) and (II. 45). We then find that for a $\Delta F = 0$ transition where $\Delta m = m_1 - m_2$, the constants are given by

$$A = K\left[J^{F}_{F,m_2} - J^{F}_{F,m_1}\right]$$

$$B_+ = K^2\left[(J^{F+1}_{F,m_1})^2 - (J^{F\mp1}_{F,m_2})^2\right],$$

$$B_- = K^2\left[(J^{F-1}_{F,m_1})^2 - (J^{F-1}_{F,m_2})^2\right],$$

$$C_+ = K^3\left\{(J^{F+1}_{F,m_1})^2\left[J^{F}_{F,m_1} - J^{F+1}_{F+1,\,m_1}\right]\right.$$

$$\left. - (J^{F+1}_{F,m_2})^2\left[J^{F}_{F,m_2} - J^{F+1}_{F+1,m_2}\right]\right\}, \qquad \text{(VII. 5)}$$

and

$$C_- = K^3\left\{(J^{F-1}_{F,m_1})^2\left[J^{F}_{F,m_1} - J^{F-1}_{F-1,m_1}\right]\right.$$

$$\left. - (J^{F-1}_{F,m_2})^2\left[J^{F}_{F,m_2} - J^{F-1}_{F-1,m_2}\right]\right\},$$

where

$$K = \frac{g_J \mu_o}{h}$$

The extension of Eq. (VII. 1) to a $\Delta F = 1$ transition is easily accomplished by using the proper hyperfine-structure separations in the calculation and then adding the appropriate $\Delta\nu$ to the result obtained.

It should be mentioned that the usefulness of this routine is rather limited, in view of the other routines now available which solve the Hamiltonian exactly. However, it does possess one advantage; since the formula it solves is expressed in closed form, it is about a factor of ten faster than the other routines that use a numerical method of solution.

2. Routine JO-8

This program, written by F. S. Baker (BAK 60) for the IBM 653, solves the zero-field Hamiltonian [Eq. (II. 32) plus an octupole term] to obtain the relation between the hyperfine-structure separations and the interaction constants a, b, and c. The program calculates the differences of the coefficients of a, b, and c, for all combinations of F levels corresponding to a particular I and J, using the formula

$$\Delta\nu_{F_i, F_j} = \frac{W_{F_i} - W_{F_j}}{h} \qquad \text{(VII. 6)}$$

$$= \Delta K^{a}_{ij}\ a + \Delta K^{b}_{ij}\ b + \Delta K^{c}_{ij}\ c,$$

where

$$\frac{W_F}{h} = \frac{C}{2}\, a + \frac{3/4\ C(C+1) - I(I+1)\ J(J+1)}{2I(2I-1)\ J(2J-1)}\, b \qquad \text{(VII. 7)}$$

$$+ \frac{5\left\{C^3+4C^2+4/5C[-3I(I+1)J(J+1)+I(I+1)+J(J+1)+3] - 4I(I+1)J(J+1)\right\}}{4I(I-1)(2I-1)J(J-1)(2J-1)}\, c,$$

with $\frac{C}{2} = (F, m\,|\vec{I}\cdot\vec{J}|F, m) = \frac{F(F+1) - I(I+1) - J(J+1)}{2}$

and $$|I + J| \geq F \geq |I - J|.$$

The values of ΔK_{ij} have been tabulated for all values of I and J from 1 to 8. The program can also be used to calculate these coefficients for I or J greater than 8, but it was not deemed necessary to tabulate them.

3. Routine JO-9

This program, written for the 653 by the author, is a modification of W. A. Nierenberg's Routine 009 (MAR 59). It computes the eigenvalues of the Hamiltonian given in Eq. (II. 52) as a function of magnetic field, and prints out tables of frequency versus magnetic field for given values of a, b, and ΔH, the desired increment in the magnetic field. It will do this for any arbitrary transition, and the operator can choose either a dimensional or dimensionless output.

The method of solution employs the recursion formulae given in Eqs. (II. 57) and (II. 58) to solve the determinantal equation

$$D_p(X, H) = 0. \qquad \text{(VII. 8)}$$

The calculation must start at H=0, where the root is easily obtained and identified. This root is then used as the trial root after the field is incremented by the amount ΔH, and the equation is solved by using Newton's method:

$$\Delta X = - \frac{D_p}{\frac{\partial D_p}{\partial X}} . \qquad \text{(VII. 9)}$$

The next trial root is then taken as $X' = X - \Delta X$, and Eq. (VII. 9) is again evaluated using X'. The iteration is halted when ΔX is smaller than some arbitrary number, usually chosen as 10^{-4} Mc/sec. The result for that field is then printed out, the field is incremented by ΔH, and the procedure is repeated.

Because of the no-m-cross rule, we will not have different levels possessing the same m value crossing each other, and thus it is safe to follow the root up in magnetic field by using the method we have described. (We need not worry about roots of different m,

since the particular submatrix we solve depends on the m value chosen.) However, if two levels of the same m approach each other closely, some caution must be used, since it is possible for the routine to jump levels if the increment in field is chosen too large.

The routine also calculates the derivative of the frequency with respect to magnetic field, using Eqs. (II. 58) and (II. 59) and the relations

$$\frac{\partial X}{\partial H} = - \frac{\dfrac{\partial D_p}{\partial H}}{\dfrac{\partial D_p}{\partial X}} \qquad \text{(VII. 10)}$$

and

$$\frac{\partial \nu}{\partial H} = \frac{\partial X_1}{\partial H} - \frac{\partial X_2}{\partial H} . \qquad \text{(VII. 11)}$$

4. Routine JO-10

This program, written for the 653 by the author, fits the observed resonances by a least-squares method, using a and b as the parameters to be varied. The program must be given starting values for a, b, and the term values for each transitions. The starting term values can be obtained with Routine JO-9.

The problem is to find the minimum of the function

$$N = \sum_i (f_i - X_{1i} + X_{2i})^2 \omega_i , \qquad \text{(VII. 12)}$$

where f is the observed resonance frequency and X_1 and X_2 are the term values for that transition. The weighting factor ω is given by

$$\omega = \frac{1}{(\delta f)^2 + \left(\dfrac{\partial f}{\partial H}\right)^2 (\partial H)^2} , \qquad \text{(VII. 13)}$$

where δf and δH are the uncertainties in the observed frequency and magnetic field, while $\partial f/\partial H$ is calculated by the program.

The method of finding the minimum of Eq. (VII. 12) is based on the procedure developed by W. A. Nierenberg (NIE 59). The following equations in δa and δb are set up:

$$\frac{\partial^2 N}{\partial a^2}\,\delta a + \frac{\partial^2 N}{\partial a \partial b}\,\delta b = \frac{\partial N}{\partial a} \qquad \text{(VII. 14a)}$$

$$\frac{\partial^2 N}{\partial b \partial a}\,\delta a + \frac{\partial^2 N}{\partial b^2}\,\delta b = \frac{\partial N}{\partial b}\,. \qquad \text{(VII. 14b)}$$

Using the starting value of a and b, we solve these equations for δa and δb. The new trial values of a and b are obtained from

$$a' = a - \delta a$$
$$b' = b - \delta b. \qquad \text{(VII. 15)}$$

This procedure is continued until N reaches its minimum and begins oscillating due to rounding-off errors. This value of N at the minimum is of course χ^2. The variances in a and b are given by

$$(\Delta a)^2 = \frac{\dfrac{\partial^2 N}{\partial b^2}}{\Delta}$$

and (VII. 16)

$$(\Delta b)^2 = \frac{\dfrac{\partial^2 N}{\partial a^2}}{\Delta},$$

where Δ is the determinant of the system of equations (VII. 14).

All the derivatives required for solution of Eqs. (VII. 14) may be obtained by differentiating Eq. (II. 57). These derivatives are listed by Marino (MAR 59). To calculate X_1 and X_2 we use the same procedure that was employed in Routine JO-9. The magnetic field and its uncertainty are calculated from the calibration frequency and its uncertainty by using the Breit-Rabi equation.

Since g_I is in general unknown, it is calculated after each iteration, using the new value of a and Eq. (II. 7). This of course presupposes that a and g_I are known for some other isotope of that element, which is usually the case. If we wish to test the sign of g_I, we can run

the problem using both signs, and the χ^2 will give an estimate of the probability that one assumption is favored over the other.

4. Routine Hyperfine

This program, written by D. H. Zurlinden for the IBM 704, is an improvement and extension of Routine JO-10. The improvement is that the program calculates the required starting values of X_1 and X_2 from the given starting values of a and b. If desired, it will also calculate X_1 and X_2 anew after each iteration, starting from zero field and using the new value of a and b obtained from the previous iteration. This prevents the program from jumping levels and greatly helps the convergence if very poor initial values of a and b are chosen.

The program has also been extended to include g_J as one of the parameters to be fit by the data. This is very useful for work on the transuranic elements or some of the rare earths where the g_J is not known. The program is presently being rewritten to include g_I as a parameter, and also to solve the problem for I or J = 1/2.

The method of solution for more than two parameters is essentially the same as that outlined in the previous section, but now the system of equations is given by

$$\sum_i \frac{\partial^2 N}{\partial x_i \partial x_j} \delta x_i = \frac{\partial N}{\partial x_j} . \qquad \text{(VII. 17)}$$

Using given starting values for the x_i, we solve these equations for the δx_i and then try the new values

$$x_i'' = x_i - \delta x_i \qquad \text{(VII. 18)}$$

This is repeated until N reaches a minimum.

6. Consistency of Programs

Since the programs described above are very complex, it is extremely likely that errors in programming will appear. Most errors can be found quite easily, but it is possible that a small but significant error might be overlooked. Since it is virtually impossible to do the calculations by hand, there is no way to check any one program. However, if there are two routines written independently by two different programmers which solve essentially the same problem, they can be used to check each other.

Since there was some question as to whether or not the g_I term was being calculated correctly in Hyperfine, JO-9 was used to calculate fictitious frequencies at arbitrary fields using a certain value of a and b. This information was then used as input data for the Hyperfine routine. If both routines were programmed correctly, Hyperfine should converge to the values of a and b (and g_J, if varied) that were used in JO-9 to calculate the frequencies, and we should get $\chi^2 = 0$. The actual χ^2 obtained was about 10^{-3}, which is undoubtedly due to rounding-off errors. To be certain that the g_I correction was being applied correctly, the g_I for the comparison isotope was varied in such a manner as to give the unknown g_I the values 0, $1/2g_{I_o}$, g_{I_o}, $3/2g_{I_o}$, and $2g_{I_o}$ where g_{I_o} is the correct value. The result is shown in Fig. 39, where we have plotted χ^2 versus g_I for the two different modes of operation of the program, that is, first with only a and b varying, and then with g_J varying also. We see that we obtain a parabola with its minimum at g_{I_o}, which is exactly what we should expect to observe if the programs have no errors.

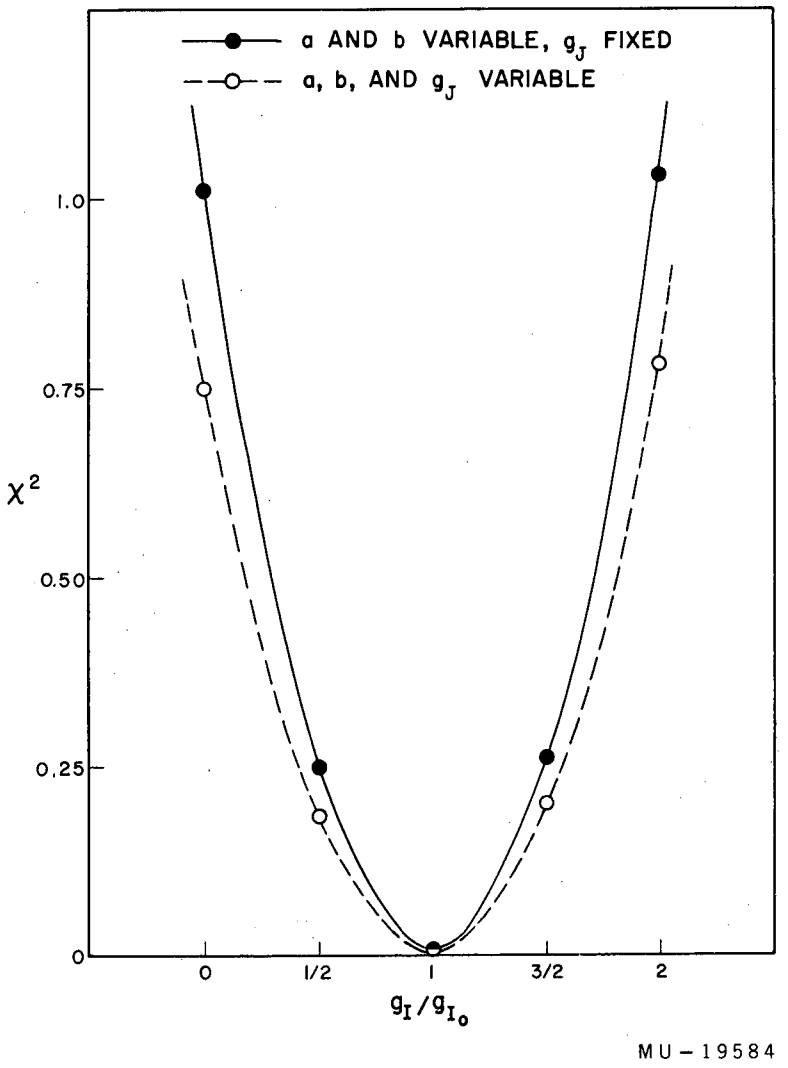

Fig. 39. The value of χ^2 obtained with Hyperfine as g_I is varied about its true value g_{I_o}, using fictitious input data calculated by JO-9.

REFERENCES

BAK 60. Forrest S. Baker, University of California, private communication, 1960.

BEC 48. G. E. Becker and P. Kusch, Phys. Rev. 73, 584 (1948).

BED 52. B. Bederson and V. Jaccarino, Phys. Rev. 87, 228 (1952).

BIT 49. F. Bitter, Phys. Rev. 76, 150 (1949).

BLI 57. R. J. Blin-Stoyle, Theories of Nuclear Moments (Oxford University Press, London, 1957), 88 pp.

BOH 50. A. Bohr and V. F. Weisskopf, Phys. Rev. 77, 94 (1950).

BOH 53. A. Bohr and B. R. Mottleson, Kgl. Danske Videnskab Selskab, Mat.-fys. Medd. 27, 16 (1953).

BOI 76. L. de Boisbaudran, Compt. rend. 82, 168 (1876) and ibid. 81, 493 (1875).

BOI 78. L. de Boisbaudran and E. Jungfleisch, Phil. Mag. 5, Ser. 5, 319 (1878).

BRE 31. G. Breit and I. I. Rabi, Phys. Rev. 38, 2082 (1931).

CAM 31. J. S. Campbell and R. F. Bacher, Phys. Rev. 38, 1906 (1931).

CAM 32. J. S. Campbell, Phys. Rev. 40, 1040 (1932).

CAM 33. J. S. Campbell, Nature 131, 204 (1933).

CAS 36. H. B. G. Casimir, On the Interaction between Atomic Nuclei and Electrons (Teyler's Tweede Genootschap, Haarlem, 1936).

CLE 54. W. W. Clendenin, Phys. Rev. 94, 1590 (1954).

COH 57. E. R. Cohen, K. M. Crowe, and J. W. M. DuMond, The Fundamental Constants of Physics, (Interscience Publishers, New York, 1957).

CON 57. E. U. Condon and G. H. Shortley, Theory of Atomic Spectra (Cambridge University Press, Cambridge, England, 1957).

CRA 49. M. F. Crawford and A. L. Schawlow, Phys. Rev. 76, 1310 (1949).

DAL 54. R. T. Daly, Jr. and J. H. Holloway, Phys. Rev. 96, 539 (1954).

EDM 57. A. R. Edmonds, Angular Momentum in Quantum Mechanics (Princeton University Press, Princeton, 1957).

EIS 58. J. Eisinger and V. Jaccarino, Revs. Modern Phys. 30, 528 (1958).

EWB 59, W. Bruce Ewbank, The Nuclear Spins and Magnetic Moments of Certain Gold and Silver Isotopes (thesis), UCRL-8756, June 1959.

EWB 60. W. Bruce Ewbank, University of California, private communication (1960).

FIS 46. R. A. Fisher, Statistical Methods for Research Workers (Oliver & Boyd, Edinburgh, 1946).

FOL 48. H. M. Foley and P. Kusch, Phys. Rev. 73, 412 (1948).

FOL 50. H. M. Foley, Phys. Rev. 80, 288 (1950).

FOW 22. A. Fowler, Report on Series in Line Spectra (Fleetway Press, London, 1922).

GAL 58. C. J. Gallagher, Jr., and S. A. Moszkowski, Phys. Rev. 111, 1282 (1958).

GAR 50. W. R. S. Garton, Nature 166, 317 (1950).

GOO 58. L. S. Goodman and W. J. Childs, Bull. Am. Phys. Soc. II, 3, 21 (1958).

GOU 33. S. Goudsmit, Phys. Rev. 43, 636 (1933).

HAR 28. P. Harteck, Z. physik. Chem 134, 1 (1928).

HAX 49. O. Haxel, J. H. D. Jensen, and H. E. Suess, Phys. Rev. 75, 1766 (1949); Z. Physik 128, 295 (1950).

HUB 58. J. C. Hubbs, R. Marrus, and J. L. Worcester, Phys. Rev. 110, 934 (1958).

JAC 32. D. A. Jackson, Z. Physik 74, 291 (1932).

JAC 32a. D. A. Jackson Z. Physik 75, 229 (1932).

KEL 35. K. K. Kelley, U. S. Bur. Mines Bull. 383, 1935.

KIE 59. L. J. Kieffer, W. J. Childs, and L. S. Goodman, Bull. Am. Phys. Soc. II, 4, 10 (1959).

KOS 52. G. F. Koster, Phys. Rev. 86, 148 (1952).

KUS 47. P. Kusch and H. M. Foley, Phys. Rev. 72, 1256 (1947).

KUS 48. P. Kusch and H. M. Foley, Phys. Rev. 74, 250 (1948).

KUS 50. P. Kusch, Phys. Rev. 78, 615 (1950).

LUR 56. A. Lurio and A. G. Prodell, Phys. Rev. 101, 79 (1956).

MAR 59. Lawrence L. Marino, Some Nuclear Properties of Bi^{206}, Tl^{200}, Th^{201}, Th^{202}, In^{109}, In^{110m}, and In^{111} (thesis) UCRL-8721, April 6, 1959.

MAY 48. M. G. Mayer, Phys. Rev. 74, 235 (1948).

MAY 49. M. G. Mayer, Phys. Rev. 75, 1969 (1949).

MAY 55. M. G. Mayer and J. H. D. Jensen, Elementary Theory of Nuclear Shell Structure (John Wiley and Sons, New York, 1955).

MEG 52. W. F. Meggers and R. J. Murphy, J. Research Natl. Bur. Standards 48, 334RP2320 (1952).

MOO 52. C. E. Moore, Atomic Energy Levels, N.B.S. Circular No. 467; 1952.

NIE 58. William A. Nierenberg, University of California, private communication, 1958.

NIE 59. William A. Nierenberg, A Method for Minimizing a Function of n Variables, UCRL-3816-Rev, August 1959.

NOR 51. L. W. Nordheim, Revs. Modern Phys. 23, 322 (1951).

NOY 58. H. Noya, A. Arima, and H. Horie, Supp. of Progr. Theor. Phys. No. 8, 33 (1958).

PAS 22. F. Paschen and R. Götze, Seriengesetze der Linienspektren (Julius Springer, Berlin, 1922).

PET 60. F. Russell Petersen, University of California, unpublished work, 1960.

POU 48. R. V. Pound, Phys. Rev. 73, 1112, and ibid 74, 228 (1948).

RAB 38. I. I. Rabi, J. R. Zacharias, S. Millman, and P. Kusch, Phys. Rev. 53, 318 (1938).

RAM 56. N. F. Ramsey, Molecular Beams (Oxford University Press, London, 1956).

REN 40. N. A. Renzetti, Phys. Rev. 57, 753 (1940).

RIC 55. M. Rice and R. V. Pound, Phys. Rev. 99, 1036 (1955).

ROS 32. J. E. Rosenthal and G. Breit, Phys. Rev. 41, 459 (1932).

SAW 29. R. A. Sawyer and R. J. Lang, Phys. Rev. 34, 712 (1929)

SCH 36. H. Schüler and H. Korsching, Z. Physik 103, 434 (1936).

SCH 37. T. Schmidt, Z. Physik 106, 358 (1937).

SCH 55. C. Schwartz, Phys. Rev. 97, 380 (1955).

SCH 55a. C. Schwartz, Phys. Rev. 99, 1035 (1955).

SCH 57. C. Schwartz, Phys. Rev. 105, 173 (1957).

SHU 57. Howard A. Shugart, The Nuclear Spins, Hyperfine-Structure Separations, and Magnetic Moments of Cs^{127}, Cs^{129}, Cs^{130}, and Cs^{132} (thesis), UCRL-3770, May 15, 1957.

SMI 51. K. F. Smith, Nature 167, 942 (1951).

SUN 56. Robert J. Sunderland, The Nuclear Spins of Rb^{82}, Rb^{83}, and Rb^{84} (thesis), University of California, 1956.

SWI 24. E. H. Swift, J. Am. Chem. Soc. 46, 2375 (1924).

UHL 22. H. S. Uhler and J. W. Tanch, Astrophys. J. 55, 291 (1922).

WAL 55. H. E. Walchli, A Table of Nuclear Moment Data, Supplement II, ORNL-1469, February 1, 1955.

WAY 55. K. Way, R. W. King, C. L. McGinnis, and R. van Lieshout, Nuclear Level Schemes, AEC Report TID-5300, June 1955.

WOR 57. J. L. Worcester, J. C. Hubbs, and W. A. Nierenberg, Bull. Am. Phys. Soc. II, 2, 316 (1957).

WOR 57a. John L. Worcester, Spin and Hyperfine-Structure Measurements of two Neutron-Deficient Gallium Isotopes (thesis), UCRL-3868, 1957.

ZAC 42. J. R. Zacharias, Phys. Rev. 61, 270 (1942).